EXPRESSION ANALYSIS AND BEHAVIORAL ASSAYS IN *DROSOPHILA* CMT MODELS

by

Cansu Küey

B.S., Molecular Biology and Genetics, Bilkent University, 2012

Submitted to the Institute for Graduate Studies in
Science and Engineering in partial fulfillment of
the requirements for the degree of
Master of Science

Graduate Program in Molecular Biology and Genetics
Boğaziçi University

2015

To my family and friends...

ACKNOWLEDGEMENTS

I would like to express my deepest gratitude to my supervisor Prof. Esra Battaloğlu, for her excellent guidance, caring, patience, and providing me with an exceptional atmosphere for doing research.

I would like to express my sincere thanks to my co-advisor Assoc. Prof. Arzu Çelik for her guidance, valuable critics and support whenever I needed.

I would like to thank my committee members, Prof. Hande Çağlayan, Assoc. Prof. Uygar Tazebay and Prof. Müge Türet who took their most valuable time to evaluate my thesis. It is an honor to receive feedback from them about my work.

I would also like to thank Sven Vilain for helping me to solve the methodological issues during my research.

I would like to thank Begüm Gökerküçük, who as a great friend, my research would not have been possible without her helps. Also, I would like to express my sincere thanks to my friends and labmates Burçak, Kaya, Kerem, Merve, Burak and Burcu for their moral support and precious friendship. I also wish to thank Lab 204 and Fly Lab members.

I would like express my deepest thanks to my family for their support and encouragement with their best wishes.

Lastly, I would like to acknowledge Scientific and Technological Research Council of Turkey (TÜBİTAK) and Scientific Research Projects (BAP) for supporting me and this project (112T275 and 7563P).

ABSTRACT

EXPRESSION ANALYSIS AND BEHAVIORAL ASSAYS IN *DROSOPHILA* CMT MODELS

Charcot–Marie–Tooth (CMT) disease is the most common inherited disorder of the peripheral nervous system. It is characterized by progressive distal sensory loss and weakness, muscle atrophy in hands and lower legs, and skeletal deformities. Up to date, approximately 40 genes have been associated with CMT. *GDAP1* is one of the few CMT-causative genes in which recessive or dominant mutations lead to demyelinating, axonal or intermediate forms of the disease with ranging onset and/or severity. *MTMR2* mutations cause autosomal recessively inherited CMT subtype, CMT4B1 that is a demyelinating form with high severity and early-onset. MTMR2 is known to have a role in endocytosis and membrane trafficking, which are crucial mechanisms for neurons. Therefore, both *GDAP1* and *MTMR2* are good candidates to study CMT from behavioral and functional aspects. In this study, we aimed to develop *Drosophila* models for CMT focusing on the fly homologues of these genes, *CG4623* and *mtm*, respectively. In the first part, we verified up- and down-regulation of *CG4623* and overexpression of *mtm* at the mRNA level as we aimed to model the disease by altering the expression levels of these genes. Negative geotaxis assay revealed that altering *CG4623* expression levels affected the climbing behavior of the flies in an age-dependent manner recapitulating the CMT phenotype of progressive motor performance decline. In addition, expression level alterations of *CG4623* yielded slightly lowered survival with statistical significance. However, RNAi knockdown of *mtm* resulted in pupal lethality. We have also generated a polyclonal antibody against mtm that allowed us to quantify expression at the protein level and could be further used in functional studies. Lastly, we aimed to verify the fly lines that were generated to knock-out *CG4623* and *mtm* by IMAGO approach. However, our studies showed that IMAGO flies cannot be used in further studies as the targeting vector was integrated incorrectly to their genome. In the scope of this study, we showed that the CMT models that have been developed can be used in further studies to elucidate the CMT pathogenesis and understand the roles of these genes in disease.

ÖZET

DROSOPHILA CMT MODELLERİNDE ANLATIM ANALİZİ VE DAVRANIŞSAL ÇALIŞMALAR

Charcot–Marie–Tooth (CMT) hastalığı periferik sinir sisteminin en sık görülen kalıtsal hastalığıdır. Progresif distal duysal kayıp ve zaaf, el ve alt bacakta atrofi ve iskelet bozukluklarıyla seyretmektedir. Bugüne dek yaklaşık 40 gen CMT ile ilişkilendirilmiştir. *GDAP1*, hastalığın demiyelizan, aksonal ve ara formlarına yol açan, baskın veya çekinik seyredebilen mutasyonları olan az sayıdaki genden biridir. *MTMR2* mutasyonları ise hastalığın şiddetli ve erken başlangıçlı bir tipi olan otozomal çekinik demiyelizan CMT alt tipine (CMT4B) neden olmaktadır. MTMR2 proteininin nöronlar için hayati öneme sahip olan endositoz ve membran trafiğinde rol oynadığı bilinmektedir. Bu sebeple, *GDAP1* ve *MTMR2* genleri hastalığın davranışsal ve işlevsel çalışmaları için uygun adaylardır. Bu çalışmada bu genlerin sinek homologları olan *CG4623* ve *mtm* genlerine odaklanarak CMT için *Drosophila* modelleri geliştirmeyi amaçladık. İlk bölümde, hastalığı genlerin anlatım düzeylerindeki değişimlerle modellemeyi amaçladığımız için, *CG4623*'ün yüksek ve düşük anlatımını ve *mtm* geninin yüksek anlatımını mRNA düzeyinde doğruladık. Negatif jeotaksis yöntemi ile de, progresif motor performans azalması görülen CMT fenotipinde olduğu gibi, değişen *CG4623* anlatım seviyelerinin sineklerin tırmanma davranışını yaşa bağlı olarak etkilediği gösterildi. Ayrıca, *CG4623*'ün anlatım seviyesindeki değişikliklerin sağkalımda küçük fakat istatistiksel olarak anlamlı bir azalmaya yol açtığı belirlenmiştir. Bununla birlikte *mtm*'nin anlatım seviyesinin düşürülmesi pupada ölüme neden olmuştur. Bu çalışmada, protein düzeyinde anlatım seviyesini saptama olanağı sağlayan ve ileride işlevsel çalışmalarda kullanılabilecek olan poliklonal *mtm* antikoru da geliştirildi. Çalışmanın son bölümünde, *CG4623* ve *mtm* genlerinin IMAGO yöntemi ile genomdan silinmesi için üretilmiş olan sineklerin doğrulanması amaçlandı. Çalışmalar hedef vektörün genoma yanlış entegrasyonu nedeniyle IMAGO sineklerinin ileri aşamalarda kullanılamayacağını göstermiştir. Bu çalışma ile, geliştirilen CMT modellerinin hastalık patogenezi ve bu genlerin hastalıktaki rollerinin aydınlatılması için gelecekte kullanılabileceği gösterilmiştir.

TABLE OF CONTENTS

LIST OF FIGURES

LIST OF TABLES

LIST OF ACRONYMS/ABBREVIATIONS

AARS	alanyl-tRNA synthetase
AD	Autosomal Dominant
APS	Ammonium peroxodisulfate
AR	Autosomal Recessive
attB	Attachment site B
attP	Attachment site P
BAC	Bacterial Artificial Chromosome
BLAST	Basic Local Alignment Search Tool
bp	basepair
BSA	Bovine Serum Albumin
cDNA	Complementary Deoxyribonucleic Acid
$C_{24}H_{39}NaO_4$	Sodium deoxycholate
CNS	central nervous system
CMT	Charcot-Marie-Tooth disease
CMAP	compound motor action potential
CT	Comperative Threshold Cycle
dH_2O	distilled H2O
DNA	deoxyribonucleic acid
DMSO	Dimethyl sulfoxide
Drp1	Dynamin-related protein 1
EDTA	Ethylenediaminetetraacetic acid
ELISA	Enzyme-Linked ImmunoSorbent Assay
Fis1	Fission 1
FLP	Flippase
FRT	Flippase recognition target
GARS	glycyl-tRNA synthetase
GDAP1	Ganglioside-induced differentiation-associated protein 1

GDAP1L1	Ganglioside-induced differentiation-associated protein 1 like 1
gDNA	genomic DNA
GSH	glutathione
GST	glutathione S-transferase
GFP	green fluorescent protein
GRAM	Glucosyltransferase, Rab-like GTPase activators and myotubularins
GTP	guanosine triphosphate
HA	Homology arm
HD	hydrophobic domain
HEPES	4-(2-hydroxyethyl)-1-piperazineethanesulfonic acid
HMSN	hereditary motor and sensory neuropathy
hpRNA	hairpin RNA
HRP	Horse raddish peroxidase
IMAGO	integrase-mediated approach for gene knock-out
IP3	Inositol trisphosphate
IPTG	Isopropyl β-D-1-thiogalactopyranoside
kb	kilobase
KCl	Potassium Chloride
kDa	kilodalton
KH_2PO_4	Potassium Phosphate
KOAc	Potassium Acetate
LB	Luria Bertani
LiCl	Lithium Chloride
LMNA	Lamin A/C
Marf	Mitochondrial assembly regulatory factor
MFN1	Mitofusin 1
MFN2	Mitofusin 2
$MgCl_2$	Magnesium Chloride
$MgCl_26H_2O$	Magnesium chloride hexahydrate

MPZ	Myelin protein zero
MTM	Myotubularin
MTMR2	Myorubularin-related protein 2
MTMR5	Myorubularin-related protein 5
MTMR13	Myorubularin-related protein 13
MOM	Mitochondrial Outer Membrane
NaCl	Sodium Chloride
$NaHCO_3$	Sodium Bicarbonate
NaH_2PO_4	Monosodium phosphate
NaOAc	Sodium Acetate
NCV	Nerve conduction velocity
n.s.	not significant
OE	overexpression
O/N	overnight
OPA1	Optic Atrophy Protein 1
PCR	Polymerase Chain Reaction
PH GRAM	Pleckstrin homology glucosyltransferases, rab-like GTPase activators and myotubularin
PI	Phosphatidyl inositol
PI3P	phosphoinositol 3-phosphate
$PI3,5P_2$	phosphoinositol 3,5-biphosphate
PMP-22	Peripheral myelin protein 22
PNS	peripheral nervous system
qRT-PCR	quantitative Reverse Transcription-PCR
RING	Rapid-Iterative Negative Geotaxis
ROS	reactive oxygen species
RMCE	recombinase mediated cassette exchange
RNA	ribonucleic acid
RNAi	ribonucleic acid interference
SBF1	SET binding factor 1
SDS	Dodecylsulfate Sodium Salt

SEM	Standart Error of Mean
siRNA	small interfering RNA
TCA	Trichloroacetic acid
TEMED	N,N,N′,N′-Tetramethylethylenediamine
TM	transmembrane domain
UAS	upstream activating sequence
UV	Ultraviolet
VDRC	Vienna Drosophila Resource Center
YARS	tyrosyl-tRNA synthetase

1. INTRODUCTION

Charcot–Marie–Tooth (CMT) disease also known as Hereditary Motor and Sensory Neuropathy (HMSN) was classically described in the 19th century. Although, it is the most common inherited peripheral neuropathy with a prevalence of 1 to 2500 (Skre, 1974), a curative treatment is not available yet. Typical symptoms of the disease are progressive distal sensory loss and weakness, muscle atrophy in hands and lower legs, and skeletal deformities (Figure 1.1; Reilly *et al.*, 2011; Patzko and Shy, 2011) all caused by motor deficiencies. Although, patients might need mobility aids and/or orthopedic surgery in later years of life, life expectancy is normal in most types of CMT. Thus, CMT is not classified as a lethal disease.

Figure 1.1. Clinical features of CMT. Proximal and distal leg wastings, clawed hands and *pes cavus* (adapted from Reilly *et al.*, 2011).

The disease is classified as demyelinating (CMT1) and axonal (CMT2) type according to electrophysiological and neuropathological findings. In demyelinating CMT, the nerve conduction velocities (NCV) of the patients are less than 38 m/s, and onion bulb formation in myelin sheath is followed by neurodegeneration. NCVs are normal in axonal CMT, but amplitudes of compound motor action potentials (CMAP) are low (Harding and Thomas, 1980). Axonal loss is followed by myelin sheath deformation in these patients as

a secondary effect. The third subtype of the disease is the intermediate form in which NCVs are between 25-45 m/s. Patients with this subtype show symptoms of both demyelinating and axonal forms (Davis *et al.*, 1978).

CMT is a clinically and genetically heterogeneous disease. The symptoms usually begin to appear around adolescence; however, depending on the causative gene and mutation identified, the onset and severity of the symptoms may vary between patients. The inheritance pattern of the disease can be autosomal dominant (AD), autosomal recessive (AR) or X-linked, and up to date approximately 40 disease-causing genes have been identified (Timmerman *et al.*, 2014). Duplication of a 1.4 Mb region on chromosome 17p.11.2, including the *peripheral myelin protein 22* (*PMP22*) gene is the causative mutation in most of the autosomal dominant CMT cases. Interestingly, deletion of the same region causes Hereditary Neuropathy with Liability to Pressure Palsies (HNPP) suggesting a dosage dependent mechanism (Berger *et al.*, 2006). Other genes associated with AD-CMT include *myelin protein zero* (*MPZ*), *mitofusin 2* (*MFN2*) and aminoacyl-tRNA synthetase genes: *AARS*, *GARS*, and *YARS*. Autosomal recessive forms of the disease are reported more frequently in certain regions with high percentage of consanguineous marriages such as the Middle East and Mediterranean basin (Juarez and Palau, 2012). The onset of AR-CMT is usually in the first decade, and the symptoms are more severe compared to AD-CMT (Patzko and Shy, 2011). Genes associated with AR-CMT include *Ganglioside-induced differentiation-associated protein 1* (*GDAP1*; *myotubularin-related protein 2* (*MTMR2*), and *Lamin A/C* (*LMNA*) (Tazir *et al.*, 2013).

Identifying the cellular functions of CMT-associated proteins and clarifying the molecular mechanisms involved in CMT are critical to understand the disease pathogenesis. CMT-associated proteins are located in Schwann cells and peripheral neurons and are known to be involved in various cellular processes including myelination, membrane trafficking and mitochondrial dynamics (Figure 1.2, Berger *et al.*, 2006; Patzko and Shy, 2011). However, the exact roles of most CMT proteins still remain to be understood. Generation of *in vivo* disease models is the most efficient approach to elucidate the functions of these proteins and underlying cellular and molecular mechanisms of disease pathogenesis. Furthermore, these animal models could be used in drug development for CMT.

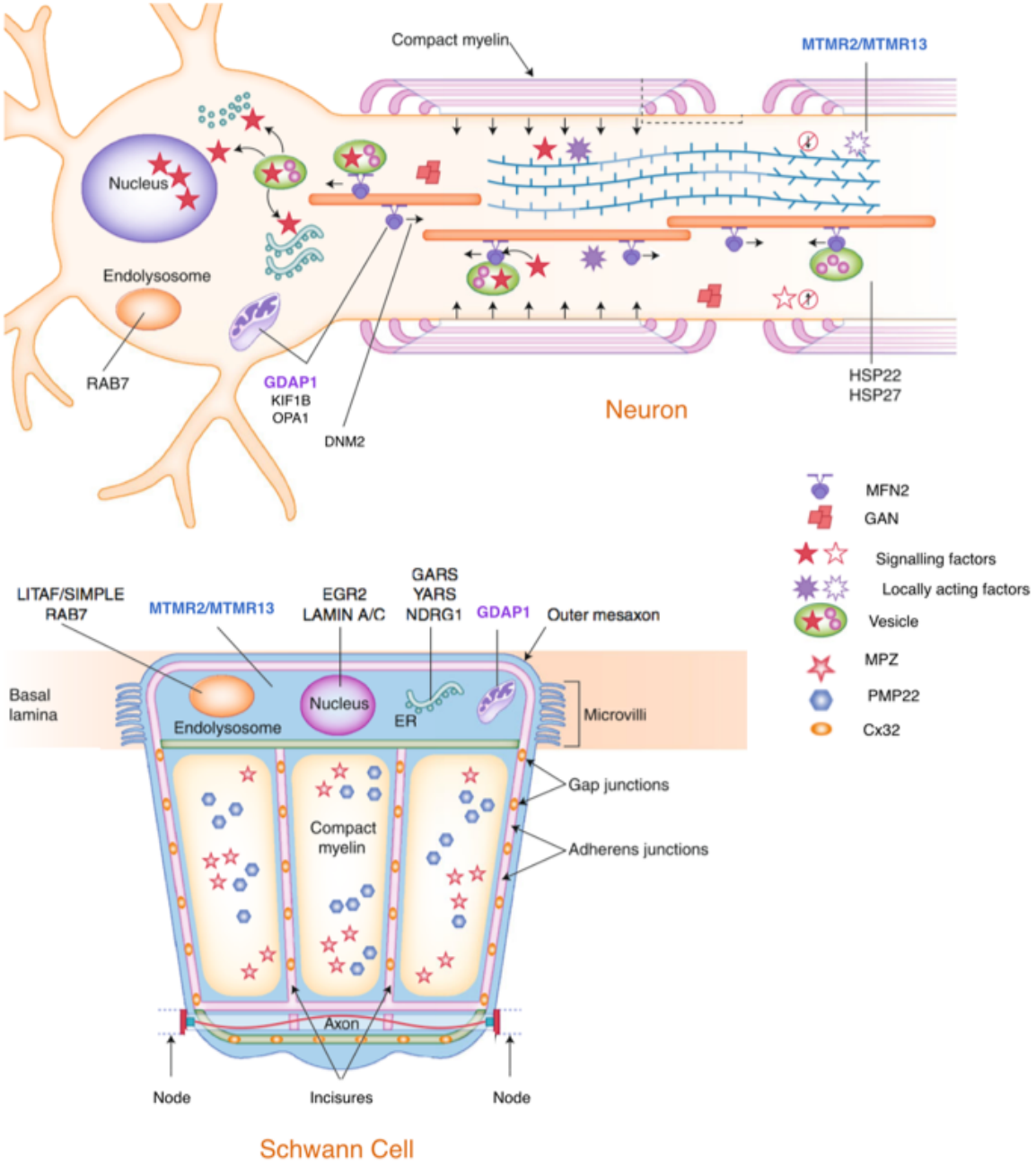

Figure 1.2. Proteins and intracellular pathways associated with CMT (adapted from Patzko and Shy, 2011).

1.1. *GDAP1*

Ganglioside –induced differentiation-associated protein 1 (*GDAP1*) is one of the few CMT-causative genes in which mutations lead to several forms of CMT. Dominant or recessive *GDAP1* mutations can cause demyelinating, axonal or intermediate forms of CMT with ranging onset and/or severity.

GDAP1 is most frequently responsible for demyelinating autosomal recessive CMT subtype CMT4A that with early onset and high severity. CMT4A is an aggressive subtype, and the symptoms can appear during early childhood or even at infancy; thus, patients often become wheelchair-bound in the second decade of life (Zuchner and Vance, 2004). Vocal cord paresis (hoarse voice) is also a common feature of this subtype suggesting central nervous system (CNS) involvement (Boerkoel *et al.*, 2003). The life expectancy is normal in CMT4A; however, it could be affected due to secondary complications (Zuchner and Vance, 2004).

GDAP1 mutations causing axonal autosomal dominant form of the disease are rare and known as CMT2K subtype. Patients display a milder phenotype and the onset of the disease is late with slower progression compared to the recessive subtypes (Claramunt *et al.*, 2005; Cassereau *et al.*, 2011). Other rare *GDAP1* mutations are associated with intermediate AR-CMT, which is also a severe early-onset neuropathy like CMT4A except that patients have intermediate nerve conduction velocities (Senderek *et al.*, 2003).

GDAP1 has six exons, and it encodes a protein of 358 amino acids that belongs to the Glutathione S-transferase family. The protein is expressed ubiquitously, especially in neurons (Pedrola *et al.*, 2005, 2008) and Schwann cells (Niemann et al., 2005), and has five domains: two glutathione S-transferase domains (GST-N and GST-C), a α4-α5 loop, a hydrophobic domain (HD), and a transmembrane domain (TM) (Figure 1.3, Marco *et al.*, 2004; Niemann *et al.*, 2009). Existence of GST domains suggests its involvement in oxidative stress mechanisms since the major role of GSTs is detoxification by conjugating glutathione to electrophilic substrates. GDAP1 is anchored to the mitochondrial outer membrane via its transmembrane domain and has a function in the mitochondrial fission process (Figure 1.4, Niemann *et al.*, 2005; Pedrola *et al.*, 2005; Niemann *et al.*, 2014; Lopez Del Amo *et al.*, 2014). *Ganglioside–induced differentiation-associated protein 1-like 1* (*GDAP1L1*), which is expressed in the central nervous system, is the paralogue of GDAP1 in humans. Although GDAPL1 has two GST domains and a transmembrane domain, it is normally cytosolic unlike GDAP1 (Figure 1.3, Niemann *et al.*, 2005; Shield *et al.*, 2006).

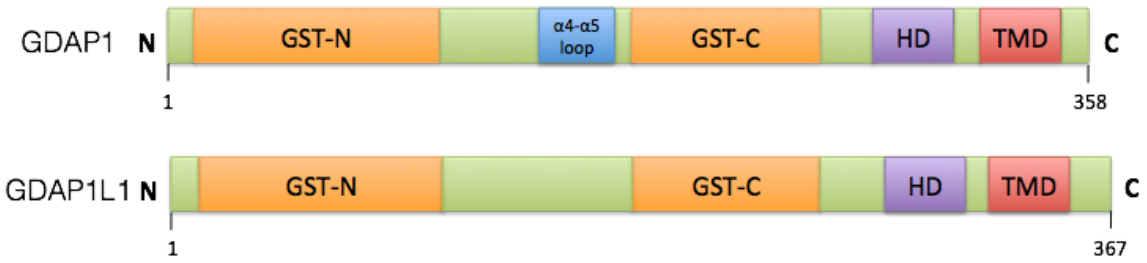

Figure 1.3. Representative domain structure of GDAP1 and GDAP1L1 proteins. GDAP1 and GDAP1L1 share two GST domains, a hydrophobic domain and a transmembrane domain.

Before 2014, several *in vitro* studies have been performed to elucidate the function of *GDAP1* in mitochondrial processes. Mitochondria are mobile and dynamic organelles that undergo fusion and fission continuously (Figure 1.4). These opposing processes control the morphology, which is crucial for proper functioning of mitochondria (Ni *et al.*, 2014). Considering the role of mitochondria as the power supply of the cells, disruptions in its morphology and dynamics distress cells with high energy demands, for instance, neurons. Mutations in genes encoding proteins involved in fusion (*MFN2* and *OPA1*) or fission (like *Drp1*) cause various neurodegenerative diseases including CMT (Chen and Chan, 2009; Detmer and Chan, 2007). Furthermore, it has been shown that overexpression of *GDAP1* causes formation of fragmented mitochondria in cell lines (Niemann *et al.*, 2005; Pedrola *et al.*, 2008) whereas, knockdown of *GDAP1* results in formation of tubular mitochondria (Niemann *et al.*, 2005). Also, it is found that GDAP1 activity is dependent on other fission factors *Drp1* and *Fis1*, but expression of recessive CMT-associated *GDAP1* mutations in cell lines decreases the fission of mitochondria, while dominant mutations damage the fusion process (Niemann *et al.*, 2009). The same group also showed that GDAP1 has a regulatory role not only in mitochondrial fission, but also in the fission process of peroxisomes (Huber *et al.*, 2013) Another study suggests involvement of GDAP1 in the transport of mitochondria by interacting with RAB6B and caytaxin. In the same study *in vitro* downregulation of *GDAP1* resulted in disrupted mitochondrial distribution in the cell pointing out to the possibility that mitochondrial motility impairments might be the cellular factor underneath the CMT pathophysiology. It was have also indicated that calcium homeostasis is disturbed upon downregulation of *GDAP1*, and abnormal positioning of mitochondria in the cell might be the cause of this abnormality (Pla-Martin *et al.*, 2013).

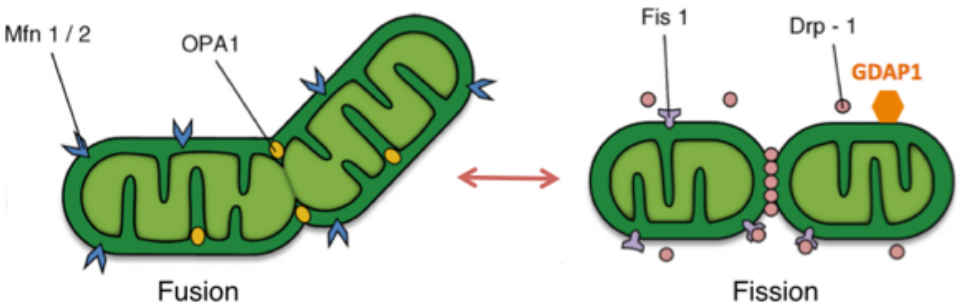

Figure 1.4. Mitochondrial dynamics and involved proteins (adapted from Kuzmicic *et al.*, 2011).

Other *in vitro* studies investigated the role of GDAP1 in oxidative stress since GDAP1 has two GST domains. In general GSTs can be cytosolic or membrane-bound and their function is to catalyze the conjugation of glutathione, an antioxidant, to electrophilic substrates such as harmful chemicals and reactive oxygen species (ROS) as a protection against oxidative stress (Eaton and Bammler, 1999). Even though, Shield and her colleagues could not observe any GST activity or glutathione binding in purified GDAP1 protein - probably due to the lack of TM domain in the purified version (Shield *et al.*, 2006) - it has been shown that overexpression of only wild-type *GDAP1* - not the recessively mutated CMT-associated versions - in neurons provided protection against oxidative stress; however, knockdown of GDAP1 gave rise to a proneness to oxidative stress; overall strengthening the role of GDAP1 as a GST (Noack *et al.*, 2012).

A *GDAP1* knockout mouse model of CMT has been generated in 2014. Decreased NCVs and hypomyelination was observed in the knockout mice around 19 months of age which is consistent with the age-related progression of CMT in humans. The observation of phenotype is also seen when GDAP1 is knocked out in Schwann cells exclusively. Larger mitochondria were observed in the axons only in the complete knockout suggesting a disruption in mitochondrial morphology was caused by neuronal loss of GDAP1. It has been shown that loss of GDAP1 results in oxidative stress since the mitochondrial DNA content was increased as a response in the peripheral nervous system of knockout mice. GDAP1L1 replaces the loss of GDAP1 in the central nervous system by translocation to the outer membrane of mitochondria from the cytoplasm, explaining the unaffected CNS in CMT patients (Niemann *et al.*, 2014).

1.1.1. *CG4623* is the *Drosophila* Homologue of *GDAP1*

CG4623 was shown to be the *Drosophila* homologue of *GDAP1* and *GDAP1L1* by bioinformatics analysis (Marco *et al.*, 2004) and the newly generated fly model (Lopez del Amo *et al.*, 2014). *CG4623*, located on the third chromosome of the fly, encodes for a protein of 327 aminoacids. The GST domains and transmembrane domain of GDAP1 and CG4623 proteins have been conserved (Figure 1.5), and they share 29% identity and 46% similarity at the amino acid level, indicated by Protein BLAST (Altschul *et al.*, 1997; Altschul *et al.*, 2005). *CG4623* is expressed in the hindgut, midgut and malphigian tubules of late embryos according to the transcriptome analyses by FlyAtlas and modENCODE projects. Lopez del Amo and colleagues detected expression not only in the same tissues but also in the anal pads and antenno-maxillary sense organs of first instar larvae. It is also suggested that this pattern of expression might indicate a function in oxidative stress defense since it resembles expression patterns of other proteins involved in protection mechanisms against reactive oxygen species (Lopez del Amo *et al.*, 2014).

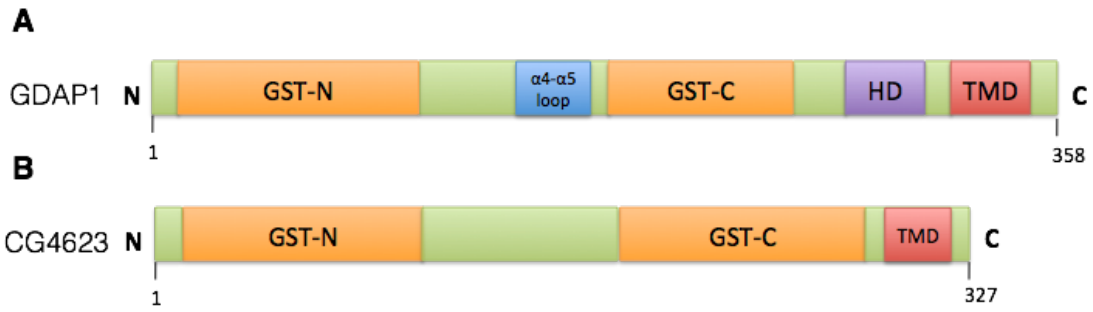

Figure 1.5. Representative domain structure of GDAP1 and CG4623 proteins. GDAP1 and CG4623 share two GST domains and a transmembrane domain.

Lopez del Amo and colleagues verified that the *CG4623* gene is the fly homolog of *GDAP1* by partial rescue of the downregulation phenotype in *Drosophila* with overexpression of human *GDAP1*. It is shown that changes in *CG4623* expression level (up- and downregulation) in the retina using retina-specific drivers resulted in degeneration in the adult retina, which is a part of the *Drosophila* peripheral nervous system. Similar experiments using muscle-specific drivers resulted in degeneration of muscles with increasing severity in an age-dependent manner. Mitochondria in the muscle fibers were larger in size upon downregulation of *CG4623*, whereas smaller mitochondria were

observed in flies which *CG4623* was overexpressed, consistent with the findings of previous *in vitro* studies and the mouse model explained above. Muscular degeneration and alteration in mitochondrial morphology seen with muscle-specific expression level changes imply a tissue-autonomous, neuron-independent function of CG4623. Furthermore, the effects of *CG4623* expression levels on mitochondrial morphology imply a role in mitochondrial dynamics (Lopez del Amo *et al.*, 2014).

CMT models described above indicate abnormalities in mitochondrial morphology and dynamics due to changes in GDAP1 levels suggesting that animal models recapitulating these phenotypes seem promising to study the effect of mitochondrial defects leading to peripheral neuropathies.

1.2. *MTMR2*

Myotubularin-related protein-2 (*MTMR2*) mutations cause autosomal recessively inherited demyelinating CMT subtype, CMT4B1 (Bolino *et al.*, 2000). This subtype, like other autosomal recessively inherited ones, has a very early onset in childhood and shows severe symptoms with rapid progression. Patients generally exhibit reduced NCVs (<20 m/s), distal and proximal weaknesses, *pes cavus*, clawed hands and scoliosis, and are usually wheelchair-bound in their adulthood (Houlden *et al.*,2001; Parman *et al.*, 2004; Tazir *et al*., 2013). Diaphragmatic and facial weaknesses are also documented. Patients of one of the initially described CMT4B1 families, an Italian family studied in 1996, had a life of 40-50 years on average, which is lower than the normal average life expectancy (Quattrone *et al.*,1996). However, there have not been any other records of lifetime in the literature. The characteristic phenotype of CMT4B is the focally folded myelin pointed out in the nerve biopsies of the patients (Saporta and Shy, 2013) implicating a defect in membrane trafficking required for the maintenance of the myelin sheaths.

MTMR2 is located on chromosome 11q22 and encodes for a protein of 643 aminoacids that belongs to the myotubularin family of proteins in humans. Myotubularins are highly conserved dual-specific phosphatases that dephosphorylate phosphoinositol 3-phosphate (PI3P) (Figure 1.6) and phosphoinositol 3,5-biphosphate ($PI3,5P_2$) *in vitro*. These phosphoinositols act as secondary messengers in endocytosis and various membrane

trafficking events by recruiting effector proteins (Berger *et al.*, 2006). *In vitro* studies showed that PI3Ps are located in the early endosomes whereas PI3,5P_2s are located in the late endosomes, and PI3,5P_2 levels are elevated during endolysosomal fusion (Dove *et al.*, 2009; Li *et al.*, 2013). This specific substrate distribution suggests that myotubularins regulate endocytosis and membrane trafficking in the cell.

Some of the inactive members of the myotubularin family form dimers with the active ones to govern the subcellular localization of the phosphatase (Kim *et al.*, 2013). MTMR2 is an active myotubularin, and it has been shown that an inactive member MTMR13 (Figure 1.7) physically interacts with MTMR2 *in vitro* (Robinson and Dixon, 2005). Mutations in *MTMR13* also result in an autosomal recessive form of CMT, known as CMT4B2.

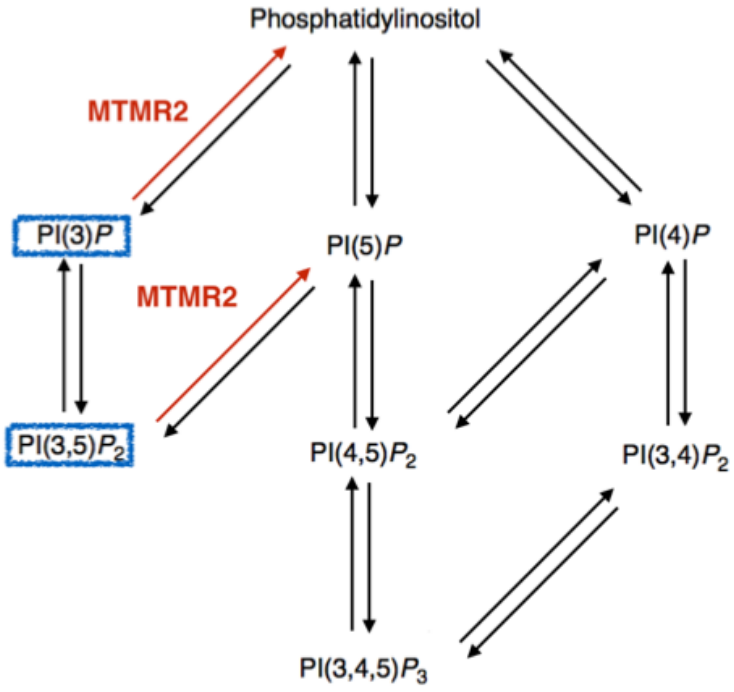

Figure 1.6. MTMR2 dephosphorylates PI3P and PI3,5P_2 (adapted from Wishart and Dixon, 2002).

MTMR2 is mainly a cytosolic protein (Robinson and Dixon, 2005; Lorenzo *et al.*, 2006) with four domains: PH GRAM (Pleckstrin homology glucosyltransferases, rab-like GTPase activators and myotubularin) domain, phosphatase domain, coiled-coil domain and PDZ domain (Figure 1.7). MTMR2 binds to its substrates, PI3P and PI3,5P_2 from its PH-

GRAM domain and remove phosphate with its catalytically active phosphatase domain. The coiled-coil domain is involved in dimerization and association to membranes, and the PDZ- binding domain has a role in protein-protein interactions (Hsu and Mao, 2014).

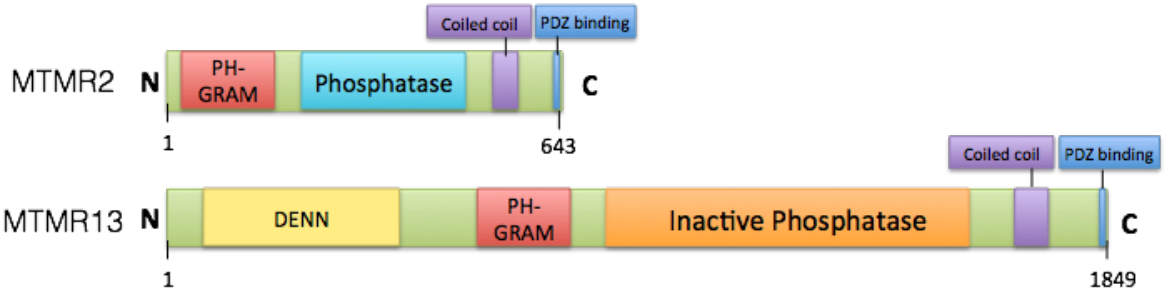

Figure 1.7. Representative domain structure of MTMR2 and MTMR13 proteins. MTMR2 and MTMR13 share a PH-GRAM domain, coiled-coil domain and a PDZ binding domain.

Two mouse models of MTMR2 have been generated. Bolino and colleagues generated *Mtmr2-null* mice in which *Mtmr2* protein is truncated and nonfunctional. The behavioral and electrophysiological analyses performed revealed neuromuscular abnormalities. Moreover, knockout mice showed a similar phenotype to CMT4B patients including the presence of focally folded myelin structure in the peripheral nerves. Schwann cell exclusive loss of Mtmr2 protein was sufficient to create the CMT4B phenotype; however, motor-neuron exclusive loss resulted in no effect suggesting a primary effect on Schwann cells. It was also shown that Mtmr2 interacts with discs large protein 1 (Dlg1) which is a scaffolding molecule in Schwann cells (Bolino *et al.*, 2004) suggesting that this interaction might be necessary for membrane homeostasis. A year later, Bonneick and colleagues generated *Mtmr2-mutant* mice mimicking a recessively segregated mutation in one of the CMT4B families. They have also observed the peripheral nerve exclusive myelin outfolding phenotype. Furthermore, they have concluded that this pathologic phenotype is progressive in an age-dependent manner. Occasional axonal damage was also reported without a change in NCVs up to 16 months of age (Bonneick *et al.*, 2005). Both studies concluded that *Mtmr2* is expressed ubiquitously both in neurons and Schwann cells implicating that the disease pathogenesis caused by *MTMR2* mutations might arise due to its effect both on Schwann cells and neurons.

A more recent study not only verified the expression pattern of *Mtmr2*, but also identified a new interaction partner of Mtmr2 in neurons and Schwann cells. Vaccari and colleagues generated *Mtmr2/Fig4* double null mutant mice, and showed that Fig4 ablation rescued the myelin outfolding phenotype seen in *Mtmr2* mutants which provides an evidence of the antagonistic work of two proteins on generation of PIP3,5P_2s (Vaccari *et al.*, 2011). Other neuronal interaction partners of MTMR2 protein were also found *in vitro* (Previtali *et al.*, 2003; Lee *et al.*, 2010). These findings may shed light onto our understanding of MTMR2 pathology.

1.2.1. *mtm* is the *Drosophila* Homologue of *MTMR2*

Myotubularin (mtm), the fly orthologue of human *MTMR1/MTMR2* genes, is located on the second chromosome of the fly, and it encodes a protein of 619 aminoacids (69.8 kD). Mtm and MTMR2 proteins have conserved PH-GRAM and phosphatase domains in common (Figure 1.8), and they share 58% identity and 76% similarity at the amino acid level, indicated by Protein BLAST (Altschul *et al.*, 1997; Altschul *et al.*, 2005).

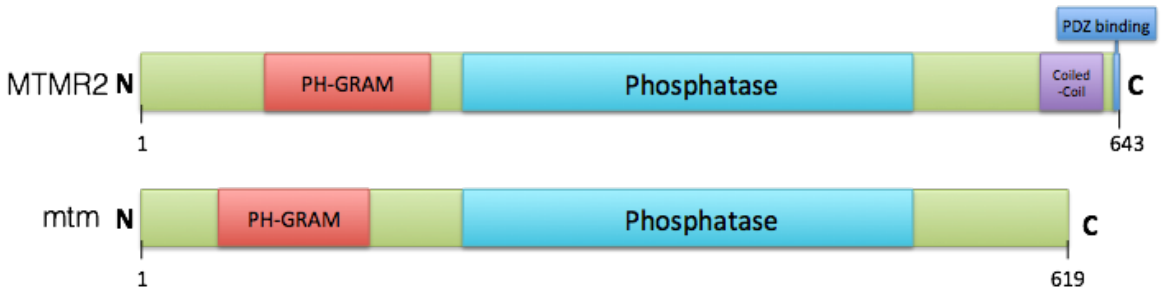

Figure 1.8. Representative domain structure of MTMR2 and mtm proteins. MTMR2 and mtm share a PH-GRAM domain and a phosphatase domain.

In 2010, Velichkova and colleagues reported the generation of null and truncated mutants of *Drosophila myotubularin (mtm)*. They identified PIP3s as the substrate of mtm, and showed that mtm is crucial for proper endocytosis by regulation of PIP3 pools. This function of mtm is required for cortical remodeling in hemocytes, in other words immune cells that respond to wounding. Mtm also has a role in homeostasis of endolysosomes. Additionally, it was shown that all mtm mutants are larval lethal, and hemocyte-specific downregulation of *mtm* results in pupal lethal phenotype, which can be rescued by

overexpression of *mtm* or human *MTMR2*. Meaning that phosphatase function of mtm in immune cells is crucial in development of the fly (Velichkova *et al.,* 2010). However, they have not performed any experiments to test the neuronal function of mtm. Recently, Merve Kılınç from our laboratory observed abnormal synaptic morphology in neuromuscular junctions of *mtm* null and neuron-specific *mtm* knockdown flies suggesting that function of mtm is necessary for the formation of proper synaptic structures (Kılınç, 2013).

1.3. *Drosophila melanogaster*

Drosophila melanogaster, the fruit fly, has been used in biology for over a hundred years, and *Drosophila* studies led to the understanding of genetics with discoveries such as the notion of chromosomes as carriers of heritable traits and gene structures (Morgan, *et al.*, 1915; Lewis, 1978; Nusslein-Volhard and Wieschaus, 1980). In the new millennia fruit fly is highly preferred as a model organism to investigate mechanisms underlying diseases since essential biological processes are similar between humans and *Drosophila.*

The lifecycle of *Drosophila* is very rapid when compared to other higher model organisms. At 25°C, the fertilized egg becomes an embryo within one day, and goes through larval stages (first, second, and third instar) in the following five days. Third instar larvae become pupae at day seven, and the pupae become an adult three days later. In other words it takes 10 days after fertilization for an adult to emerge. The lifespan of *Drosophila* is two months in average at 25°C and around one month at 29°C. Also, females live longer than males. However, changing the culture conditions *i.e.* temperature and food type can help to increase the lifespan. This short lifecycle of *Drosophila* enables researchers to investigate the effects of various genetic and/or environmental factors on the organism throughout its lifetime since it is less time consuming. For instance, longevity assays are frequently used when comparing effects of different genetic mutations in the fly.

Drosophila has a sophisticated nervous system despite its small size. Although it lacks Schwann cells, the wrapping glial cells provide protection and support to the neurons. Furthermore, the adult fly is capable of performing complex behaviors such as learning and memory, aggression, climbing, and flight navigation (Pandey and Nichols, 2011). Assays that analyze these behaviors have been established throughout the years.

External stimuli such as light, odors and gravity can be used to trigger motor behavior in fruit flies or larvae (Jose *et al.*, 2013). Negative geotaxis assay is one of the most commonly used assays to analyze the motor behavior of adult flies. It assesses an innate escape response of flies that is their behavior of climbing against gravity after they are tapped to the bottom of the container (Gargano *et al.*, 2005). This assay is an established method to detect the motor deficits in neurodegenerative disorders.

After *Drosophila* and human genomes are fully sequenced in the early 2000's, studies using fruit fly as a model organism to investigate disease mechanisms gained momentum since its genome was strikingly similar to humans. About 75% of genes associated with human diseases have homologs in one of the four chromosome of *Drosophila* (Bier, 2005; Jackson, 2008; Lloyd and Taylor, 2010; Yamamoto, *et al.*, 2014), and between flies and mammals, the overall sequence identity of two homologous genes is around 40% and it can rise up to 90% in conserved functional domains (Pandey and Nichols, 2011). Moreover, well-established genetic tools to manipulate the *Drosophila* genome were already present in the field. Most commonly used tools include balancer chromosomes that prevent homologous recombination and hold an allele of interest in heterozygous state, Gal4-UAS binary system that allows spatiotemporal regulation of a gene, and *P*-elements, transposons that randomly insert to the genome that are used in mutagenesis and transgenesis. Certain *P*-elements can be used to generate null alleles by deletion of sequences flanking the site of integration by imprecise excision (Lloyd and Taylor, 2010). Also, *P*-element vectors with markers can be used to insert sequences to the fly genome with random or site-specific integration (Hummel and Klambt, 2008).

It is relatively less time consuming to study a disease in *Drosophila* compared to vertebrate models. First of all, it is cost-efficient and easy to take care of *Drosophila* in the laboratory. Considering the short life cycle and enormous number of progeny that emerge in one cross, conducting drug screens on *Drosophila* is very feasible. Drugs can be delivered in various ways such as direct injection and mixing with the food (Lu and Vogel, 2009; Pandey and Nichols, 2011). These advantages led to the usage of *Drosophila* as a model organism in elucidating disease mechanisms and search for therapeutic targets in many neurodegenerative diseases like Alzheimer's, Parkinson's and Amyotrophic Lateral Sclerosis (Lu, 2009). Several fruit fly models of Charcot-Marie-Tooth disease have been

generated in recent years. A genetic screen that investigated effects of mutations on dendrite and axon morphogenesis in 2007 showed that the mutations in the *Drosophila* homolog of glycyl-tRNA synthetase (*GARS*) gene displayed CMT-like phenotypes (Chihara *et al.*, 2007). In 2009, Storkebaum and his collegues generated a CMT model by introducing CMT-causing dominant mutations of tyrosyl-tRNA synthetase gene (*YARS*) to its fly homolog (Storkebaum *et al.*, 2009). Other *Drosophila* models of CMT have been developed in later years, for CMT causative genes *rab7* and *GARS* (Cherry *et al.*, 2013; Ermanoska *et al.*, 2014). Very recently, a *Drosophila* model for *GDAP1* was developed, which has been described in Section 1.1 (Lopez del Amo *et al.*, 2014).

1.3.1. Gal4-UAS Binary System

Spatiotemporal transcriptional regulation is a critical approach to investigate functional properties of genes. The Gal4-UAS binary system in *Drosophila* allows researchers to express their gene of interest in specific tissues or at a certain time frame for over two decades (Brand and Perrimon, 1993). The basic principle of this binary system is the binding of Gal4, a yeast transcription factor, to the Upstream Activating Sequence (UAS), which results in the expression of the gene residing downstream of UAS. The system is composed of two fly lines, the UAS responder line and the Gal4 driver line. Responder lines are generated by cloning the gene of interest to the downstream of UAS. The gene of interest may vary from Green Flourescent Protein (GFP) to human disease-causing genes. The Gal4 sequence is inserted to the downstream of an endogenous regulatory element (promoter or enhancer), so that Gal4 expression will mimic the pattern of the original gene regulated by the element. When a responder line is crossed with a driver line, the expression of the gene of interest is activated upon binding of Gal4 to UAS in the progeny carrying both Gal4 and UAS alleles. Thus, the gene of interest would be expressed in the same pattern with Gal4 (Figure 1.9). Importantly, this binary approach allows the responder lines to stay transcriptionally inactive unless they are crossed with a driver (Duffy, 2002). Various driver lines specific for different tissues have already been developed by researchers and are available in *Drosophila* stock centers. One of the most frequently used lines is *the* actin5C-Gal4 line, which drives the ubiquitous expression of the gene of interest when crossed with a UAS line since actin is expressed in the whole organism. In the nSyb-Gal4 line, Gal4 is under the control of the neuronal synaptobrevin

promoter, which originally regulates a protein that is only expressed in neurons; thus, this driver is used for neuronal expression or downregulation of the gene of interest.

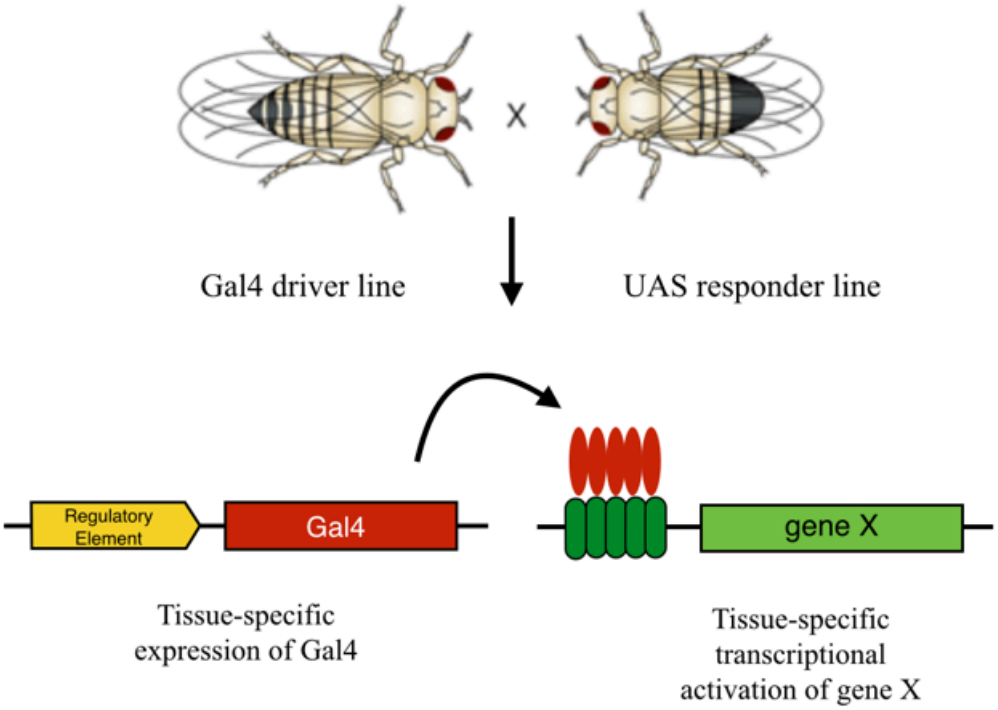

Figure 1.9. The Gal4-UAS Binary System. Crossing Gal4 driver lines to UAS responder lines allows expression of any gene of interest under the control of specific regulatory elements (adapted from Miratul *et al.*,2002).

Gal4-UAS system can be used to overexpress a human or *Drosophila* gene by generation of a UAS line specific for that gene. A UAS construct with the gene of interest in the downstream can be integrated to the genome by using *P*-element vectors such as *pUAST* for random integration and *pUASTattB* for site-specific integration. *attB* sites in the site-specific integration vector are originally bacterial attachment sites that are used in phage integration to the bacterial genome along with their phage counterparts, *attP* sites. After the injection of the vector, *attB* sites and *attP* sites, specifically placed in the fly genome, recombine with each other in the presence of a recombinase, and allow insertion of the UAS construct with gene of interest.

It is also possible to achieve the spatiotemporal downregulation of a gene by using the Gal4-UAS system. Responder lines carrying the RNAi construct for downregulation in

the downstream of UAS has been generated for many genes, and are commercially available at the Vienna Drosophila Resource Center (VDRC). Upon crossing with a driver line, a hairpin RNA (hpRNA) is expressed under the control of the Gal4 line promoter, and cleaved into small interfering RNAs (siRNAs) by Dicer enzyme. Then, these siRNAs conduct the degradation of target mRNA (http://stockcenter.vdrc.at/control/howtornaidmel). A UAS-Dicer construct can also be integrated to the genome of any Gal4 RNAi line to increase the efficiency of knockdown.

1.3.2. Integrase-Mediated Approach for Gene Knock-Out (IMAGO)

In 2009, Choi and colleagues modified the ends-out homologous recombination and created Integrase-Mediated Approach for Gene Knock-Out (IMAGO), which allows knock-in of any DNA sequence to the *Drosophila* genome once the knock-out is generated (Choi *et al.*, 2009).

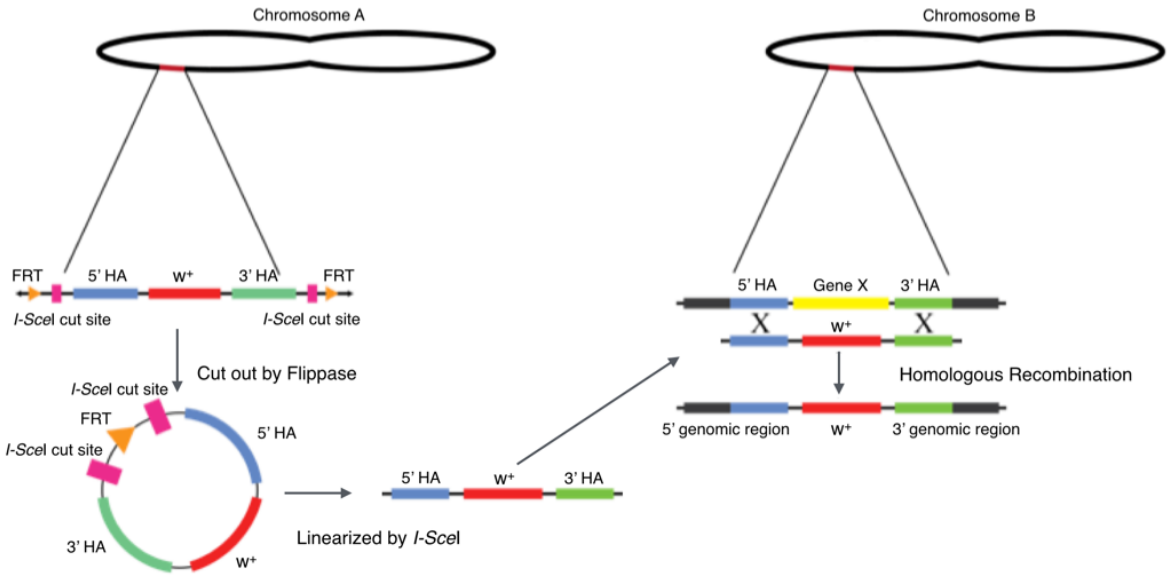

Figure 1.10. Gene targeting and knock out via homologous recombination (adapted from Yıldırım, 2013).

IMAGO vector pPwhite-STAR containing the marker gene w^+ (red eye) with two attP sites at both ends that are flanked by 5' and 3' homology arms of the gene of interest is integrated randomly to the fly genome by *P*-element transformation. The vector is cut out from the genome and linearized by heat-shock induced flippase (Flp) and *I-Sce*I

activity, respectively. Recombination occurs between the linearized DNA fragment and the target locus since the fragment has homologous sequences to the flanking regions of the gene of interest. Thus, the knock-out is generated by the replacement of the gene of interest with the marker gene, w^+ via homologous recombination (Figure 1.10). After the knock-out is generated, knock-in constructs are inserted to the genome by ΦC31 integration. The attP sites on both ends of the marker gene allow recombination between the marker gene and attB flanked knock-in constructs in the presence of ΦC31 integrase.

2. AIM OF THE STUDY

In this study, our aim is to develop *Drosophila* models for Charcot-Marie-Tooth disease by focusing on two causative genes, *Ganglioside-induced differentiation-associated protein 1 (GDAP1)* and *myotubularin-related protein 2 (MTMR2).*

In the first part of the study, we aim to model CMT in flies by altering the expression levels of *GDAP1* and *MTMR2* fly homologues*, CG4623* and *mtm*, respectively. Therefore, we verified down-regulation of *CG4623* and overexpression of *CG4623* and *mtm* by qRT-PCR. Since the CMT patients present progressive distal weakness we performed negative geotaxis assay to investigate whether our models can recapitulate these symptoms. We also produced an antibody against mtm that can be used in further studies to unravel the role of the protein in disease pathogenesis via analyzing its expression pattern and subcellular localization. Finally, we assessed the effect of expression level alterations of *CG4623* and *mtm* on the lifespan in order to investigate whether recapitulation of CMT has an influence on the survival of the flies.

In the last part of the study, we aim to verify the fly lines that were generated to knock-out *CG4623* and *mtm* by IMAGO approach. For this purpose, we examined the genotype of the flies by performing test crosses in addition to the different molecular genetic approaches.

3. MATERIALS

3.1. Biological Materials

3.1.1. The Model Organism: *Drosophila melanogaster*

The *Drosophila melanogaster* fly lines used in this study are listed below in Table 3.1. All of these flies were kept in incubators set to 25°C and 80% humidity with 12 hour light / 12 hour dark cycle unless stated otherwise. Nutri-Fly Bloomington Formulation fly food with addition of 5.5 ml Propionic acid per liter was used in raising the flies. All fly lines were bought from Bloomington Drosophila Stock Center at Indiana University, USA except *IMAGO CG4623 L1* and *L2*, *IMAGO mtm L1* and *L2* were generated by our lab (Kılınç, 2013; Yıldırım, 2013); *UAS-Dicer;;nSyb-Gal4* and $mtm^{\Delta 77}$*/CyO*, $mtm^{\Delta 210}$*/CyO and UAS:eGFP-hMTMR2/CyO* were kindly donated by Verstreken Lab (VIB, Belgium) and Kiger Lab (USCD, USA) respectively.

Table 3.1. *Drosophila melanogaster* lines used in this study.

Genotype	Chromosome	Description
Canton-S	-	Wild type, red eye
IMAGO CG4623 L1	I	Expected to contain IMAGO targeting vector for *CG4623*, Line 1
IMAGO CG4623 L2	I	Expected to contain IMAGO targeting vector for *CG4623*, Line 2
IMAGO MTM L1	I	Expected to contain IMAGO targeting vector for *mtm*, Line 1
IMAGO MTM L2	I	Expected to contain IMAGO targeting vector for *mtm*, Line 2
UAS-Dicer	I	Expresses Dicer-2 under UAS control
w^{1118}	I	White eye
y,v	I	Yellow body color and vermillion eye
y,w	I	Yellow body color and white eye
actin5C-Gal4	II	Ubiquitous driver

Table 3.1. *Drosophila melanogaster* lines used in this study (cont.).

CyO	II	Balancer chromosome with curly wings
CyO, GFP	II	Balancer chromosome with curly wings and GFP expression
CyO, Roi	II	Balancer chromosome with curly wings and rough eye
KK Control	II	Control line of *UAS-CG4623 RNAi* that does not contain KK RNAi sequence
$mtm^{\Delta 77}$	II	Null mutant allele of *mtm*
$mtm^{\Delta 210}$	II	Null mutant allele of *mtm*
Sco	II	Missing bristles scutellum
sp	II	Supernumerary bristles marker
UAS-CG4623 RNAi (KK)	II	Expresses double stranded RNAi of *CG4623* under UAS control
UAS:eGFP-hMTMR2	II	Overexpresses human MTMR2
Ubi>stop>Stinger	II	Contains FRT sites, expresses GFP ubiquitously if cut with flippase
hs:Flp, hs:I-Sce1	II or III	Expresses flippase and I-SceI upon heat shock
hs:hid	II or III	Heat shock lethal
eyFLP	III	Expresses flippase under control of *eyeless* promoter
MKRS	III	Short bristles marker
n-Syb-Gal4	III	Neural driver
TM2	III	Balancer chromosome with large halteres
TM3, Sb	III	Balancer chromosome with shorter bristles
TM6B, Tb	III	Balancer chromosome with tubby marker
TRIP Control	III	Control line of *UAS-mtmTRIP* that does not contain TRIP RNAi sequence
UAS-CG4623 OE1	III	Overexpresses *CG4623*, Line 1

Table 3.1. *Drosophila melanogaster* lines used in this study (cont.).

UAS-CG4623 OE2	III	Overexpresses *CG4623*, Line 2
UAS-CG4623 OE3	III	Overexpresses *CG4623*, Line 3
UAS-mtm OE1	III	Overexpresses *mtm,* Line 1
UAS-mtm OE2	III	Overexpresses *mtm*, Line 2
UAS-mtm OE3	III	Overexpresses *mtm*, Line 3
UAS-mtm RNAi (TRIP)	III	Expresses double stranded RNAi of *mtm* under UAS control

3.1.2. *Escherichia coli*

Rosetta strain of *E.coli* that was transformed with pET30a vector containing *mtm* cDNA (LD28822) was used in this study for antibody generation purposes. Transformation of bacteria has been was performed previously in our laboratory by Kaya Akyüz (Akyüz, 2013).

3.1.3. Rabbits

Rabbits were provided by the animal facility in Bogazici University Center for Life Sciences and Technologies. Two New Zealand rabbits were used in this study for antibody generation purposes. They were bred on a 12-hour light / 12-hour dark cycle at 21 – 25°C. Food and water were provided *ad lib*. All use and handling of animals were in accordance with Bogazici University Ethics Committee guidelines.

3.2. Chemicals and Enzymes

In this study the following list of chemicals and enzymes were used (Table 3.2).

Table 3.2. List of chemicals and enzymes.

Chemical	Supplier and product code
β-mercaptoethanol	Merck Millipore, Germany (805740)
1 kb DNA Ladder	Thermo Scientific, USA (SM0311)
Acetic acid	Merck Millipore, Germany (100056)

Table 3.2. List of chemicals and enzymes (cont.).

Acetone	Sigma-Aldrich, USA (650501)
Acrylamide	Sigma-Aldrich, USA (A3553)
Agarose	Prona Agarose, Biomax, EU (124543PR)
APS	Fluka, Germany (09914)
Benzonase Nuclease	Merck Millipore, Germany (70664)
Bis-Acrylamide	Sigma-Aldrich, USA (M7279)
Bromophenol blue	Merck Millipore, Germany (111746)
BSA	Sigma-Aldrich, USA (A2153)
Chloramphenicol	Applichem, Germany (7495)
$C_{24}H_{39}NaO_4$	Sigma-Aldrich, USA (30970)
Citric acid	Sigma-Aldrich, USA (251275)
Complete, EDTA-free (protease inhibitor coctail)	Roche, Germany (11873580001)
Coomassie Brilliant Blue R250	Merck Millipore, Germany (112553)
DMSO	Merck Millipore, Germany (102952)
EDTA	Sigma-Aldrich, USA (34549)
Ethanol	Panreac, Spain (131086.1214)
Ethidium bromide solution	Sigma-Aldrich, USA (E1510)
Formaldehyde	Sigma-Aldrich, USA (47608)
Freund's complete adjuvant	Sigma-Aldrich, USA (F5881)
Freund's incomplete adjuvant	Sigma-Aldrich, USA (F5506)
Glucose (D)	Sigma-Aldrich, USA (G8270)
Glycerol	Sigma-Aldrich, USA (G5516)
Glycine	Sigma-Aldrich, USA (G8898)
HCl	BDH, England (2850744)
HEPES	Sigma-Aldrich, USA (H4034)
ImmunoCruz Western Blotting Luminol Reagent	Santa Cruz Biotechnology, UAS (sc-2048)
IPTG	Promega, USA (V395A)
Isopropanol	Sigma-Aldrich, USA (24137)
Kanamycin	Life Technologies, USA (11815-024)

Table 3.2. List of chemicals and enzymes (cont.).

KCl	Sigma-Aldrich, USA (P9541)
KH_2PO_4	Merck Millipore, Germany (529568)
KOAc	Merck Millipore, Germany (104820)
LB broth	Difco, France, (244620)
LiCl	Sigma-Aldrich, USA (L9650)
Methanol	Sigma-Aldrich, USA (24229)
$MgCl_2$	Carlo Erba Reagenti, Italy (349357)
$MgCl_26H_2O$	Carlo Erba Reagenti, Italy (7791186)
NaCl	Merck Millipore, Germany (106404)
$NaHCO_3$	Sigma-Aldrich, USA (S7277)
NaH_2PO_4	Merck Millipore, Germany (567549)
NaOAc	Merck Millipore, Germany (1.06265)
NaOH	Riedel-de Haen, Germany (06203)
NP-40	Fluka, Germany (74385)
PageRuler Prestained Protein Ladder	Thermo Scientific, USA (26616)
Phenylmethanesulfonyl fluoride (PMSF)	Sigma Aldrich, USA (P7626)
Phenol-chloroform-isoamyl alcohol	Sigma-Aldrich, USA (77617)
Phosphate buffered saline (10X)	Life Technologies, USA (70011-044)
Propionic Acid	Merck Millipore, Germany (800605)
RiboRuler High Range RNA Ladder	Thermo Scientific, USA (SM1821)
SDS	Merck Millipore, Germany (822050)
Sodium azide	Sigma-Aldrich, USA (438456)
Sodium citrate	Merck Millipore, Germany (106448)
Sucrose	Sigma-Aldrich, USA (S0389)
SYBR Premix Ex Taq (2x) (Tli RNaseH Plus	Takara, Japan (RR420A)
Taq DNA polymerase (recombinant)	Thermo Scientific, USA (EP0405)
TCA	Merck Millipore, Germany (100807)
TEMED	Sigma-Aldrich, USA (T7024)

Table 3.2. List of chemicals and enzymes (cont.).

Trehalose	Sigma-Aldrich, USA (T9531)
Tris	Sigma-Aldrich, USA, (T1503)
Triton X-100	Sigma-Aldrich, USA (T8787)
Tween 20	Riedel-de Haen, Germany (63158)
Urea	Sigma Aldrich, USA (U5378)

3.3. Buffers and Solutions

The buffers, solutions, and their contents are listed in Table 3.3, 3.4 and 3.5.

Table 3.3. List of buffers and solutions used in this study.

Buffer or solution	**Content**
1% agarose gel	1X TAE Buffer 1% Agarose 0.5% Ethidium Bromide
1X TAE buffer	40 mM Tris-Cl 1 mM EDTA 0.1% Acetic acid
Buffer A	100 mM Tris-Cl (pH 7.5) 100 mM EDTA 100 mM NaCl 0.5% SDS
Ethidium bromide solution	10 mg/ml in dH_2O

Table 3.4. List of buffers and solutions used in antibody generation.

Buffer or Solution	**Content**
Lysis Buffer (pH 8.0)	0.1 M NaH_2PO_4 7 M Urea 0.01 M Tris-Cl (pH 8.8) 0.1 mM PMSF 3 unit/ml Benzonase Nuclease

Table 3.4. List of buffers and solutions used in antibody generation (cont.).

Wash Buffer (pH 6.3)	0.1 M NaH_2PO_4 8 M Urea 0.01 M Tris-Cl (pH 8.8) 0.1 mM PMSF
Elution Buffer (pH 4.5)	0.1 M NaH_2PO_4 8 M Urea 0.01 M Tris-Cl (pH 8.8) 0.1 mM PMSF
Strip Buffer for Nickel Column Cleaning	50 mM KH_2PO_4 0.3 M NaCl 0.1 M EDTA
Gel Extraction Elution Buffer (pH 7.5)	50m M Tris-Cl 150 mM NaCl 0,1 mM EDTA
Sodium Citrate-Glucose Solution	2.3% Sodium citrate 0.8% Citric acid 2.2% Glucose (D) in 100 ml dH_2O
BBT Buffer	1X PBS 0.1% BSA 0.1% Tween 20
Fixation Solution	3.7% Formaldehyde Solution in HL3
HL-3 Solution	110 mM NaCl 5 mM KCl 10 mM $NaHCO_3$ 5 mM HEPES 30 mM Sucrose 5 mM Trehalose 10 mM $MgCl_2$ (pH 7.2)
PBS (1X)	100 ml PBS (10X) 900 ml dH_2O

Table 3.5. List of buffers and solutions used in SDS-PAGE analysis and Western Blotting.

Buffer or solution	Content
Non-ionic Fly Lysis Buffer	20 mM Tris-Cl (pH 6.8) 50 mM NaCl 1% NP-40 2 mM EDTA 1X Complete, EDTA-free (protease inhibitor cocktail)
Protein Sample Buffer (6X)	300 mM Tris-Cl (pH 6.8) 12 mM EDTA 60 % Glycerol 12 % SDS 6 % β-mercaptoethanol 0.04 % Bromophenol blue
Coomassie Blue Solution	50 % Methanol 10 % Acetic Acid 0.05 % Coomassie R250
Destaining Solution	30% Isopropanol 10% Acetic Acid
Running Buffer	25 mM Tris 250 mM Glycine 0.2 % SDS
Transfer Buffer	25 mM Tris 200 mM Glycine 20 % Methanol
Tris-Buffered Saline (TBS)	20 mM Tris-Cl (pH 8.0) 150 mM NaCl
TBS with Tween-20 (TBS-T)	0.1 % Tween-20 in TBS
Blocking solution	5% BSA in 1X TBS-T
Stripping Solution	62,5 mM Tris-Cl (pH 6.8) 2% SDS 0.7% beta-mercaptoethanol

All of the other buffers and solutions are purchased ready-made (such as 10X PBS) or prepared according to the manufacturers' instructions (such as LB broth).

3.4. Kits

The following kits are used in this study: RNeasy Mini Kit (Qiagen, Netherlands, 74106) for RNA isolation; RevertAid First Strand cDNA Synthesis Kit (Thermo Scientific, USA, K1622) for cDNA synthesis; Pierce BCA Protein Assay Kit (Thermo Scientific, USA, 23227) to measure protein concentrations.

3.5. Oligonucleotide Primers

Lyophilized primers synthesized at Macrogen company (South Korea), were suspended in dH_2O to reach a final concentration of 100 mM and stored at -20°C. Primers used in qRT-PCRs for expression analysis and PCRs for checking IMAGO targeting vector integration to the fly genome can be found in Table 3.6 in detail.

Table 3.6. The names, sequences, and the Tm of primers used in qRT-PCRs and PCRs.

Primer Name	**Primer Sequence (5'→3')**	**T_m (°C)**
actin79b_RT_FP	ATGTATCCAGGTATCGCTGAC	59.5
actin79b_RT_RP	TGCTTGGAGATCCACATCTG	58.4
CG4623_RT1_FP	GCCAATAAGCCAGTGCTCTTC	61.2
CG4623_RT1_RP	GCCCTTGGGATTGAGGTTTAG	61.2
mtm_RT_FP	TTGAGTTCAACGAGCACTTC	56.4
mtm_RT_RP	AATACTGGTCCAGCGACG	56.3
IMAGO_CG4623_SCR_F	TGTCCCACACCTTCTCATCGCACTC	64
IMAGO_CG4623_SCR_R	AGCGAGCACAGCTACCAGAATAATC	60
CG4623_IMG_SCRF_CK	TCAGACCGTGGACATTCAAG	58.4
mtm_IMG_SCRF_CK	GCTCCAGGTCGGCTATTCTC	62.5
WplusIMG_SCRR_CK	CACTATTTGTTTGTGCGATTGCG	60.9
CG4623_5HS3	CAACAAGGTGCTCGACGAGA	60.5

Table 3.6. The names, sequences, and the Tm of primers used in qRT-PCRs and PCRs (cont.).

CG4623_5HRS2	AGCAAAATACCCATGGGTCG	58.4
CG9115_5H_S2	CGCTGAATAAATGTCCGCTC	58.4
CG9115_5H_S4	AGCTGAAGCTGACGCACTC	59.5
CG9115_5H_S5	GGCTAGAGCGTTATCGTTG	57.5
CG9115_5H_T1	GCGCAGGATCAGTGTATG	56.3

3.6. Antibodies

The following antibodies were used in Western Blotting experiments in this study (Table 3.7 and 3.8).

Table 3.7. List of primary antibodies used in Western Blot.

Antigen	Host	Dilution	Producer
actin	Goat	1000	Santa Cruz Biotechnology, USA (sc1616)
His-probe	Mouse	1000	Santa Cruz Biotechnology, USA (sc8036)
mtm	Rabbit	2500	Our Laboratory (CMT LAB)
mtm (pre-adsorbed)	Rabbit	1000	Our Laboratory (CMT LAB)

Table 3.8. List of secondary antibodies used in Western Blot.

Target	Host	Tag	Dilution	Producer
Goat	Donkey	Horse radish peroxidase	5000	Santa Cruz Biotechnology, USA (sc2620)
Rabbit	Goat	Horse radish peroxidase	3000	Santa Cruz Biotechnology, USA (sc2030)
Mouse	Donkey	Horse radish peroxidase	2000	Santa Cruz Biotechnology, USA (sc2314)

3.7. Disposable Materials

Disposable materials used in this study are listed in Table 3.9. Glassware and plastic consumables were sterilized by autoclaving at 121°C for 15 minutes unless they were provided as sterile.

Table 3.9. The list of disposable materials.

Material	Producer
96-well Piko PCR plate	Thermo Scientific, USA (SPL0961)
Adhesive Seal for Piko PCR plates	Thermo Scientific, USA (ASF-0020)
Centrifuge tubes, 15 ml	Becton, Dickinson and Company, USA
Centrifuge tubes, 50 ml	Becton, Dickinson and Company, USA
Culture tubes, 14 ml	Greiner Bio-One, Belgium
Filtered tips	Fisher Scientific, UK
Flugs	Flystuff, Genesee Scientific, USA (49-101)
Fly tubes	Gür Plastik, Turkey
Microcentrifuge tubes, 0.5 ml	Fisher Scientific, UK
Microcentrifuge tubes, 1.5 ml	Fisher Scientific, UK
Microcentrifuge tubes, 2 ml	Fisher Scientific, UK
Pasteur pipettes	Isolab, Germany
PCR tubes (200 µl)	Fisher Scientific, UK
PCR strips (8 well)	Fisher Scientific, UK
Pestle and mortar	Boeco, Germany
Petri dishes (60 mm)	Isolab, Germany
Pipette tips	Fisher Scientific, UK
PVDF Western Blotting Membrane	Roche, Germany (33010040001)
Scalpel	Bayha, Germany
Serological pipette, 50 ml	Greiner Bio-One, Belgium
Syringe, 50 ml	Set, Turkey
Syringe Filter, 0.22 um	Sartorius Stedim Biotech, Germany
Syringe Filter, 0.45 um	Sartorius Stedim Biotech, Germany
Test tubes, 20 ml	Greiner Bio-One, Belgium (169101)

3.8. Laboratory Equipment

Laboratory equipment used in this study is listed in Table 3.10.

Table 3.10. The list of laboratory equipment.

Equipment	Producer
Autoclave	Astell Scientific Ltd., UK
Blotting apparatus	Mini Trans-Blot Cell, Bio-Rad, USA
Centrifuges	Allegra X-22R, Beckman Coulter, USA Centrifuge 5415, Eppendorf, Germany J2-21 Centrifuge, Beckman, USA
Chemiluminescence Detection System	Stella, Raytest, Germany
Cold room	Birikim Elektrik Soğutma, Turkey
Dissection forceps	FST, USA
Documentation System	Gel Doc XR, Bio-Rad, USA
Electronic Balance	UW6200H, Shimadzu, Japan
Electrophoresis	Mini Sub Cell, Bio-Rad, USA Hybaid tank, Thermo Scientific USA
Electrophoresis (vertical)	Mini PROTEAN Tetra Cell, Bio Rad, USA PROTEAN II xi Cell, Bio-Rad, USA
The Flowbuddy	Flystuff, Genesee Scientific, USA
Fly CO_2 Pads	Flystuff, Genesee Scientific, USA
Fly homogenizer	Kontes Pellet Pestile Motor, Fisher Scientific, UK
Fly homogenizer heads	Fisher Scientific, UK
Fly incubators	TK 120, Nüve, Turkey TK 600, Nüve, Turkey
Fluorescence stereomicroscope	MZ16FA, Leica, Germany
Freezers	-20 ºC, Arçelik, Turkey -80 ºC, Thermo Forma, USA
Heat Block	DRI-Block DB-2A, Techne, UK
Hybridization Oven	Hybaid Shaken Stack, Thermo Scientific

Table 3.10. The list of laboratory equipment (cont.).

Laboratory bottles	Isolab, Germany
Magnetic stirrer	Speed Safe, Hanna Instruments, USA MK 418, Nüve, Turkey
Micropipettes	Gilson, USA
Microwave oven	Arçelik, Turkey
Nickel Column	Qiagen, Netherlands
Peristaltic pump	2115 Multiperpex, LKB Bromma, Sweden
pH meter	HI 208 Hanna Instruments, Romania
PikoReal 96 Real-Time PCR System	Thermo Scientific, USA
Power supply	Power Pac, Bio-Rad, USA
Refrigerators	+4º C Arçelik, Turkey
Shaker	SL 350, Nüve, Turkey Orbital Shaker, Thermo Scientific, USA
Sonicator	Sonoplus, Bandelin, Germany
Spectrophotometer	ND-1000, NanoDrop, USA DU 730, Beckman Coulter, USA
Stereomicroscope	SZ61, Olympus, Japan
Test tube rack	Verstreken Laboratory, VIB, Belgium
Thermal cycler	C1000 Thermal Cycler, Bio-Rad, USA
Vortex mixer	Nuvemix, Nüve, Turkey
Water bath	BM 302, Nüve, Turkey

4. METHODS

4.1. Downregulation of *CG4623* in *Drosophila*

Homozygous *CG4623* RNAi line (*UAS-CG4623 RNAi*) and its control line (*KK control*) were obtained from the Vienna Drosophila Stock Center (VDRC). They were crossed with ubiquitous or neuronal drivers.

4.1.1. Crossing Scheme for Ubiquitous Downregulation of *CG4623* by RNAi

Actin5C-Gal4 is used to drive the ubiquitous downregulation of *CG4623*. To generate flies in which *CG4623* is downregulated in the whole organism, *CyO, Roi* balanced *actin5C-Gal4* line was crossed with homozygous *CG4623* RNAi line (Figure 4.1) and progeny carrying both alleles was selected. Crosses were kept at 25°C and 80% humidity. F1 progeny that does not show *CyO, Roi* phenotypes (curly wing and rough eye) were selected.

$$\male ; \mathrm{UAS-CG4623\ RNAi;} \quad \mathrm{X} \quad ; \frac{\mathrm{actin5C-Gal4}}{\mathrm{CyO,Roi}} ; \ \female$$

$$; \frac{\mathrm{actin5C-Gal4}}{\mathrm{UAS-\ CG4623\ RNAi}} ;$$

Figure 4.1. Crossing scheme of ubiquitous *CG4623* downregulation. F1 progeny was selected against *CyO, Roi*.

Adult flies with ubiquitously downregulated *CG4623* were used in quantitative Reverse Transcription-PCR, Negative Geotaxis Assay and Longevity Assay. *CyO, Roi* balanced *actin5C-Gal4* line was crossed with *KK control* or w^{1118}, and F1 progeny carrying *actin5C-Gal4* allele was used as the control in all experiments stated above.

4.1.2. Crossing Scheme for Neuron-Specific Downregulation of *CG4623* by RNAi

UAS-Dicer;;nSyb-Gal4 is used to drive the downregulation of *CG4623* specifically in neurons. Homozygous *UAS-Dicer;;nSyb-Gal4* line (donated by Verstreken Laboratory, Belgium) was crossed with homozygous *CG4623* RNAi line (Figure 4.2). Crosses were kept at 29°C and 70% humidity to enhance Dicer enzyme activity.

$$\male ; \mathrm{UAS-CG4623\ RNAi;} \quad \mathrm{X} \quad \mathrm{UAS-Dicer;;\ nSyb-Gal4}\ \female$$

$$\downarrow$$

$$\frac{\mathrm{UAS-Dicer}}{+};\ \frac{\mathrm{UAS-CG4623\ RNAi}}{+};\ \frac{\mathrm{nSyb-Gal4}}{+};$$

Figure 4.2. Crossing scheme of neuronal *CG4623* downregulation. All F1 progeny was collected.

Adult flies in which *CG4623* is downregulated specifically in neurons were used in Negative Geotaxis Assay. *UAS-Dicer;;nSyb-Gal4* was crossed with *KK control*, and F1 progeny was used as the control in Negative Geotaxis Assay.

4.2. Overexpression of *CG4623* in *Drosophila*

Overexpression lines of *CG4623, UAS-CG4623 OE1, OE2, OE3,* were generated and balanced with *TM3, Sb* balancer (short bristles) previously in our laboratory by Kaya Akyüz (Akyüz, 2013). Since their background was white-eyed wild type, w^{1118} was used as a control.

4.2.1. Crossing Scheme for Ubiquitous Overexpression of *CG4623*

Actin5C-Gal4 is used to drive the ubiquitous overexpression of *CG4623*. To generate flies in which CG4623 is overexpressed in the whole organism, *CyO,Roi* balanced *actin5C-Gal4* line was crossed with *TM3, Sb* balanced *CG4623* OE lines (Figure 4.3). Crosses were kept at 25°C and 80% humidity. F1 flies without *TM3, Sb* and *CyO, Roi* (short bristles, curly wing and rough eye) phenotypes were selected for further studies.

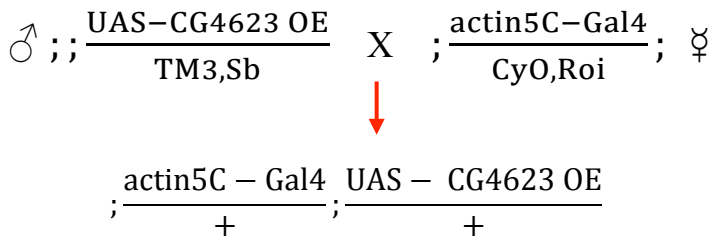

Figure 4.3. Crossing scheme of ubiquitous *CG4623* overexpression. F1 progeny was selected against *CyO, Roi* and *TM3, Sb*.

Adult flies with ubiquitously overexpressed *CG4623* were used in qRT-PCR, Negative Geotaxis Assay and Longevity Assay. *CyO, Roi* balanced *actin5C-Gal4* line was crossed with w^{1118}, and F1 progeny carrying *actin5C-Gal4* allele was used as the control in all experiments stated above.

4.2.2. Crossing Scheme for Neuron-Specific Overexpression of *CG4623*

UAS-Dicer;;nSyb-Gal4 is used to drive the overexpression of *CG4623* specifically in neurons. Homozygous *UAS-Dicer;;nSyb-Gal4* line was crossed with *TM3, Sb* balanced *CG4623* OE lines (Figure 4.4). Crosses were kept at 25°C and 80% humidity.

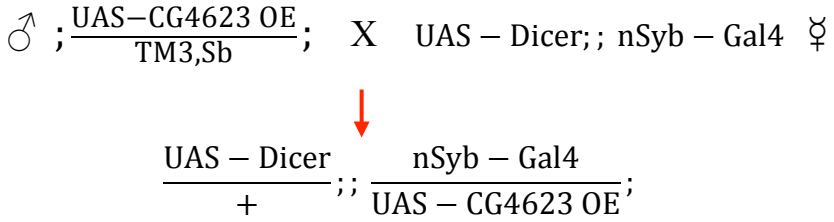

Figure 4.4. Crossing scheme of neuronal *CG4623* overexpression. F1 progeny was selected against *TM3, Sb*.

Adult flies with *CG4623* is overexpressed specifically in neurons were used in Negative Geotaxis Assay. *UAS-Dicer;;nSyb-Gal4* was crossed with w^{1118}, and F1 progeny was used as the control in Negative Geotaxis Assay.

4.3. *CG4623* IMAGO Targeting Vector Integration Verification in *Drosophila*

A targeting vector for IMAGO has been generated previously in our laboratory to knock-out the *CG4623* gene. The vector has been transferred to fly embryos by microinjection by Genetic Services, Inc., USA (Yıldırım, 2013). Integration of the targeting vector to the fly genome was tested in this study by crossing, homozygous *CG4623* IMAGO lines with an *eyFLP* line in which *eyFLP* was recombined with *TM3, Sb* (short bristles) balancer (Figure 4.5). These flies carry a flippase enzyme that is active in the eye and can flip out the *w+* (red eye) gene inside the vector by cutting from the two flanking FRT sites. The IMAGO targeting vector prepared in our lab was designed to contain the red eye gene as a marker; thus, we expected to get white-eyed flies in the correct integration of the vector in the engineered flies.

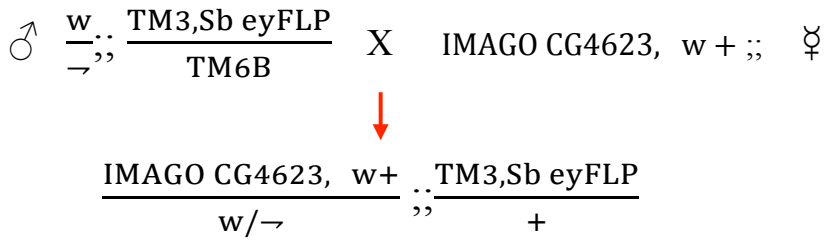

Figure 4.5. Crossing scheme for IMAGO verification. F1 progeny is selected for *TM3, Sb.*

4.4. Downregulation of *mtm* in *Drosophila*

Homozygous *mtm* RNAi line (*UAS-mtm RNAi*) and its control line (*TRIP control*) were obtained from Vienna Drosophila Stock Center (VDRC). They were crossed with a ubiquitous driver.

4.4.1. Crossing Scheme for Ubiquitous Downregulation of *mtm* by RNAi

Actin5C-Gal4 is used downregulate *mtm* ubiquitously. To generate flies in which *mtm* is downregulated in the whole organism, *CyO, Roi* balanced *actin5C-Gal4* line was crossed with homozygous *mtm* RNAi line (Figure 4.6). Crosses were kept at 25°C and 80% humidity. F1 progeny that does not show *CyO, Roi* phenotypes (curly wing and rough eye) were selected.

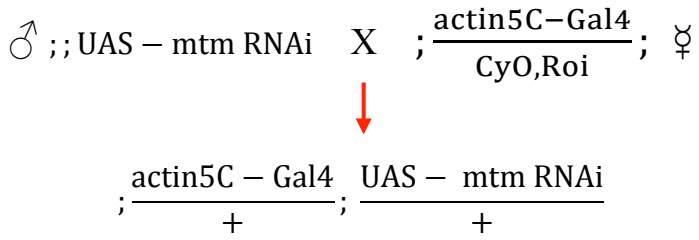

Figure 4.6. Crossing scheme of ubiquitous *mtm* downregulation. F1 progeny was selected against *CyO, Roi*.

Adult flies with ubiquitously downregulated *mtm* were used in Longevity Assay. *CyO, Roi* balanced *actin5C-Gal4* line was crossed with *TRIP control*, and F1 progeny carrying *actin5C-Gal4* allele was used as the control in Longevity Assay.

4.4.2. Crossing Scheme to Generate *mtm* Null Mutants

Velichkova and co-workers generated *mtm*-deficient flies using *P*-element excision (Velichkova *et al*., 2010). They generated null excision alleles ($mtm^{\Delta 77}$ and $mtm^{\Delta 210}$) that were kindly donated to our laboratory, and was balanced with CyO GFP (curly wings and GFP expression) by Merve Kılınç previously in our lab (Kılınç, 2013). The compound heterozygous mutant larvae were selected according to the crossing scheme in Figure 4.7 and were used in pre-adsorption of polyclonal anti-mtm antibody.

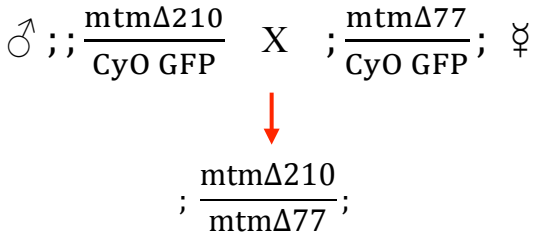

Figure 4.7. Compound heterozygous null mutant larvae of *mtm* were generated by crossing two *P*-element excision mutants. Larvae were selected against GFP under fluorescence stereomicroscope.

4.5. Overexpression of *mtm* in *Drosophila*

Overexpression lines of *mtm, UAS-mtm OE1, OE2, OE3*, were generated and balanced with *TM3, Sb* balancer previously in our laboratory by Kaya Akyüz (Akyüz, 2013). Since their background was white-eyed wild type, w^{1118} was used as control.

4.5.1. Crossing Scheme for Ubiquitous Overexpression of *mtm*

Actin5C-Gal4 is used to drive the ubiquitous overexpression of *mtm*. To generate flies in which *mtm* is overexpressed in the whole organism, *CyO,Roi* balanced *actin5C-Gal4* line was crossed with *TM3, Sb* balanced *mtm* OE lines (Figure 4.8). Crosses were kept at 25°C and 80% humidity. F1 flies without *TM3, Sb* and *CyO, Roi* (short bristles, curly wing and rough eye) phenotypes were selected for further studies.

$$\text{♂};;\frac{\text{UAS−mtm OE}}{\text{TM3,Sb}} \quad \text{X} \quad ;\frac{\text{actin5C−Gal4}}{\text{CyO,Roi}};\ \text{♀}$$

$$\downarrow$$

$$;\frac{\text{actin5C} - \text{Gal4}}{+};\frac{\text{UAS} - \text{ mtm OE}}{+}$$

Figure 4.8. Crossing scheme of ubiquitous *mtm* overexpression. F1 progeny was selected against *CyO, Roi* and *TM3, Sb.*

Adult flies with ubiquitously overexpressed *mtm* were used in qRT-PCR and Longevity Assay. *CyO, Roi* balanced *actin5C-Gal4* line was crossed with w^{1118}, and F1 progeny carrying *actin5C-Gal4* allele was used as the control in experiments stated above.

4.5.2. Crossing Scheme for Overexpression of *hMTMR2*

Fly lines with *UAS-hMTMR2* were generated by Velichkova and co-workers to overexpress human homolog of *mtm, MTMR2* gene in flies; and were kindly donated to our laboratory (Velichkova et al., 2010). *Actin5C-Gal4* is used to drive the ubiquitous overexpression of *hMTMR2*. *CyO, Roi* balanced *actin5C-Gal4* line was crossed with *CyO* balanced *UAS-hMTMR2* (Figure 4.9). Crosses were kept at 25°C and 80% humidity.

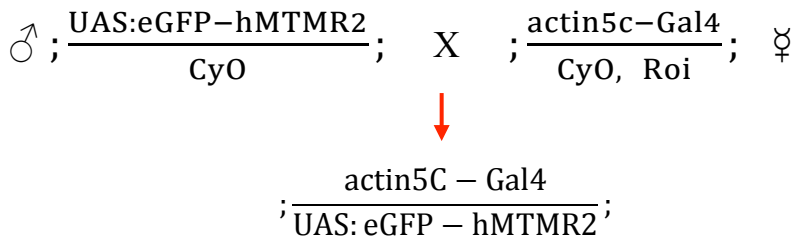

Figure 4.9. Crossing scheme of ubiquitous *hMTMR2* overexpression. All F1 progeny was collected since *CyO/CyO, Roi* is lethal.

Adult flies with ubiquitously overexpressed *hMTMR2* were used in Longevity Assay. *CyO, Roi* balanced *actin5C-Gal4* line was crossed with w^{1118}, and F1 progeny carrying *actin5C-Gal4* allele was used as the control in Longevity Assay.

4.5.3. Crossing Scheme for Rescue with *hMTMR2*

In order to see whether *hMTMR2* overexpression can rescue the *mtm* downregulation phenotype, fly line was generated by combining *UAS:eGFP-hMTMR2* and *UAS-mtm RNAi* alleles. First, fly line carrying *UAS:eGFP-hMTMR2* allele and fly line carrying *UAS-mtm RNAi* were balanced with a quadruple balancer (*w*; *sp/CyO*; *MKRS/TM2*, *w*:white eye, sp:supernumerary bristles, *CyO*: curly wings, *MKRS*: short bristles, *TM2*: large halteres) two times, separately (Figure 4.10 and 4.11). Finally, *UAS:eGFP-hMTMR2* and *UAS-mtm RNAi* alleles were combined by crossing two balanced lines (Figure 4.12).

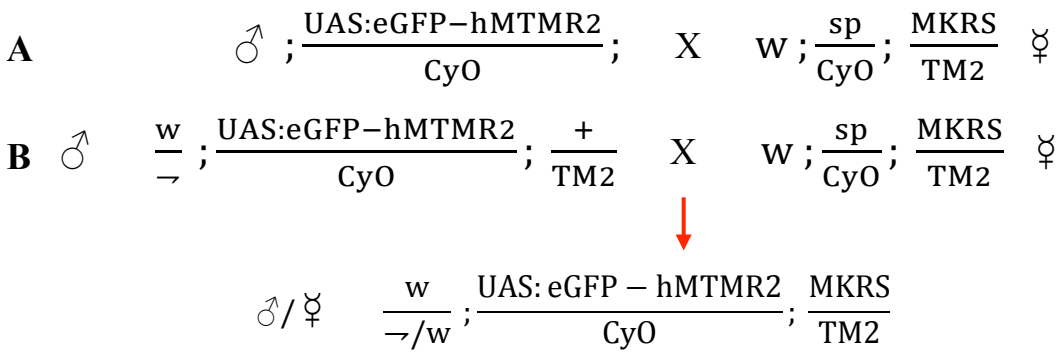

Figure 4.10. Balancing *UAS:eGFP-hMTMR2* line. (A) Adult males were selected for red eye, *CyO* and *TM2;* against *sp* and *MKRS*. (B) Adults were selected for red eye, *CyO*, *TM2* and *MKRS;* against *sp*. *UAS:eGFP-hMTMR2* has w^{+}(red eye) as a marker.

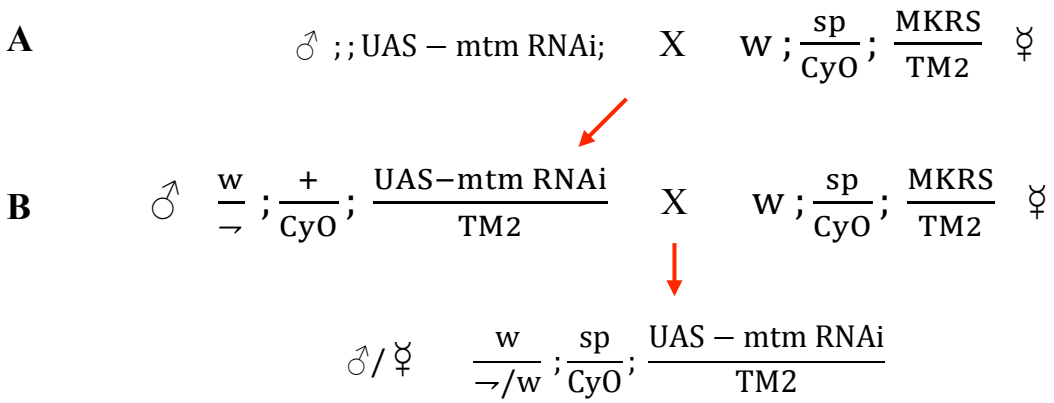

Figure 4.11. Balancing *UAS-mtm RNAi* line. (A) Adult males were selected for red eye, *CyO* and *TM2;* against *sp* and *MKRS*. (B) Adults were selected for red eye, *CyO*, *TM2* and *sp;* against *MKRS*. *CyO/CyO* and *TM2/TM2* are lethal; *UAS-mtm RNAi* has w^+(red eye) asa marker.

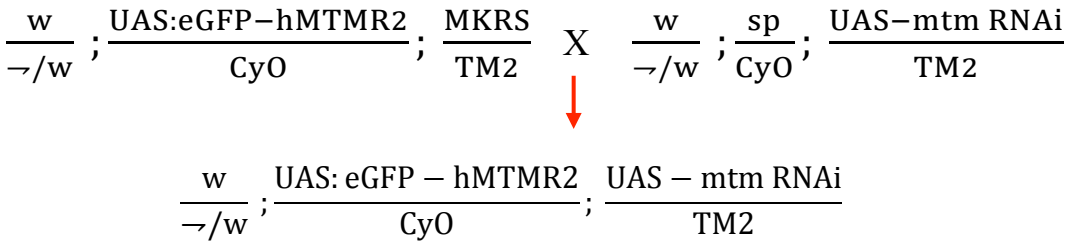

Figure 4.12. Combination of *UAS:eGFP-hMTMR2* and *UAS-mtm RNAi* alleles. Adults were selected for red eye, *CyO* and *TM2*; against *sp* and *MKRS*. *CyO/CyO* and *TM2/TM2* are lethal; *UAS-mtm RNAi* has *w+*(red eye) as a marker.

4.6. *mtm* IMAGO Targeting Vector Verification in *Drosophila*

A targeting vector for IMAGO has been generated previously in our laboratory to knock-out the *mtm* gene. The vector has been transferred to fly embryos by microinjection by Genetic Services, Inc., USA (Kılınç, 2013). Integration of the targeting vector to the fly genome was tested in this study by crossing homozygous *mtm* IMAGO lines with an *eyFLP* line in which *eyFLP* was recombined with *TM3,Sb* (short bristles) balancer (Figure 4.13). These flies carry a flippase enzyme that is active in the eye and can flip out the w^+ (red eye) gene inside the vector by cutting from the two flanking FRT sites. The IMAGO targeting vector prepared in our lab was designed to contain the red eye gene as the

marker; thus, we expected to get white-eyed flies in the correct integration of the vector in the engineered flies.

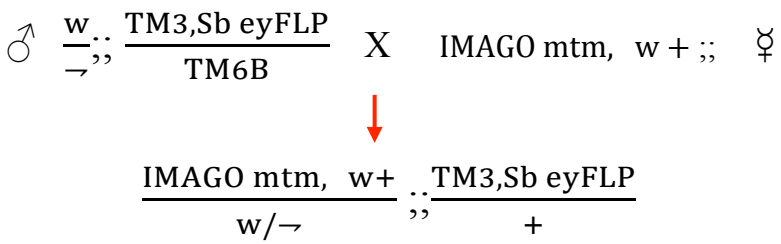

Figure 4.13. Crossing scheme for IMAGO verification. F1 progeny was selected for *TM3, Sb.*

4.7. Behavioral Assays

4.7.1. Negative Geotaxis Assay

A modified version of Rapid-Iterative Negative Geotaxis (RING) protocol was used to assess the climbing ability of adult flies with different genotypes (Gargano, *et al.*, 2005; Nichols *et al.*, 2012). Clean test tubes containing around ten flies of same genotype, sex and age were placed on a test tube rack to minimize the variation. The rack was tapped down three to four times so that all the flies were at the bottom of the tube. In order to observe the climbing behavior that is caused by negative geotaxis only, thus eliminate the phototactic behavior, indirect horizontal illumination from the back of the tubes was used. The climbing behavior of the flies was recorded by using a video camera (Nikon D90, Japan) that was one meter away from the tubes (Figure 4.14). The distance climbed by each fly was measured from images taken 5 seconds after the tapping by using ImageJ software. The average climbing distance of all flies in a tube was calculated. The experiment was repeated four or five times for the same group of flies and the average of four or five trials was calculated. Biological quadruplets were used for each genotype and its control. A two-tail paired Student's t-test was performed between experiment and control groups for statistical analysis.

Figure 4.14. Negative geotaxis setup.

4.7.2. Longevity Assay

Around two hundred flies of the same genotype and sex were collected in 24 hours after eclosion from pupae, and grouped in around twenty flies per vial. Flies were grown at 25°C and were followed over 90 days by transferring them to a fresh food-containing vial and counting the number of dead flies every 3 days. The longevity curves were drawn and statistically analyzed using an online tool called OASIS (Yang *et al.*, 2011).

4.8. Molecular Biology Techniques

4.8.1. Isolation of Total RNA From Flies

RNeasy Mini Kit was used to extract total RNA from flies. Fourteen young adult flies (around 10 days old, equal number of males and females) of same genotype were selected and frozen at -80°C for 10 minutes. Frozen flies were homogenized in 350 µl of lysis buffer (Buffer RLT) with 3.5 µl β-mercaptoethanol, and the protocol supplied with the kit was followed. Total RNA was eluted in 30 µl RNase-free water, and stored at -80°C. Concentrations of total RNA were measured using ND-1000, NanoDrop spectrophotometer.

4.8.2. Reverse Transcription and cDNA Synthesis

RevertAid First Strand cDNA Synthesis Kit was used to synthesize cDNA from total RNA isolated. According to the protocol supplied, 1-4 µg of total RNA was used for reverse transcription. After the synthesis, cDNAs were diluted to a final concentration of 10 ng/µl and stored at -80°C.

4.8.3. Quantitative Reverse Transcription-PCR (qRT-PCR)

For qRT-PCR, SYBR Premix Ex Taq was used to prepare the reaction mix of 10 µl as found in Table 4.1.

Table 4.1. qRT-PCR setup.

Component	Volume (µl)
dH_2O	2.6
SYBR Premix Ex Taq 2X	5
Forward primer (10 µM)	0.2
Reverse primer (10 µM)	0.2
cDNA template (10 ng/µl)	2

For amplification the following conditions were used (Table 4.2).

Table 4.2. Cycling conditions for qRT-PCR.

Cycle	Step	Temperature (°C)	Duration
1	Initial Denaturation	95	30 sec
40	Denaturation	95	5 sec
	Annealing	55	10 sec
	Elongation	72	10 sec
1	Melting Curve	60-95	holds 1 sec at each 0.2°C increment

The reactions were run in PikoReal 96 Real-Time PCR System. Actin79b was used as a reference gene. Experimental triplicates were done to avoid pipetting errors. The data was analyzed using Microsoft Excel. Comparative CT ($2^{-\Delta\Delta CT}$) method was used to calculate fold difference between cDNA samples of a genotype and its control. The experiment was repeated for each genotype and its control for three times. Two-tail paired Student's t-test was used between experiment and control groups for statistical analysis.

4.8.4. Isolation of Genomic DNA from Flies

Fourteen young adult flies (around 10 days old, equal number of males and females) of the same genotype were selected and frozen at -80°C for 10 minutes. Frozen flies were homogenized in 200 µl of Buffer A and incubated at 65°C for 30 minutes. After cooling the samples at room temperature, 400 µl of 5 M KOAc and 6 M LiCl were added and mixed in a 1:2.5 ratio. The samples were incubated on ice for 10 minutes and centrifuged at 13,200 rpm at room temperature for 15 minutes. The supernatant was transferred to a new 1.5 ml tube and 600 µl of phenol-chloroform mixture (1:1) was added. After vigorous shaking for 15 seconds, the samples were centrifuged at 12,000 g at room temperature for 5 minutes. The aqueous phase was transferred to a new 1.5 ml tube. The steps from phenol-chloroform addition to transfer of aqueous phase were repeated three times. The last aqueous phase was mixed with 0.7 volume of isopropanol and centrifuged at 13,200 rpm at 4°C for 15 minutes. Isopropanol was removed after centrifugation and 70% ethanol was added without disturbing the pellet. The samples were centrifuged at 13,200 rpm at room temperature for 10 minutes. The supernatant was discarded and the pellet was air-dried for 1-2 hours. The dry pellet was dissolved in 75 µl of dH_2O by shaking for 1-2 hours at room temperature. The genomic DNA was stored at -20°C.

4.8.5. Gradient PCR

For gradient PCR *Taq* DNA Polymerase Recombinant was used to prepare the reaction mix of 25 µl as shown in Table 4.3 unless stated otherwise in the text.

Table 4.3. Gradient PCR setup.

Component	Volume (µl)
dH_2O	16.2
10X Taq Buffer with KCl	2.5
$MgCl_2$ (25 mM)	1.5
Forward primer (10 µM)	1
Reverse primer (10 µM)	1
dNTP (10 mM)	0.5
Taq DNA polymerase (5 u/µl)	0.3
Genomic DNA template (100 ng/µl)	2

For amplification the following conditions were used unless stated otherwise in the text (Table 4.4).

Table 4.4. Cycling conditions for gradient PCR.

Cycle	Step	Temperature (°C)	Duration
1	Initial Denaturation	95	5 min
35	Denaturation	95	45 sec
	Annealing	50-60	45 sec
	Elongation	72	1 min per kb
1	Final Elongation	72	10 min
1	Hold	4	hold

After the amplification, the product was stored at 4°C.

4.8.6. Nested PCR

For the first PCR *Taq* DNA Polymerase Recombinant was used to prepare the reaction mix of 50 µl as found in Table 4.5 unless stated otherwise in the text.

Table 4.5. First PCR setup.

Component	Volume (µl)
dH_2O	21.5
10X Taq Buffer with KCl	5
$MgCl_2$ (25 mM)	3
Forward primer (10 µM)	2
Reverse primer (10 µM)	2
dNTP (10 mM)	0.5
Taq DNA polymerase (5 u/µl)	1
Genomic DNA template (100 ng/µl)	15

For amplification of the first PCR the following conditions are used (Table 4.6).

Table 4.6. Cycling conditions for first PCR.

Cycle	Step	Temperature (°C)	Duration
1	Initial Denaturation	95	5 min
40	Denaturation	95	30 sec
	Annealing	50	1 min
	Elongation	72	2 min
1	Final Elongation	72	7 min
1	Hold	4	hold

For the second PCR *Taq* DNA Polymerase Recombinant was used to prepare the reaction mix of 50 µl as found in Table 4.7 unless stated otherwise in the text.

Table 4.7. Second PCR setup.

Component	Volume (µl)
dH_2O	34.5
10X Taq Buffer with KCl	5
$MgCl_2$ (25 mM)	3
Forward primer (10 µM)	2

Table 4.7. Second PCR setup (cont.).

Reverse primer (10 μM)	2
dNTP (10 mM)	0.5
Taq DNA polymerase (5 u/μl)	1
First PCR Product	2

For amplification of the second PCR the following conditions are used (Table 4.8).

Table 4.8. Cycling conditions for second PCR.

Cycle	Step	Temperature (°C)	Duration
1	Initial Denaturation	95	5 min
35	Denaturation	95	30 sec
	Annealing	60	1 min
	Elongation	72	2 min
1	Final Elongation	72	7 min
1	Hold	4	hold

The PCR product was stored at 4° C after the amplification.

4.8.7. Agarose Gel Electrophoresis

DNA samples were run on 1% agarose gel prepared with 1X TAE, with Ethidium Bromide in 10,000:1 ratio. 1 kb DNA Ladder was used to mark the length of the bands. The gel was visualized under UV in Gel Doc XR.

4.9. Polyclonal Antibody Generation

4.9.1. IPTG Induction

IPTG inducible *E. coli* cells were inoculated in 15 ml LB Broth medium with Kanamycin and Chloramphenicol in 1:1000 ratio and grown in a rotary shaker at 37°C, 200 rpm overnight. The overnight culture was diluted to a 1:60 ratio with fresh LB

containing Kanamycin and Chloramphenicol in 1:1000 ratio to a total volume of 30 ml for optimization purposes and of 650 ml for bulk protein production. Cultures were grown at 37ºC until OD_{600} value was between 0.6 – 0.8. Ten ml of culture was taken to a fresh culture tube, to be used as uninduced control in further experiments. Thousand µM IPTG was added to the culture, and both induced and uninduced cultures were grown at 20°C for 16 hours. One ml from both cultures was centrifuged at 13,200 rpm for 5 minutes. Supernatant was removed and pellets were stored at -20ºC for further use in TCA Assay. Cultures were then centrifuged at 7000 rpm for 15 minutes; pellets were collected and stored at -80ºC.

4.9.2. Trichloroacetic Acid (TCA) Assay

Pellet of one ml induced and uninduced cultures were dissolved in 100 µl of TCA by vortexing. The mixture was kept on ice for 15 minutes and centrifuged at 13,200 rpm for 2 minutes. Supernatant was removed and the pellet was dissolved in 1 ml of acetone by vortexing. The mixture was centrifuged at 13,200 rpm for 2 minutes and supernatant was removed. Pellet was dried in room temperature and stored at -20ºC to be analyzed with SDS-PAGE.

4.9.3. Protein Purification with Nickel Column

As the initial step, a nickel column to be used for protein purification was calibrated by running 5-10 ml of lysis buffer (pH 8.0, 7 M urea) through it. Bacterial pellet from 150 ml culture was dissolved in 5 ml lysis buffer with 1 µl Benzonase Nuclease. The mixture was agitated by vigorous shaking and centrifuged at 10,000 g, 4°C for 15 minutes. Supernatant was collected and run through the column. The flow through was collected. To get rid of unbound proteins, column was washed with 30-40 ml washing buffer (pH 6.3, 8 M urea) and fractions were collected in every 10 ml. After the wash, 10-15 ml of elution buffer (pH 4.5, 8 M urea) was run through the column and fractions were collected at every 1.5 ml. All buffers were run through with the help of a peristaltic pump. Lysis flow through, wash fractions and elution fractions were stored at -20ºC to be analyzed with SDS-PAGE.

4.9.4. Polyacrylamide Gel Electrophoresis (SDS-PAGE)

10% SDS-PAGE running gel was prepared according to the concentrations given in Table 4.9. After the gel was casted into the 1.5 mm glass plates, isopropanol was poured on top of it to achieve even polymerization. Isopropanol was removed after polymerization. Stacking gel was casted on top of the running gel and a comb was inserted before polymerization.

Table 4.9. SDS-PAGE gels and their contents.

Gel	Contents
10% SDS-PAGE Running Gel	375 mM Tris-Cl (pH 8.8) 10 % Acrylamide: Bisacrylamide (37.5:1) 0.1 % SDS 0.1 % APS 0.1 % TEMED
5% SDS-PAGE Stacking Gel	125 mM Tris-Cl (pH 6.8) 5 % Acrylamide: Bisacrylamide (37.5:1) 0.1 % SDS 0.1 % APS 0.1 % TEMED

An appropriate amount of 6X protein sample buffer was added to the protein samples and they were incubated at 95°C for 5 minutes for denaturation. Samples were loaded to the SDS-PAGE gel and run at 80 V until they pass the stacking gel and 100 V for 2 hours. BSA of a known concentration was used as a control to assess the concentration of the samples. PageRuler Prestained Protein Ladder was used as a marker. The gel was then stained with Coomassie Blue solution for 2 hours at room temperature. When the gel was completely blue, staining solution was removed and destaining solution was added. The gel was shaken in destaining solution for 4 hours; the solution was refreshed every half an hour.

4.9.5. Protein Extraction from SDS-PAGE

Bacteria were induced with IPTG as described in Section 4.9.1 for bulk amount of protein extraction. Bacterial pellet from 150 ml culture was dissolved in 5 ml 1X PBS with 1% Triton-X and 1 µl Benzonase Nuclease. The mixture was sonicated at 95 V for 4 cycles of 30 seconds, three times and centrifuged at 10,000 g, 4°C for 15 minutes. The supernatant was removed and stored; pellet was dissolved in 5 ml 1X PBS with 1% Triton-X. Centrifugation, removal of the supernatant and addition of 5 ml 1X PBS with Triton-X was repeated three times to get purer protein of interest in the pellet. Five ml 1X PBS was used in the last wash to get rid of excess detergent. After the washes, pellet was dissolved in 2 ml of 1X PBS and stored at -20°C. Stored supernatants and sample of dissolved pellet were analyzed with SDS-PAGE.

PROTEAN II xi Cell was used to cast a maxi SDS-PAGE gel. The gel was prepared as shown in Table 4.9 and casted as described in Section 4.9.3. However, to load more of the pellet, the wells of the gel were combined by taping 13 comb teeth together. 200 µl of bacterial pellet dissolved in 1X PBS was mixed with 40 µl of 6X protein sample buffer and denatured at 95°C for 5 minutes. 10 µl of it was loaded to a normal sized well as a sample and the rest was loaded to the combined well. Gel was run at 100 V, 4°C overnight. PageRuler Prestained Protein Ladder was used as a marker. After gel electrophoresis, the strip of the gel containing the sample and the marker was cut with a scalpel and stained with Coomassie Blue solution as described in Section 4.9.3. The rest of the gel was wrapped in plastic film to prevent it from drying, until the strip was ready. The stained strip of gel was aligned with the unstained gel portion and the band of gel that aligns with the stained protein of interest in the reference strip was cut out. The excised band was cut into pieces with a scalpel and put into a mortar. 2 ml of gel extraction elution buffer was added and the pieces were crushed until single pieces were indistinguishable. The mixture was incubated in a rotary shaker at 200 rpm, 30°C for 8 hours and centrifuged at 10,000 x *g*, 4°C for 15 minutes. Supernatant was pipetted into a new microcentrifuge tube. The pellet was dissolved in 2 ml gel extraction elution buffer and incubated in a rotary shaker at 200 rpm, 30°C overnight and centrifuged at 10,000 x *g*, 4°C for 15 minutes. The new supernatant was combined with the previous one and an aliquot of the mixture was subjected to SDS-PAGE to test the presence of interested protein.

4.9.6. Antigen Injections and Serum Collection

Once the presence and purity of the protein of interest was proven by running it on SDS-PAGE, the protein was diluted to 70 µg in 200 µl of 1X PBS and mixed with 200 µl of Freund's Complete Adjuvant, and the mixture was injected to the rabbit. Two rabbits were subjected to injections. First five protein injections were performed after every two weeks. Protein was mixed with Freund's incomplete adjuvant in injections other than the first one. 1-2 ml of blood was drawn from the ears of each rabbit 4 days after the third injection; sodium citrate-glucose was added in 1:10 ratio to prevent coagulation. Blood was centrifuged at 13,000 rpm, 4°C for 5 minutes. The serum residing on top was transferred to a new microcentrifuge tube and stored at -20°C to be used to check if the rabbits developed an immune response against the protein of interest by using it as the primary antibody against the protein of interest in Western Blot. 30 ml of blood was drawn from each rabbit 4 days after the fifth injection; sodium citrate-glucose was added in 1:10 ratio to prevent coagulation. Blood was centrifuged at 10,000 rpm, 4°C for 20 minutes; the serum residing on top was transferred to a new centrifuge tube and stored at -20°C. The sixth injection was performed a month later than the fifth, and rabbits were sacrificed. Around 100 ml of blood was drawn from each rabbit 4 days after the last injection; sodium citrate-glucose solution was added in 1:10 ratio to prevent coagulation. Blood was centrifuged at 10,000 rpm, 4°C for 20 minutes; the serum residing on top was transferred to a new centrifuge tube and stored at -20°C. Sera from fifth and sixth injection was stored to be used in purification of polyclonal antibody produced against the protein of interest.

4.9.7. Purification of Polyclonal Antibody from Rabbit Sera

Rabbit sera were sent to Prof. Fatma Yucel in Tubitak MAM, Kocaeli for antibody purification. They have used HiTrap Protein G column (GE Healthcare, UK) to purify the polyclonal antibody produced against the protein of interest. They performed Enzyme-Linked ImmunoSorbent Assay (ELISA) to distinguish the elutions from the column that had high antibody concentration. The selected elutions with high antibody concentrations, which can be used as purified antibodies against the protein of interest, were retrieved from them.

4.9.8. Protein Extraction from Flies

Fourteen young adult flies (around 10 days old, equal number of males and females) of same genotype were selected and frozen at -80°C for 10 minutes. They were homogenized for 10 seconds, three times in 210 µl of Non-ionic Fly Lysis Buffer with 1X protease inhibitor. The mixture was held on ice for 30 minute then centrifuged at 13,200 rpm for 10 minutes. After centrifugation, the supernatant containing the proteins was drawn without disturbing the oily surface, and stored at -20°C. Protein concentrations were measured using BCA Assay Kit in ND-1000, NanoDrop spectrophotometer.

4.9.9. Western Blot Analysis

Fifty µg of fly lysate or antigen of interest were mixed with 6X protein sample buffer and denatured at 95°C for 5 minutes, unless otherwise stated in the text. Samples were loaded to SDS-PAGE gel and run at 80 V until they pass the stacking gel and 100 V for 2 hours. Proteins were electroblotted to PVDF membranes in transfer buffer at 100 V for 75 minutes (1 min per 1 kDa). The membrane was washed for 5 minutes in 1X TBS-T three times and blocked with 5% BSA in 1X TBS-T at room temperature for 1 hour. Primary antibody incubation was performed in 5% BSA in 1X TBS-T overnight at 4 °C. Excess antibody was washed away with 1XTBS-T for 5 minutes, three times. Horseradish peroxidase (HRP)-conjugated secondary antibody incubation was performed at room temperature for 1 hour. After washing 5 minutes with 1X TBS-T for three times, membranes were incubated in ImmunoCruz Western Blotting Luminol Reagent and visualized by chemiluminescence detection system Stella. To detect actin protein as loading control, membranes were washed 5 minutes with 1X TBS-T for three times after visualization, and stripped by incubation with stripping solution at 50°C for 30 minutes in hybridization oven. After washing 10 minutes with 1X TBS-T for three times, blocking and antibody incubation steps were followed as stated previously. For analysis, protein levels were normalized to corresponding actin levels.

4.9.10. Pre-adsorption of Polyclonal Antibody

Around fifty null mutant larvae of the gene of interest were placed in HL-3 solution containing silicon plates. Their heads were dissected under stereomicroscope. Cuticle was ripped to expose brain and the imaginal discs. The heads were incubated in fixation solution for 20 minutes on a shaker, and then washed in BBT buffer for 20 minutes, four times. Heads were incubated in BBT buffer with polyclonal antibody produced against the protein of interest in 1:10 ratio, and incubated at 4°C for 24 hours. Pre-adsorbed antibody was removed and transferred into a new microcentrifuge tube. 0.3% sodium azide was added to store the pre-adsorbed polyclonal antibody at 4°C.

5. RESULTS

5.1. Studies on *CG4623*

We aimed to generate a *Drosophila* model for the CMT disease by achieving up- and down-regulation of *CG4623*. Thus, as the initial step for further experiments we confirmed the expression levels quantitatively at the mRNA level using qRT-PCR. To investigate whether the disease phenotypes are recapitulated in the flies we investigated the effect of altered *CG4623* expression on motor performance and lifespan of the flies by analyzing their climbing behavior and longevity, respectively. In the scope of this study, we also examined the genotype of the flies that were developed previously in our lab at the initial step of *CG4623* knock-out generation, to verify the integration of the targeting vector.

5.1.1. Determination of *CG4623* Downregulation and Overexpression

In order to determine the expression levels of *CG4623* in *CG4623* downregulation and overexpression lines, quantitative Reverse Transcription-PCR (qRT-PCR) was performed.

Ubiquitous downregulation and overexpression was achieved by crossing the *UAS-CG4623 RNAi* and *UAS-CG4623 OE* lines with *actin5C-Gal4* driver line. Expression levels were determined for F1 progeny carrying the *actin5C-Gal4*/*UAS-CG4623 RNAi* alleles and *actin5C-Gal4*;*UAS-CG4623* alleles. *Actin5C-Gal4* line was also crossed with wild-type w^{1118}, and the F1 progeny carrying *actin5C-Gal4* allele was used as the driver control. Apart from these flies, *UAS-CG4623 RNAi* and *UAS-CG4623 OE* lines were crossed with w^{1118}, and F1 progeny carrying the *UAS-CG4623 RNAi* or *UAS-CG4623 OE* allele was used as the UAS-line control, respectively. Total RNA was isolated from 14 young adult flies of each genotype, cDNA was synthesized by reverse transcription, and real time PCR was performed with CG4623_RT1 and actin79b_RT primer pairs. CG4623_RT1 primer pair was designed from the first and second exon that harbors an intron in-between, thus, it also allows detection of any genomic DNA contamination. Expected PCR product size was 159 bp for *CG4623*. One of the Actin79b_RT primers,

was designed from the exon-exon boundary of the second and third exon, thereby can only bind to cDNA (Yıldırım, 2013). Actin79b_RT primer pair amplifies a product of 167 bp. Average cycle threshold (CT) values of experimental triplicates were calculated. The deviations between CT values of experimental triplicates were low indicating that the pipetting differences were negligible. *Actin79b* was used as a reference gene; thus, *CG4623* CT values were normalized to *actin79b* CT values. The fold differences between cDNAs of *CG4623* downregulated flies and its driver and UAS-line controls; and cDNAs of *CG4623* overexpressed flies and its driver and UAS-line controls were calculated by Comparative CT ($2^{-\Delta\Delta CT}$) method and statistically analyzed. The mean fold changes indicating the expression levels compared to controls was shown in Figure 5.1.

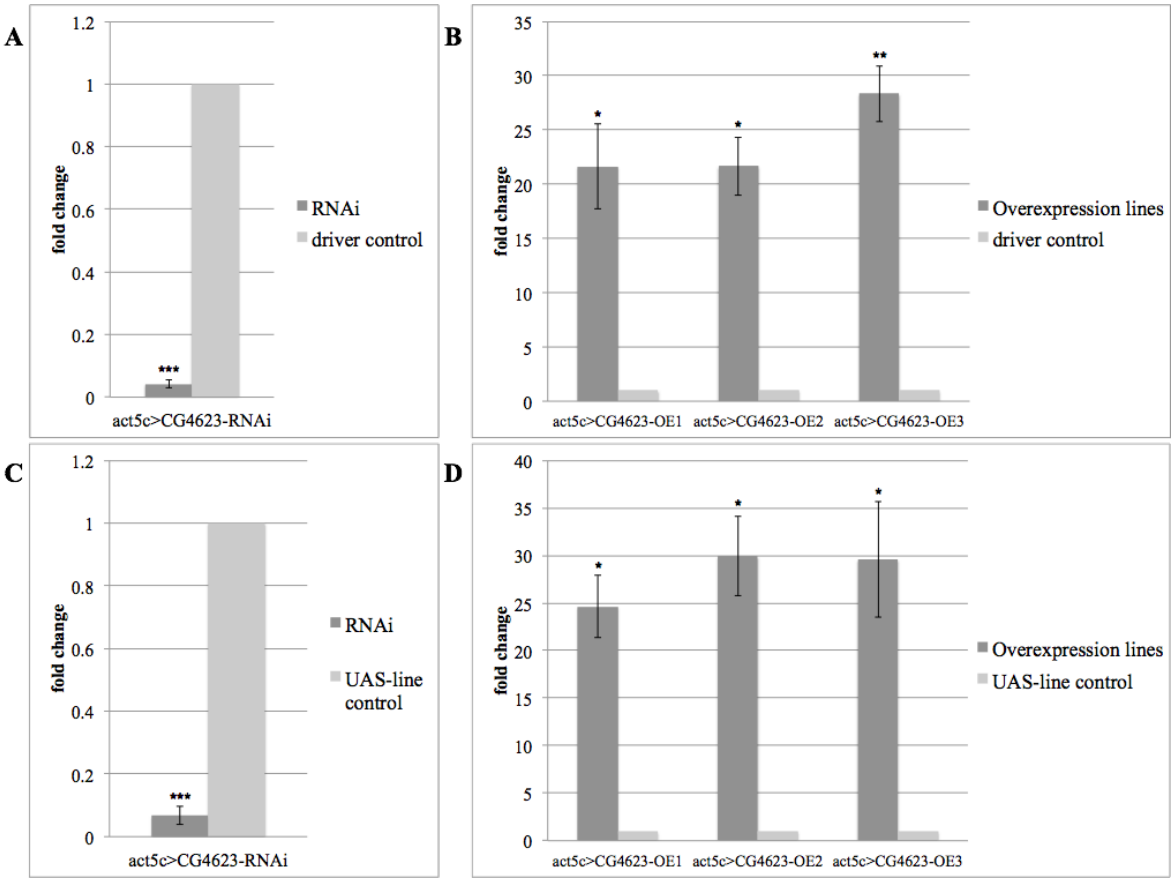

Figure 5.1. Expression level quantification of ubiquitous downregulation (A,C) and overexpression (B,D) of *CG4623* by qRT-PCR. Expression level comparison with the driver control (A,B) and the UAS-line control (C,D). Bar graphs indicate fold change of biological triplicates of act5c>CG4623-RNAi and act5c>CG4623-OE1, 2 and 3 compared to controls. Mean fold change ± SEM (n=3). ***: $P<0.001$, **: $P<0.01$, *: $P<0.05$.

When *CG4623* was ubiquitously downregulated (act5c>CG4623-RNAi), *CG4623* mRNA level was reduced by 96% compared to the driver control (Figure 5.1A), and by 93% compared to the UAS-line control (Figure 5.1C). Three different *CG4623* overexpression lines were used, and ubiquitous *CG4623* overexpression (act5c>CG4623-OE) had led to 21-fold, 21-fold and 27-fold increase in *CG4623* mRNA levels compared to the driver control, respectively (Figure 5.1B). 24-fold, 29-fold and 29-fold increase in mRNA levels was observed when ubiquitously overexpressed *CG4623* flies were compared to each UAS-line control, respectively (Figure 5.1D). Two-tail paired Student's t-test indicated that all results are statistically significant. Furthermore, the specificity of amplification with CG4623_RT1 and actin79b_RT primer pairs was confirmed by melting curve analysis. Single peaks were observed at 82°C and 86°C corresponding to specific melting temperatures of *CG4623* and *actin79b* products, respectively (data not shown). According to these results, downregulation line *UAS-CG4623 RNAi* and first overexpression line, *UAS-CG4623 OE L1* were selected to be used in further experiments.

5.1.2. Altering *CG4623* Expression Levels Affect the Climbing Behavior of *Drosophila*

To shed light onto the effects of *CG4623* expression level on the motor performance of the flies, negative geotaxis assay was performed with males and females from different age groups in which *CG4623* is ubiquitously or neuron-specifically downregulated or overexpressed.

CG4623 ubiquitous downregulation and overexpression was achieved by crossing *actin5c-Gal4* driver line with *UAS-CG4623 RNAi* and *UAS-CG4623 OE* lines. Progeny of each cross was separated by gender and age. Nine, 20 and 30 days old males and females, in which *CG4623* is ubiquitously downregulated or overexpressed, were subjected to negative geotaxis assay along with appropriate controls (*act5C>KK control* and *act5C>w*^{1118}, respectively). The climbing distance of the flies was recorded for five seconds after the start of the movement (Figure 5.2), and the assay was performed in biological quadruplicates for each genotype and age group. Mean climbing distances of males and females are depicted in Figure 5.3.

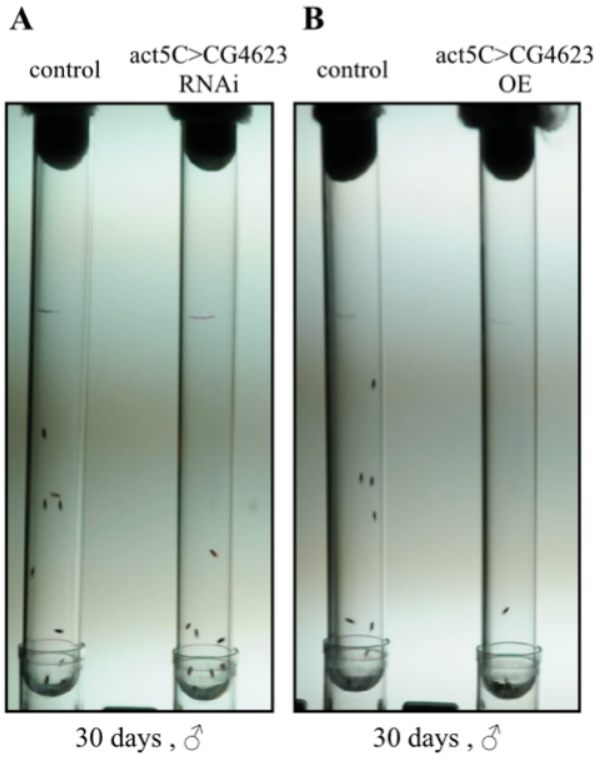

Figure 5.2. Climbing behavior of thirty days old males. act5C>CG4623 RNAi and act5C>CG4623 OE stands for ubiquitous (A) downregulation and (B) overexpression of *CG4623*, respectively.

Thirty days old males and females with ubiquitous *CG4623* downregulation climbed a shorter distance than controls at the same time period. Difference in climbing distance was not significant between younger male and female (9 and 20 days old) *CG4623* downregulated flies and their controls (Figure 5.3A,C). *CG4623* ubiquitous overexpression resulted in longer distance climbing of young, 9 days old, males and females; however, as the flies age to 30 days, these flies climbed a shorter distance than the controls (Figure 5.3B,D). Short distance climbing was also observed in 20 days old males with *CG4623* overexpression (Figure 5.3B), although no significant difference was observed in females at the same age (Figure 5.3D). These results indicate that alteration of *CG4623* expression level affects the climbing behavior of the flies. Shorter distance climbing was observed in later times in life in both ubiquitous downregulation and overexpression of *CG4623* suggesting an age-dependent phenotype.

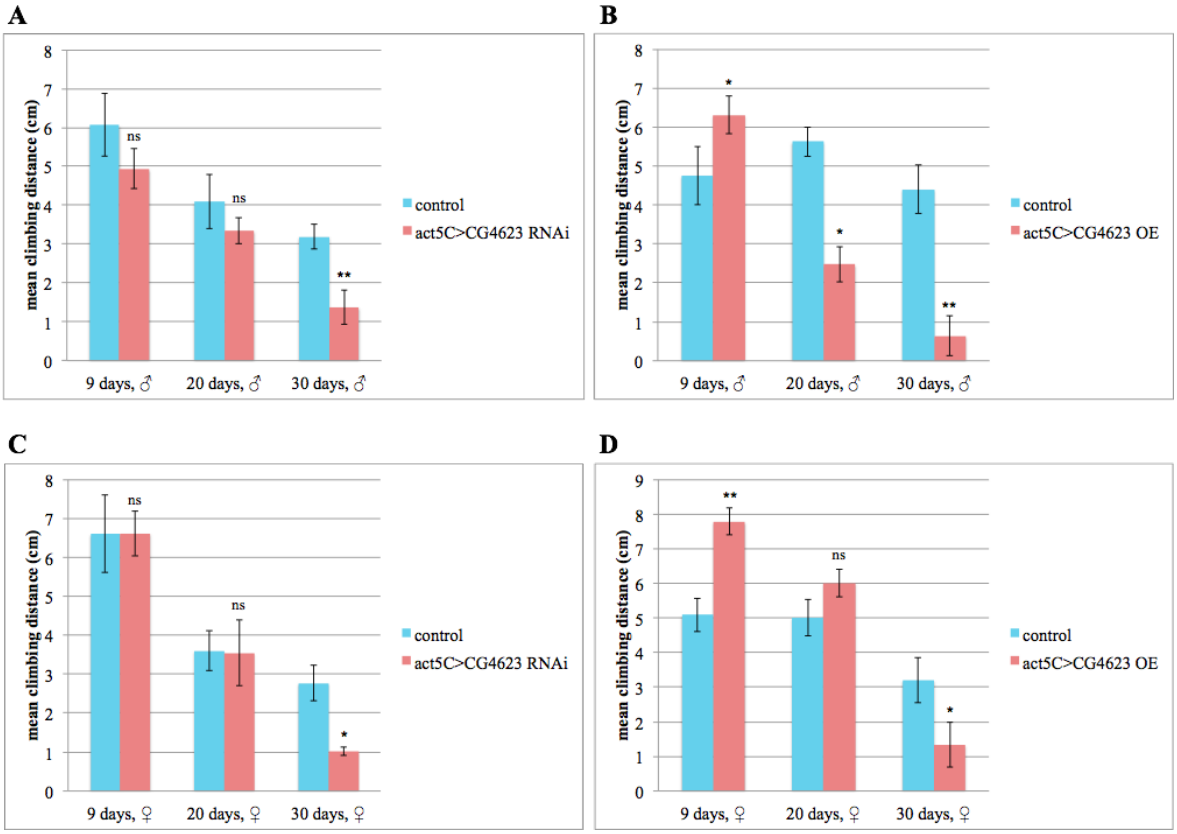

Figure 5.3. Mean climbing distance graphs for males (A,B) and females (C,D) with *CG4623* ubiquitous downregulation (A,C) and overexpression (B,D). Control in A,C stands for *actin5C-Gal4* driven *KK control*; control in B,D stands for *actin5C-Gal4* driven w^{1118}. Mean climbing distance ± SEM (n=4). **: $P<0.01$, *: $P<0.05$, ns: not significant. Student's t-test was performed between experiments and controls.

CG4623 neuron-specific downregulation and overexpression was achieved by crossing *UAS-Dicer;;nSyb-Gal4* driver line with *UAS-CG4623 RNAi* and *UAS-CG4623 OE* lines. Progeny of each cross was separated by gender and age. Neuron-specific downregulation crosses were kept in 29°C for higher downregulation efficiency; although, the lifespan of *Drosophila* is halved at this temperature. Thus, younger age groups of 9, 12, 15 days were selected from progeny of neuron-specific downregulation crosses. Males and females with neuron-specific *CG4623* overexpression were grouped as 9, 20, and 30 days old. All age groups of both genders were subjected to negative geotaxis assay along with appropriate controls (*nSyb>KK control* for downregulation and *nSyb>*w^{1118} for overexpression). The climbing distance of the flies was recorded for five seconds after the start of the movement (Figure 5.4), and the assay was performed in biological

quadruplicates for each genotype and age group. Mean climbing distances of males and females are depicted in Figure 5.5.

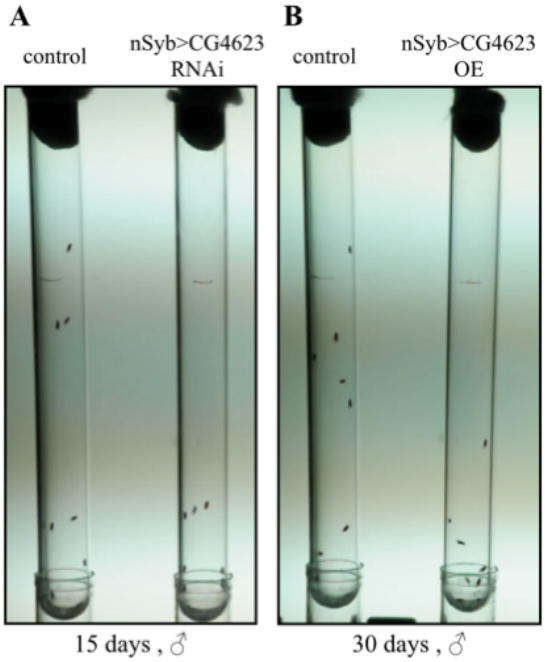

Figure 5.4. Climbing behavior of fifteen and thirty days old males. nSyb>CG4623 RNAi and nSyb>CG4623 OE stands for (A) downregulation and (B) overexpression of *CG4623* in neurons, respectively.

Males with *CG4623* downregulation in neurons (nSyb>CG4623 RNAi) climbed a shorter distance than controls at the same time period, in all age groups (Figure 5.5A). While no significant difference was observed between females with neuron-specific *CG4623* downregulation and controls in terms of climbing distance until the age of 15 days (Figure 5.5C). Strikingly, 15 days old female flies showed extremely significant climbing difference compared to controls; thus suggesting an age-dependent phenotype (Figure 5.5C). *CG4623* overexpression in neurons (nSyb>CG4623 OE) resulted in faster climbing in young (9 days old) females compared to controls; however, no significant difference was observed in males at the same age (Figure 5.5B,D). As the flies age to 30 days, males with neuron-specific *CG4623* overexpression climbed a shorter distance than controls (Figure 5.5B), which is also consistent with the results of 30 days old males having ubiquitous overexpression (Figure 5.3B).

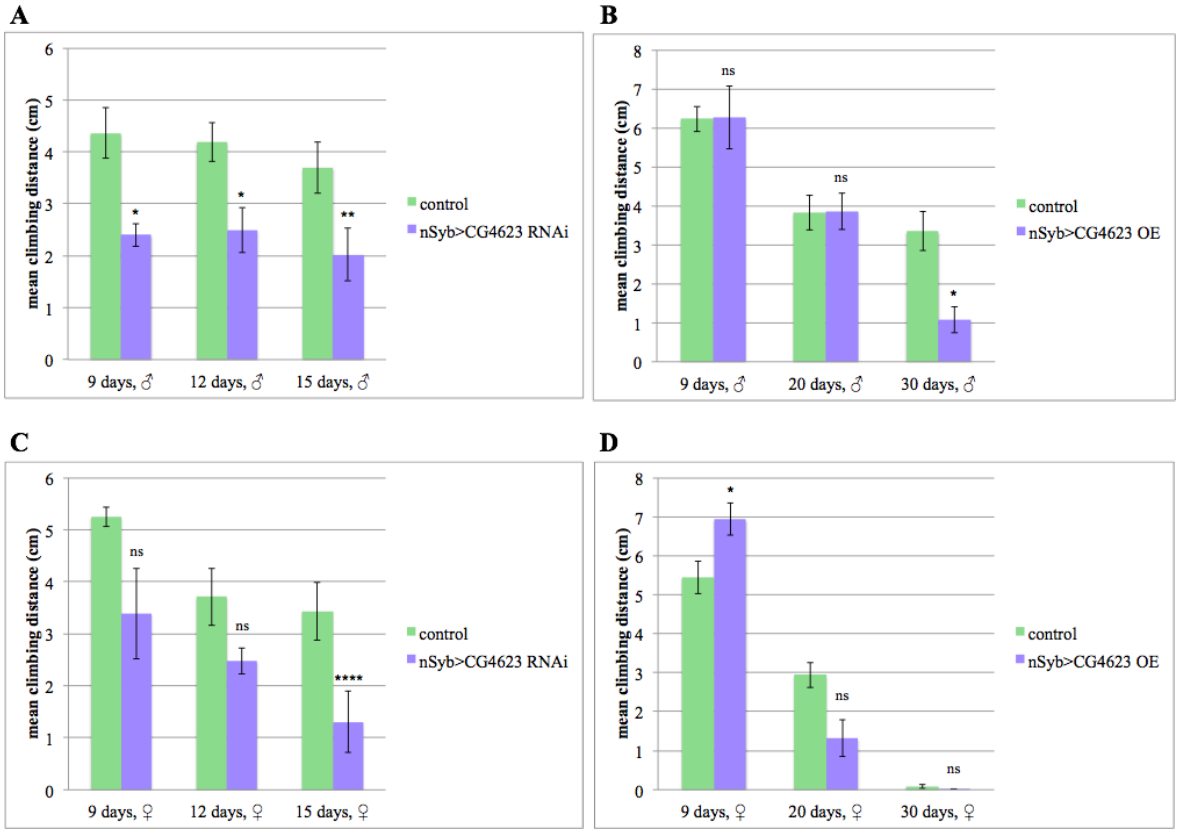

Figure 5.5. Mean climbing distance graphs for males (A,B) and females (C,D) with *CG4623* neuron-specific downregulation (A,C) and overexpression (B,D). Control in A,C stands for *UAS-Dicer;;nSyb-Gal4* driven *KK control*; control in B,D stands for *UAS-Dicer;;nSyb-Gal4* driven w^{1118}. Mean climbing distance ± SEM (n=4). ****: $P<0.0001$, **: $P<0.01$, *: $P<0.05$. Student's t-test was performed between experiments and controls.

These results show that alteration of *CG4623* expression level in neurons also affects the climbing behavior of the flies. The age-dependent short distance climbing, observed in nSyb>CG4623 RNAi females and nSyb>CG4623 OE males is consistent with the results of the negative geotaxis assay with ubiquitous expression level alterations.

5.1.3. Analysis of the Effects of *CG4623* Expression Level on *Drosophila* Lifespan

Male and female flies in which *CG4623* is ubiquitously downregulated or overexpressed were followed over 90 days along with appropriate controls, and number of dead flies was counted every 3 days. The survival plots were drawn and statistically analyzed using an online tool (Figure 5.6, Yang et al., 2011).

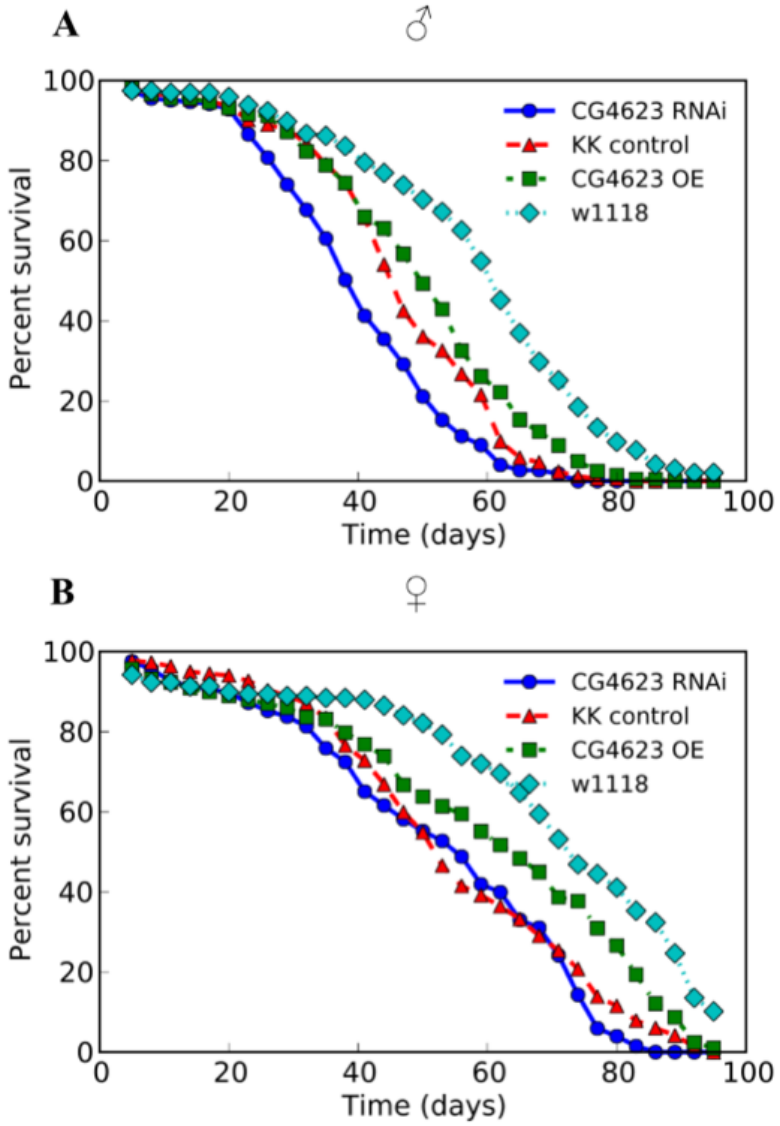

Figure 5.6. Survival plots for males (A) and females (B) with ubiquitous *CG4623* downregulation (CG4623 RNAi) and overexpression (CG4623 OE). KK control: downregulation control, w^{1118} : overexpression control. (Yang *et al.*, 2011).

CG4623 ubiquitous downregulation in males yielded slightly lowered survival percentage over the documented period compared to control (Figure 5.6A) whereas no overall difference in terms of lifespan was observed in females between *CG4623* downregulated and control flies (Figure 5.6B). Both male and female flies in which *CG4623* is ubiquitously overexpressed yielded mildly lowered survival percentage compared to control (Figure 5.6).

Detailed survival analysis in terms of mean lifespan and age in mortality percentage is listed in Tables 5.1 and 5.2 for males and females, respectively. Both survival plots and detailed analysis showed that males had lower percent survival over time compared to females.

Table 5.1. Detailed longevity analysis for males of four genotypes (Yang *et al.*, 2011).

Genotype	No. of subjects	Restricted mean			Age in days at % mortality				
		Days	Std. error	95% C.I.	25%	50%	75%	90%	95% Median C.I.
act>CG4623 RNAi	223	39.88	0.97	37.97 ~ 41.79	29	41	50	59	38 ~ 38
act>KK control	172	46.51	1.15	44.25 ~ 48.77	38	47	59	62	44 ~ 44
act>CG4623 OE	203	49.51	1.21	47.14 ~ 51.88	38	50	62	71	47 ~ 50
act>w^{1118}	195	58.83	1.40	56.09 ~ 61.57	47	62	74	80	59 ~ 62

Table 5.2. Detailed longevity analysis for females of four genotypes (Yang *et al.*, 2011).

Genotype	No. of subjects	Restricted mean			Age in days at % mortality				
		Days	Std. error	95% C.I.	25%	50%	75%	90%	95% Median C.I.
act>CG4623 RNAi	203	52.39	1.52	49.41 ~ 55.38	38	56	71	77	50 ~ 56
act>KK control	217	54.94	1.43	52.14 ~ 57.74	41	53	74	83	50 ~ 53
act>CG4623 OE	207	60.09	1.77	56.61 ~ 63.56	44	65	83	89	59 ~ 68
act>w^{1118}	207	69.06	1.78	65.57 ~ 72.55	56	74	89	-	71 ~ 77

According to detailed longevity analysis, mean lifespan of *CG4623* downregulated males was a week shorter than controls while *CG4623* downregulated females and control

flies had similar lifespan for the majority of the assay. Mean lifespan of both male and female flies in which *CG4623* is ubiquitously overexpressed was 9 days shorter than the controls, and the difference was sustained throughout the assay (Table 5.1 and Table 5.2).

Fisher's exact test was performed to males and females for statistical analysis, and results are presented in Table 5.3 and Table 5.4, respectively. *P*-values indicate that the difference between *CG4623* downregulated male flies and controls in terms of lifespan was statistically significant at every percent mortality period (Table 5.3). However, significant difference in lifespan was reached at only 90% mortality period between *CG4623* downregulated female flies and controls (Table 5.4). The lifespan difference between *CG4623* overexpressed male and female flies and controls was also statistically significant according to the *P*-values determined with Fisher's exact test (Table 5.3 and Table 5.4).

Table. 5.3. Fisher's exact test results for males (Yang *et al*., 2011).

Condition	**Statistics**			
	P-value at 25%	**P-value at 50%**	**P-value at 75%**	**P-value at 90%**
act>CG4623 RNAi vs. act>KK control	0.0002	0.0002	0.0002	0.0243
act>CG4623 OE vs. act>w^{1118}	0.0034	<0.00001	0.000023	0.000047

Table. 5.4. Fisher's exact test results for females (Yang *et al.*, 2011).

Condition	**Statistics**			
	P-value at 25%	**P-value at 50%**	**P-value at 75%**	**P-value at 90%**
act>CG4623 RNAi vs. act>KK control	0.3706	0.2413	0.8214	0.0057
act>CG4623 OE vs. act>w^{1118}	0.0001	0.0043	0.0004	0.000034

5.1.4. Investigation of *CG4623* IMAGO Targeting Vector Integration

Previously in our lab, *CG4623* mutant lines were being developed using Integrase-Mediated Gene Knock-Out (IMAGO) approach. To delete *CG4623* gene from fly genome via homologous recombination, Kerem Yıldırım designed a targeting vector carrying the

flanking homology regions of *CG4623* (Figure 5.7). Bacterial clone of the designed vector was sent to Genetic Services, Inc., USA for injection into embryos with white-eye background (*w*). After receiving vector injected *Drosophila* lines, it was observed that the flies had red eyes indicating that the targeting vector (CG4623_pP{white-STAR}) was integrated to the genome since it carried a red eye marker (w^+). Yıldırım also confirmed that the vector was integrated on the X chromosome by chromosome mapping and generated homozygous fly lines carrying the vector, *IMAGO CG4623 L1* and *IMAGO CG4623 L2*) (Yıldırım, 2013).

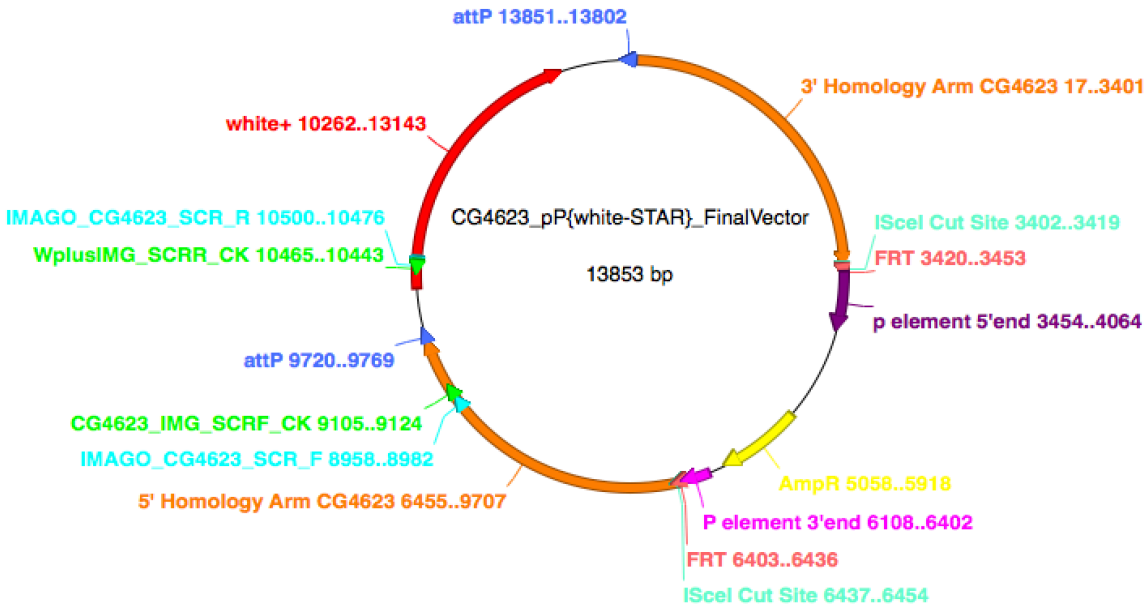

Figure 5.7. Graphic map of CG4623_pP{white-STAR} vector injected to fly embryos. Vector contains *P*-element arms for genomic integration; 5' and 3' homology arms of *CG4623*; red eye marker (w^+); FRT sites and *I-Sce*I sites for *CG4623* knock-out and attP sites for knock-ins.

In this study, genomic integration of the vector was tested. For this purpose, gradient PCR was performed with genomic DNA (gDNA) from *IMAGO CG4623 L1* and *L2* flies with IMAGO_CG4623_SCR_F and IMAGO_CG4623_SCR_R primers that were designed from 5' homology arm of *CG4623* and w^+ gene (Figure 5.7). Even though the PCR was repeated for several times, the expected band of 1543 bp, which was seen in the injected CG4623_pP{white-STAR} vector itself, was not observed in neither of the fly lines tested at any temperature (Figure 5.8).

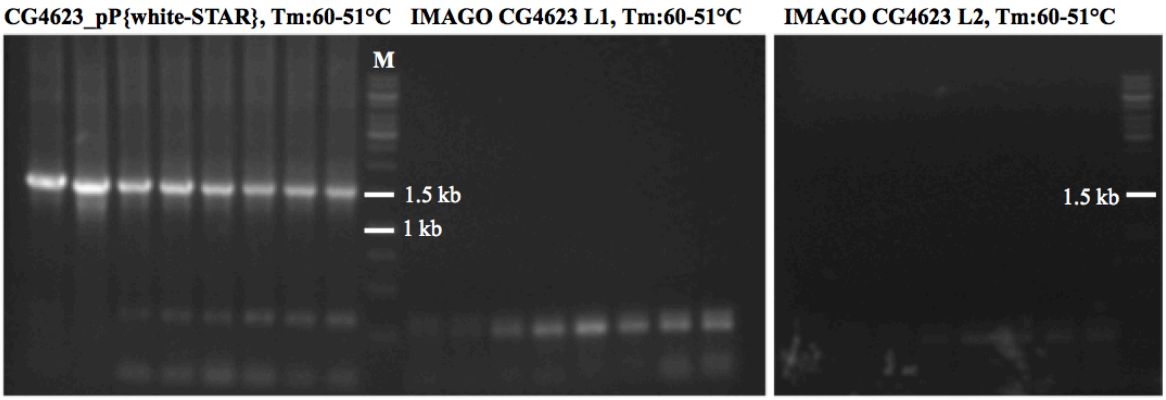

Figure 5.8. Gradient PCR with genomic DNA of *IMAGO CG4623 L1* and *L2* flies. CG4623_pP{white-STAR} vector itself is used as a positive control. Annealing temperatures were between 60°C and 51°C. M: 1 kb DNA ladder.

Since PCR with a range of annealing temperatures did not resulted in positive results, a new gradient PCR was performed with same primers and samples, but with different concentrations of $MgCl_2$ and addition of DMSO. More non-specific bands were observed as the temperature increased, and changes in $MgCl_2$ concentration did not cause any significant differences. Addition of DMSO resulted in weaker non-specific bands; however, the expected 1543 bp band was not observed in any case. In order to confirm that genomic DNA extraction was successful, another primer pair was used to amplify a 483 bp region from the genome. The existence of the expected band suggested that genomic DNA extraction from flies was successful and is not interfering with the amplification of the IMAGO insert (Figure 5.9).

A new primer pair (CG4623_IMG_SCRF_CK and WplusIMG_SCRR_CK) was designed from 5' homology arm of *CG4623* and w^+ gene to check the integration of CG4623_ pP{white-STAR} vector to the fly genome (Figure 5.7), and gradient PCR was performed with this primer pair and gDNA of *IMAGO CG4623 L1* and *L2* flies. However, the expected band of 1361bp bp was not observed in neither of the fly lines tested at any temperature. The expected fragment was observed only as the PCR product of the injected CG4623_pP{white-STAR} vector, itself (Figure 5.10).

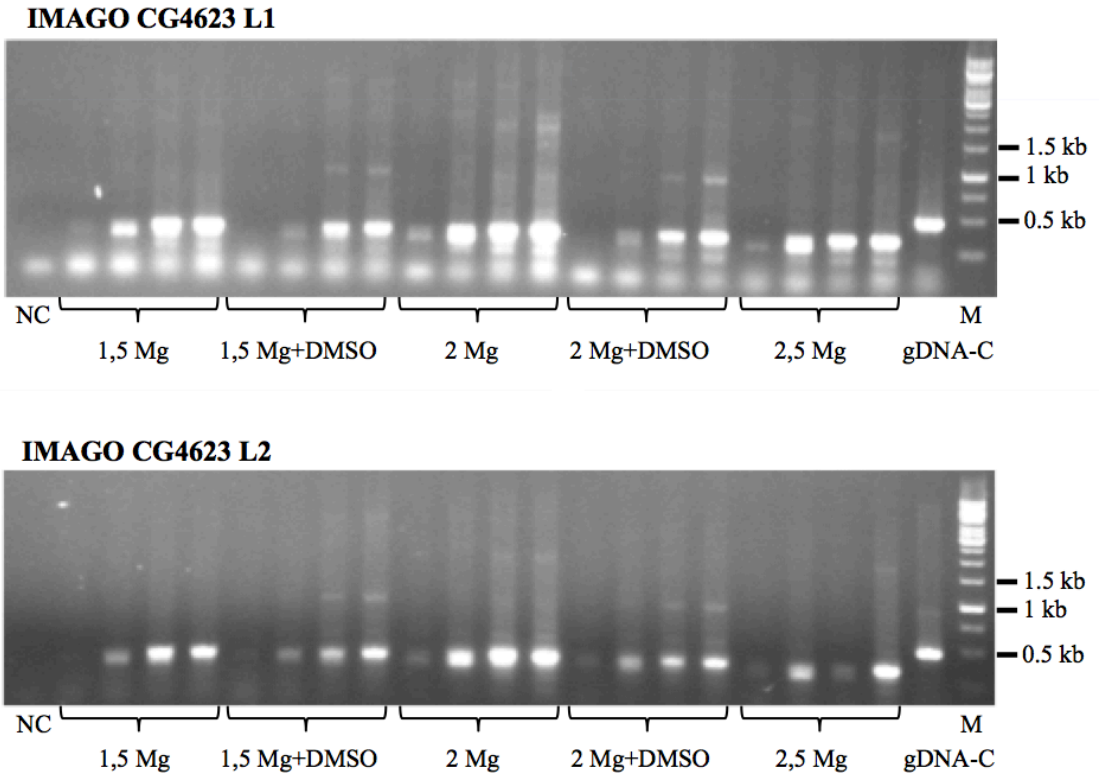

Figure 5.9. Gradient PCR with gDNA of *IMAGO CG4623 L1* and *L2* flies at increasing $MgCl_2$ concentrations and with/without DMSO. Annealing temperatures: 59.5°C, 56.4°C, 52.1°C, 50°C; $MgCl_2$ concentrations:1,5 mM, 2 mM, 2.5 mM (Left to right). NC: negative control, gDNA-C: genomic DNA control, M: 1 kb DNA ladder. CG9115_5H_S4 and CG9115_5H_T1 primer pair was used to amplify a 483 bp region as gDNA control.

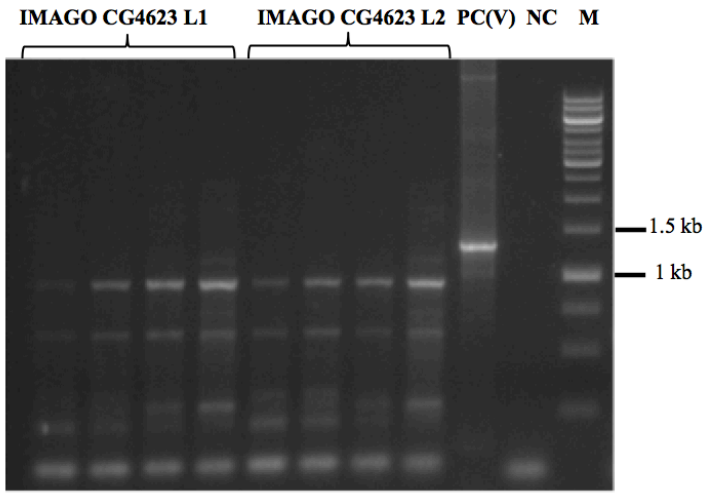

Figure 5.10. Gradient PCR with genomic DNA of *IMAGO CG4623 L1* and *L2* flies, and a second primer pair. Annealing temperatures were between 60°C and 51°C. PC(V): positive control (vector), NC: negative control, M :1kb DNA ladder.

As a final molecular approach, nested PCR was performed with both primer pairs that were used before. The first PCR was performed with gDNA of *IMAGO CG4623 L1* and *L2* flies and IMAGO_CG4623_SCR_F and IMAGO_CG4623_SCR_R primers. Then, the second PCR was performed using the product of the first PCR as the template, and CG4623_IMG_SCRF_CK and WplusIMG_SCRR_CK primers that allow amplification from an internal site of the region amplified by the primary primer pair. Both PCR products were loaded on agarose gel, after the nested PCR however, 1361 bp band expected after second PCR could not be observed (Figure 5.11).

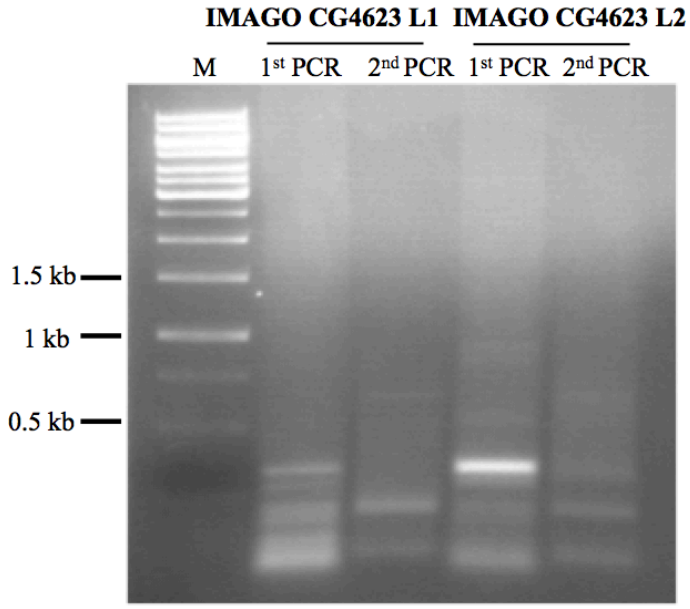

Figure 5.11. Nested PCR with genomic DNA of *IMAGO CG4623 L1* and *L2* flies. IMAGO_CG4623_SCR_F and IMAGO_CG4623_SCR_R primer pair is used in the first PCR and CG4623_IMG_SCRF_CK and WplusIMG_SCRR_CK primer pair is used in the second PCR. M: 1 kb DNA ladder.

All together these results suggests that CG4623_pP{white-STAR} vector was not integrated into the fly genome in the correct way. Although *IMAGO CG4623 L1* and *L2* lines were both red-eyed (carrying the w^+ gene somehow), a part of the 5' homology arm and the region between the 5' homology arm and w^+ gene were definitely missing.

In order to check the integration of the targeting vector to the fly genome, a different strategy was adopted. Since CG4623_pP{white-STAR} vector also contains FRT sites in

the vicinity of the homology arms (Figure 5.7), the region containing the w^+ (red eye) gene can be cut out via flippase activity. For this purpose, homozygous *IMAGO CG4623 L1* and *L2* lines were crossed with *w;;eyFLP*, *TM3,Sb/TM6B* line separately. These flies carry eyFLP, a flippase enzyme that is active in the eye; thus F1 progeny was expected to include white-eyed flies in the presence of both *IMAGO* and *eyFLP* alleles. F1 progeny was selected against *Sb* (short bristle) and screened for white-eyed flies. Even though more than 150 flies were screened for both lines, no white-eyed flies were observed (Table 5.5). These are consistent with the results of PCR experiments; thus, it was concluded that the targeting vector for IMAGO was integrated to the genome in an incorrect manner.

Table. 5.5. Screening results for F1 progeny of IMAGO targeting vector integration verification crosses.

	Number of red-eyed flies	**Number of white-eyed flies**
$\frac{\text{IMAGO CG4623,w+ L1}}{+/\rightarrow} ;; \frac{\text{TM3,Sb eyFLP}}{+}$	153	0
$\frac{\text{IMAGO CG4623,w+ L2}}{+/\rightarrow} ;; \frac{\text{TM3,Sb eyFLP}}{+}$	258	0

5.2. Studies on *mtm*

Since we aimed to generate a *Drosophila* model for the CMT disease by altering the expression levels of *mtm*, it is essential to determine the expression at both RNA and protein levels. Thus, we chose to quantify it at the RNA level by qRT-PCR, and by generating an antibody against mtm at the protein level since there was no commercially available antibody. Furthermore, we investigated the effect of altered expression levels on the lifespan of the flies by analyzing their longevity. As we have done for the *CG4623* lines generated for knock-out, we also examined the genotype of the flies that were developed previously in our lab at the initial step of *mtm* knock-out generation, to verify the integration of the targeting vector in the scope of the this study.

5.2.1. Determination of *mtm* Overexpression

Ubiquitous downregulation of *mtm* by crossing a*ctin5C-Gal4* line with *UAS-mtm RNAi* resulted in pupal lethality in the F1 progeny. Thus, qRT-PCR was performed with the overexpression lines only, to determine the expression levels of *mtm*.

Ubiquitous overexpression was achieved by crossing the *UAS-mtm OE* lines with *actin5C-Gal4* driver. Expression levels were determined for F1 progeny carrying the *UAS-mtm OE* together with *actin5C-Gal4* driver allele. *Actin5C-Gal4* line was also crossed with wild-type w^{1118}, and F1 progeny carrying *actin5C-Gal4* allele was used as the driver control. Besides, *UAS-mtm OE* lines were crossed with w^{1118}, and F1 progeny carrying the *UAS-mtm OE* allele was used as the UAS-line control.

Total RNA was isolated from 14 young adult flies of each genotype, cDNA was synthesized by reverse transcription and Real Time PCR was performed with mtm_RT and actin79b_RT primer pairs. mtm_RT primer pair was designed from the first and second exon that harbors an intron in-between to allow detection of any genomic DNA contamination. Expected PCR product size was 162 bp for *mtm*. Design of actin79b_RT primer pair is explained in Section 5.1.1, and it amplifies a product of 167 bp. Average cycle threshold (CT) values of experimental triplicates were calculated. The deviations between CT values of experimental triplicates were low indicating that the pipetting differences were negligible. *Actin79b* was used as a reference gene; thus, *mtm* CT values were normalized to *actin79b* CT values.

The fold differences between cDNAs of *mtm* overexpressed flies and its driver and UAS-line controls were calculated by Comparative CT ($2^{-\Delta\Delta CT}$) method and statistically analyzed. The mean fold changes indicating the expression levels compared to controls was shown in Figure 5.12.

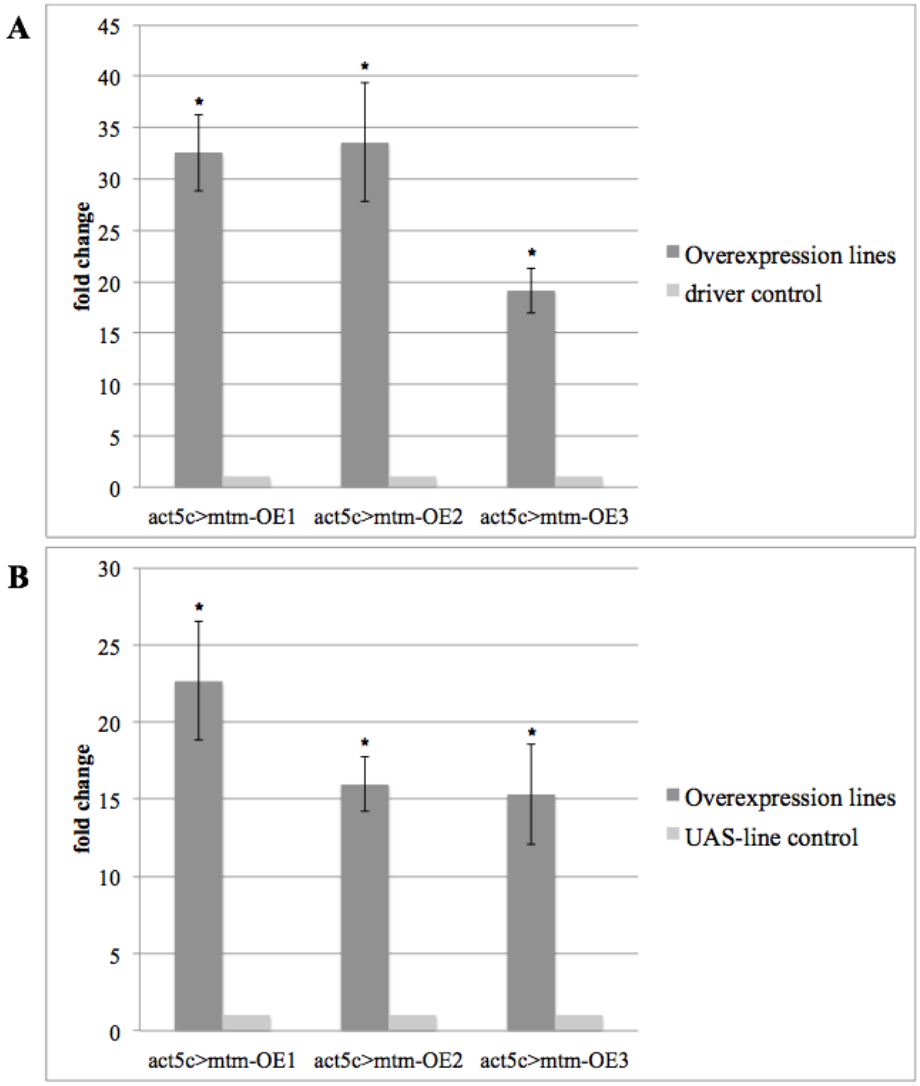

Figure 5.12. Expression level quantification for ubiquitous overexpression of *mtm* by qRT-PCR. (A) display of expression level compared with the driver control, (B) display of the expression level compared with the UAS-line control. Bar graphs indicate the mean fold change of biological triplicates of *actin5C-Gal4* driven *mtm* overexpression (act5c>mtm-OE) compared to controls. Mean fold change ± SEM (n=3). *: $P<0.05$.

For the three different *mtm* overexpression lines that were used, ubiquitous *mtm* overexpression had led to 32-fold, 33-fold, and 18-fold increase in *mtm* mRNA level compared to the driver control, respectively (Figure 5.12A). Compared to each UAS-line control, a 22-fold, 15-fold, and 14-fold increase in *mtm* mRNA levels was observed, respectively (Figure 5.12B). Two-tail paired Student's t-test indicated that all results are statistically significant. Furthermore, the specificity of amplification with mtm_RT and actin79b_RT primer pairs was confirmed by melting curve analysis. Single peaks were

observed at 86.5°C and 86°C corresponding to specific melting temperatures of *mtm* and *actin79b* products, respectively (data not shown). According to these results, first overexpression line, *UAS-mtm OE L1* was selected to be used in further experiments.

5.2.2. Polyclonal Antibody Generation against mtm

In order to generate polyclonal antibodies, high yield production of mtm protein was necessary. Thus, *mtm* was cloned into pET30a vector by Kaya Akyüz to allow IPTG induced overexpression of recombinant mtm protein with a His-tag (six histidine residues) at the amino or carboxyl terminus. He also performed the transformation of the vector into the Rosetta cells that provide rare codon tRNAs for better expression. Cells were induced with 1000 µM of IPTG at 20°C overnight, and lysed with TCA to test the induction (Figure 5.13). IPTG induction was successful based on the observation of a thick band in the induced sample corresponding to His-tagged mtm protein. Inductions with lower IPTG concentrations were performed for optimization, and 1000 µM was found to be most efficient (data not shown); thus induction conditions remained unchanged throughout the experiments.

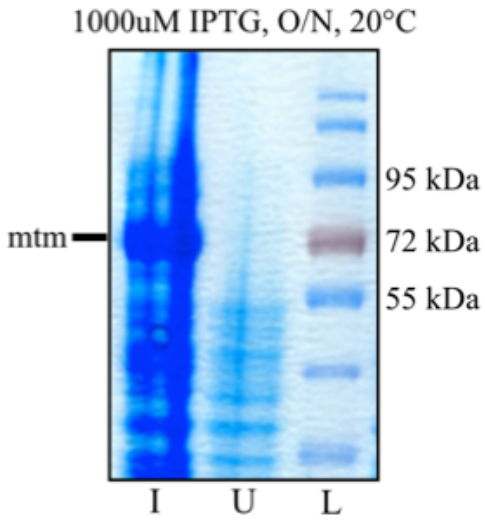

Figure 5.13. SDS-PAGE analysis of pET30aX6HIS-mtm transformed Rosetta cells that were lysed with TCA. His-tagged mtm is 74.6 kDa; I: induced, U: uninduced, L: PageRuler Prestained Protein Ladder.

Recombinant mtm protein with the His-tag (74.6 kDa) was generated for purification with the Nickel column since nickel ions hold the histidine residues. Buffers with high urea concentration at different pH values were used for Ni-column purification. Therefore, *mtm* overexpressing Rosetta cells were lysed at pH 8.0 and run through the column. Histidine residues were expected to bind to the column at high pH. Then, column was washed with wash buffer at pH 6.3, to get rid of non-specifically bounded proteins. Lastly, elution buffer with pH 4.5 was run through the column to reduce the affinity of His-tag for nickel ions and elute bounded proteins. SDS-PAGE analysis of the uninduced and induced lysates, flow through (which is collected after running the lysate through the column), wash, and elution fractions showed that mtm protein was induced in the cells; however, it could not bind to the column since it appeared at a similar amount in the induced and flow through samples. Moreover, no trace of mtm was found in the elution fractions (Figure 5.14). Therefore, we decided to use gel extraction method to purify mtm protein.

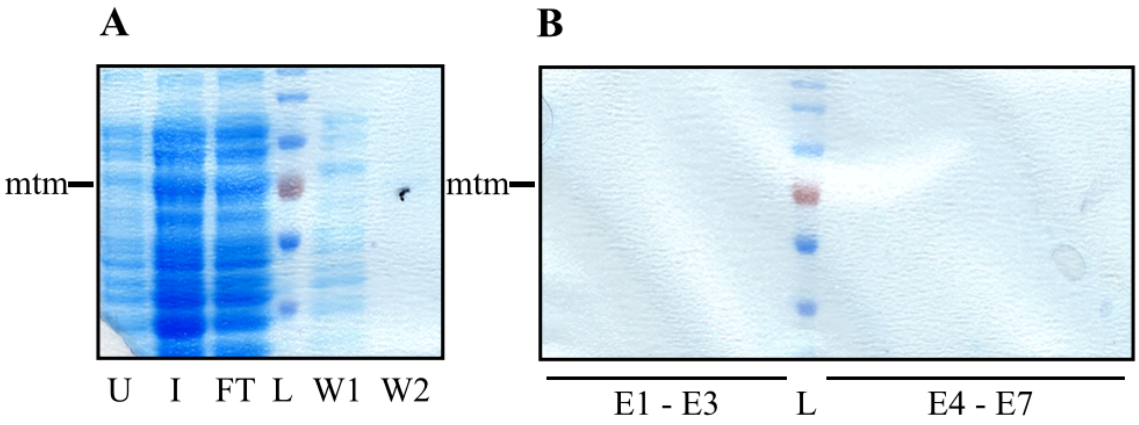

Figure 5.14. Purification of mtm protein by Nickel column. Induced (I) and uninduced (U) samples, flow through (FT), wash fractions (W1, W2) (A) and Elution fractions (E1-E7) (B) were run on polyacrylamide gel. L: PageRuler Prestained Protein Ladder.

Before gel extraction, IPTG induced cells overexpressing *mtm* were lysed with sonication in 1xPBS, centrifuged, and supernatant and pellet were run on polyacrylamide gel to determine in which phase mtm protein resides. SDS-PAGE analysis showed that mtm protein mostly resides in the pellet (Figure 5.15); therefore, we decided to perform gel extraction using the pellet.

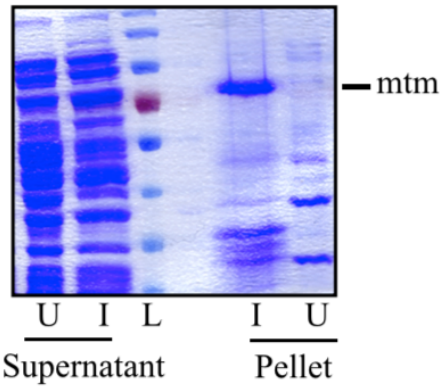

Figure 5.15. SDS-PAGE analysis of supernatant and pellet of lysed cells. U: uninduced, I: Induced, L: PageRuler Prestained Protein Ladder.

Gel extraction was performed after pellet was washed with 1xPBS and centrifuged three times to get rid of other proteins (Figure 5.16A). Then, pellet was loaded to polyacrylamide gel and region where mtm protein is found was extracted from the unstained gel. Samples containing the purified mtm protein were analyzed with SDS-PAGE afterwards (Figure 5.16B). Isolation of the mtm protein was also verified by western blotting with His-probe antibody (Figure 5.16C) that recognizes the histidine residues.

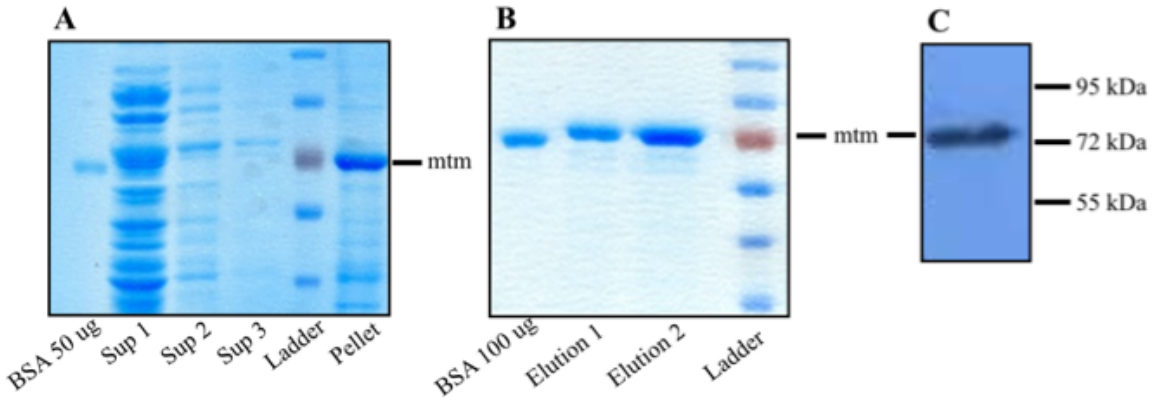

Figure 5.16. Purification of mtm protein by gel extraction. (A) SDS-PAGE analysis of the clean pellet and washes (sup) (B) SDS-PAGE analysis of elutions after gel extraction containing purified mtm protein. (C) Western blotting of purified mtm protein with anti-His antibody. BSA was loaded to assess concentration of the samples.

After a successful purification verified by western analysis, mtm protein was injected to rabbits as the antigen source. A total of six injections were performed and blood samples were collected from the animals after the third injection to test the cross-reactivity of the serum with mtm antigen. Western blotting performed on purified mtm antigen using the serum collected after 3rd injection as the primary antibody confirmed that the serum contained anti-mtm antibodies (Figure 5.17). All collected sera were sent to Prof. Fatma Yücel in TUBITAK MAM, Kocaeli for polyclonal antibody purification. They have used HiTrap Protein G column to purify the polyclonal antibodies (immunoglobulins) produced against mtm. They performed ELISA to distinguish the elution samples with the highest antibody concentrations. High antibody containing elution samples were retrieved from them to be used as polyclonal antibody source against mtm in western blotting.

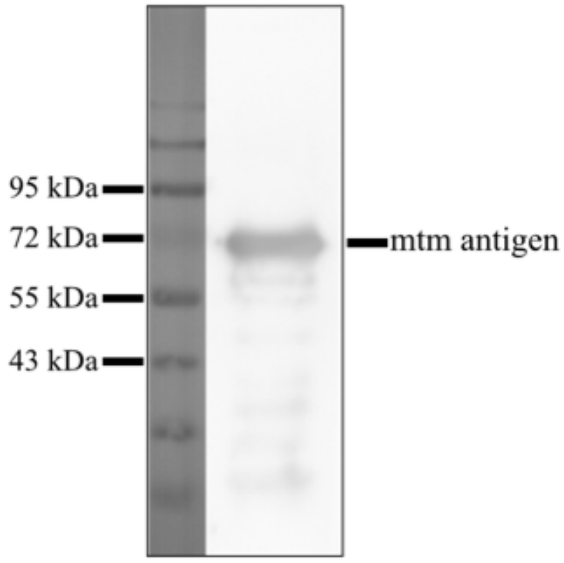

Figure 5.17. Western Blot analysis of mtm antigen using rabbit serum as the primary antibody.

5.2.2.1. Western Blot Analysis of Drosophila Lysates with Anti-mtm Antibody. Before testing the polyclonal antibody on fly lysates, a preliminary western blot was performed to verify the cross-reactivity of the purified antibody with the mtm antigen (Figure 5.18A). Purified polyclonal antibody recognized the mtm antigen showing that it can be used on fly lysates to observe the expression of endogenous mtm protein. Thus, as the next step, anti-mtm antibody was tested on lysates of wild type and ubiquitous *mtm* overexpressing flies. Overexpression of mtm was achieved by crossing the *UAS-mtm OE* line with the

ubiquitous *actin5C-Gal4* driver line. On the western blot, a thick band was observed below 72 kDa in the overexpression sample, which probably corresponds to the endogenous mtm protein of 69.8 kDa (Figure 5.18B). In order to reduce the non-specific bands especially between 43 to 95 kDa, anti-mtm antibody was pre-adsorbed by incubation in compound heterozygous mtm mutant ($mtm^{\Delta 210}/mtm^{\Delta 77}$) larvae, overnight. Western blotting repeated with the pre-adsorbed anti-mtm antibody allowed a more clear observation of the difference between endogenous mtm levels of overexpression and wild type. In addition, most of the non-specific bands were weakened, even though a total clean up was not accomplished (Figure 5.18C). These results indicate that polyclonal antibody generation was successful, and anti-mtm antibody can be used in western blotting after optimizations for cleaner results.

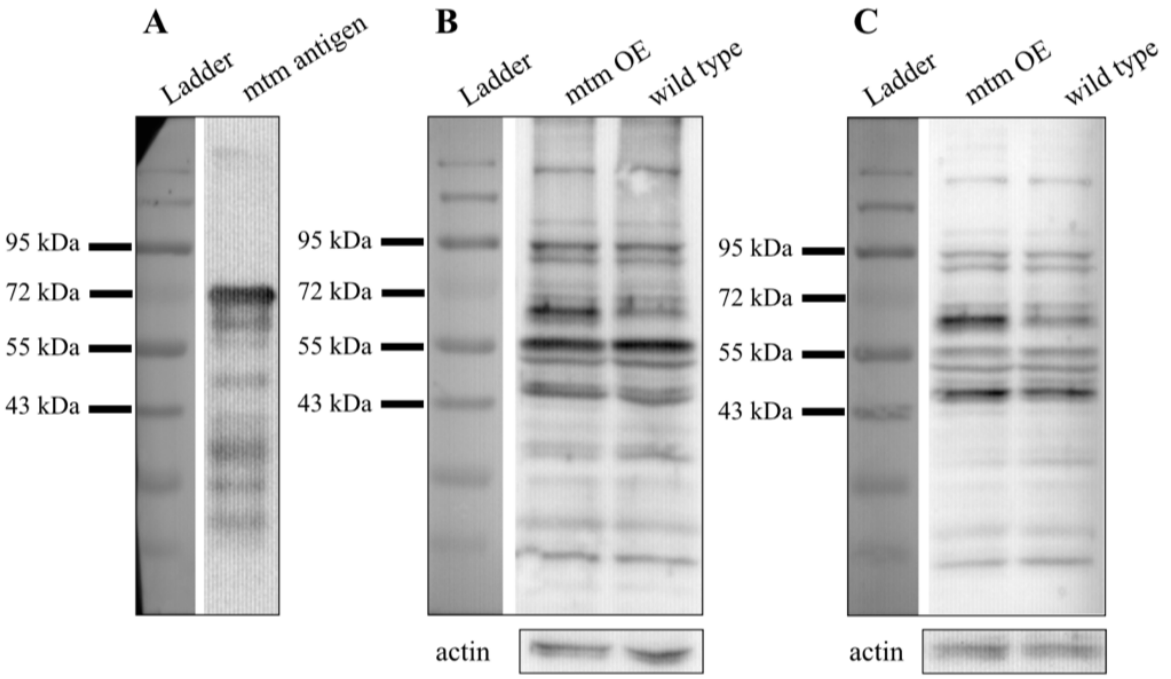

Figure 15.18. Western blot analysis of mtm antigen (A) and fly lysates (B,C) with anti-mtm (A,B) and pre-adsorbed anti-mtm antibody (C). (B,C) mtm OE stands for ubiquitous *mtm* overexpressing flies. Actin was used as loading control.

5.2.3. Analysis of the Effects of *mtm* Expression Level on *Drosophila* Lifespan

Male and female flies were followed over 90 days by counting the number of dead flies in every 3 days. The survival plots were drawn and statistically analyzed for *actin5C-*

Gal4 driven *mtm RNAi control* line, *mtm* overexpression line, *hMTMR2* overexpression line, *mtm RNAi/hMTMR2* rescue line and w^{1118} wild type line using an online tool (Figure 5.19, Yang et al., 2011).

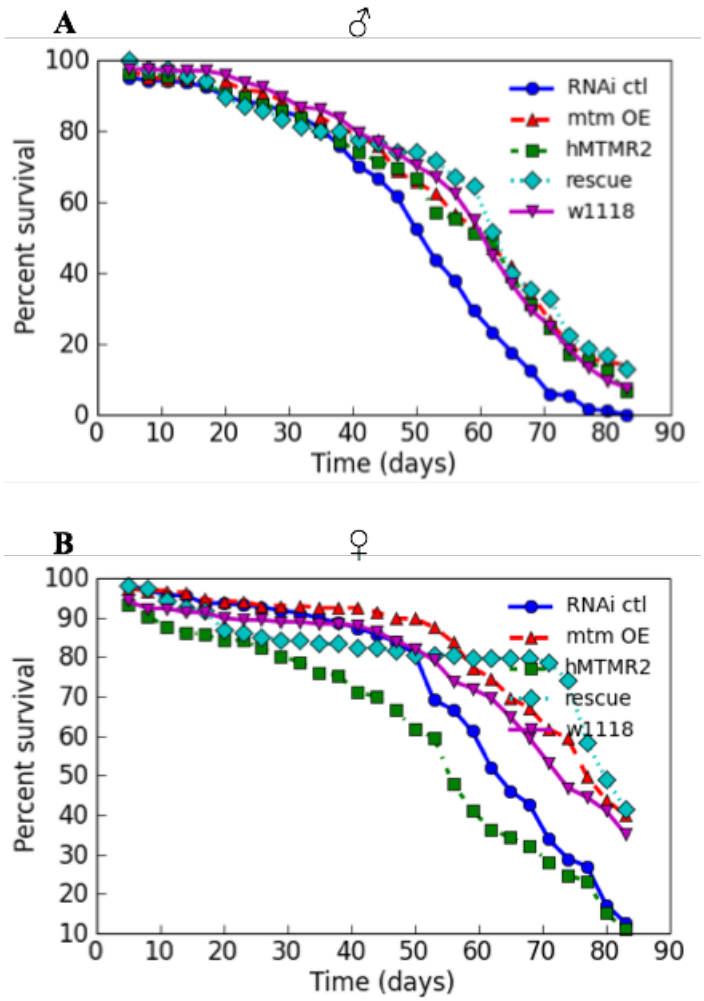

Figure 5.19. Survival plots for males (A) and females (B) of five genotypes. RNAi ctl: ubiquitous *mtm* downregulation control, mtm OE: ubiquitous *mtm* overexpression, hMTMR2: ubiquitous human *MTMR2* overexpression, rescue: ubiquitous human *MTMR2* overexpression in *mtm* downregulated background, w1118: wild type line as control. (Yang *et al.*, 2011).

Ubiquitous downregulation of mtm resulted in pupal lethality in both males and females. Longevity analysis of its control line carrying the *actin5C-Gal4* allele (RNAi ctl) proved that the lethality was not due to the presence of the RNAi cassette since control males and females were viable for quite some time. Moreover, lethality was rescued by

ubiquitous *hMTMR2* overexpression in *mtm* downregulated background both in males and females (Figure 5.19), which also verifies that *mtm* is the *Drosophila* homolog of *MTMR2*. Ubiquitous overexpression of *mtm* or *hMTMR2* did not have any effect on the lifespan of male flies (Figure 5.19A). However, *hMTMR2* overexpression resulted in lowered percent survival compared to wild type in females.

Detailed survival analysis in terms of mean lifespan and age in mortality percentage is listed in Tables 5.6 and 5.7 for males and females, respectively. Both survival plots and detailed analysis showed that males had lower percent survival over time compared to females in general except for the females with ubiquitous *hMTMR2* overexpression. They had a mean lifespan that was close to that of males with the same genotype.

Table 5.6. Detailed longevity analysis for males of five genotypes.

Genotype	**No. of subjects**	**Restricted mean**			**Age in days at % mortality**			
		Days	**Std. error**	**95% C.I.**	**25%**	**50%**	**75%**	**95% Median C.I.**
RNAi ctl	187	49.73	1.33	47 ~ 52.34	41	53	62	50 ~ 53
mtm OE	166	57.59	1.60	54.45 ~ 60.73	47	62	74	56 ~ 62
hMTMR2	105	56.14	2.07	52.08 ~ 60.21	41	62	71	53 ~ 62
rescue	85	58.86	2.32	54.31 ~ 63.41	47	65	74	62 ~ 65
w^{1118}	195	58.32	1.34	55.69 ~ 60.96	47	62	74	59 ~ 62

Table 5.7. Detailed longevity analysis for females of five genotypes.

Genotype	**No. of subjects**	**Restricted mean**			**Age in days at % mortality**			
		Days	**Std. error**	**95% C.I.**	**25%**	**50%**	**75%**	**95% Median C.I.**
RNAi ctl	204	62.09	1.35	59.43 ~ 64.74	53	65	80	62 ~ 65
mtm OE	185	70.14	1.40	67.39 ~ 72.89	62	77	-	77 ~ 80
hMTMR2	146	53.47	2.04	49.48 ~ 57.46	41	56	74	56 ~ 56
rescue	108	69.03	2.34	64.44 ~ 73.62	74	80	-	77 ~ 83

Table 5.7. Detailed longevity analysis for females of five genotypes. (cont.)

w^{1118}	207	65.88	1.60	62.76 ~ 69.01	56	74	-	71 ~ 77

According to detailed longevity analysis, mean lifespan of males were quite similar to each other except for the *mtm* RNAi control. On the other hand, females in which *hMTMR2* was ubiquitously overexpressed had a mean lifespan that was 12 days and 16 days shorter than the wild type and rescue flies, respectively.

Fisher's exact test was performed to males and females for statistical analysis, and results could be found in Table 5.8 and Table 5.9, respectively. *P*-values indicate that no significant difference was observed between males in terms of lifespan (Table 5.8). *hMTMR2* overexpression in females resulted in a shorter lifespan that was statistically significant when compared to wild type; however, the difference between *hMTMR2* overexpressed females and RNAi rescues in terms of mean lifespan was only significant at the later stages of life (Table 5.9).

Table. 5.8. Fisher's exact test results for males.

Condition	**Statistics**			
	P-value at 25%	**P-value at 50%**	**P-value at 75%**	**P-value at 90%**
mtm OE vs. w^{1118}	0.9010	0.7512	0.3663	0.7887
hMTMR2 vs. w^{1118}	0.3286	0.6276	0.7930	0.7276
rescue vs. w^{1118}	1.0000	0.3623	0.4014	0.2751
rescue vs. hMTMR2	0.6138	0.7705	0.2580	0.5616

Table. 5.9. Fisher's exact test results for females.

Condition	**Statistics**			
	P-value at 25%	**P-value at 50%**	**P-value at 75%**	**P-value at 90%**
mtm OE vs. w^{1118}	0.0307	0.3328	0.0150	0.6096
hMTMR2 vs. w^{1118}	0.0001	<0.00001	<0.00001	<0.00001
rescue vs. w^{1118}	0.6344	0.0003	0.0240	0.2724
rescue vs. hMTMR2	0.1641	<0.00001	<0.00001	<0.00001

5.2.4. Investigation of *mtm* IMAGO Targeting Vector Integration

In a previous study in our lab, *mtm* mutant fly lines were being developed using IMAGO approach. In order to delete *mtm* gene from fly genome via homologous recombination, Merve Kılınç designed a targeting vector carrying the flanking homology regions of *mtm* (Figure 5.20). Bacterial clone of the designed vector was sent to Genetic Services, Inc., USA for injection into embryos with white-eye background (*w*). After receiving vector injected *Drosophila* lines, it was observed that the flies had red eyes indicating that the targeting vector (mtm_pP{white-STAR}) was integrated to the genome since it carried a red eye marker (w^+). Kılınç also confirmed that the vector was integrated on the X chromosome by chromosome mapping and generated homozygous fly lines carrying the vector (*IMAGO mtm L1* and *IMAGO mtm L2*) (Kılınç, 2013).

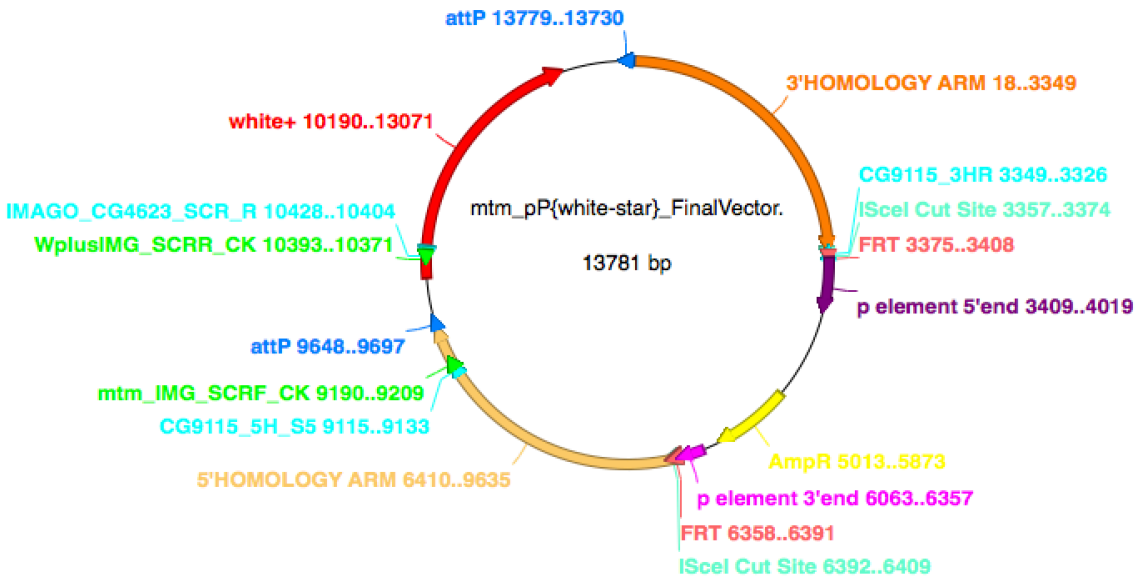

Figure 5.20. Graphic map of mtm_pP{white-STAR} vector injected to fly embryos. Vector contains *P*-element arms for genomic integration; 5' and 3' homology arms of *mtm*; red eye marker (w^+); FRT sites and *I-Sce*I sites for *mtm* knock-out and attP sites for knock-ins.

In order to verify correct genomic integration of the vector, gradient PCR was performed with gDNA from *IMAGO mtm L1* and *L2* flies with CG9115_5HS5 and IMAGO_CG4623_SCR_R primers that were designed from the 5' homology arm of *mtm* and w^+ gene (Figure 5.20). Different concentrations of $MgCl_2$ and DMSO addition were

tested to increase the efficiency and specificity of the reaction, respectively. More non-specific bands were observed as the temperature and $MgCl_2$ concentration increased. Addition of DMSO resulted in increased specificity, however, the expected PCR product was not observed. A slightly visible band was present in the vicinity of the expected size (1314 bp) in *IMAGO mtm L1*; however it was too weak to be specific. Overall, a specific band of the expected size of 1314 bp was not observed in any of the fly lines at any condition or temperature. In order to confirm that gDNA extraction was successful, another primer pair was used to amplify a 368 region from the genome. The existence of the expected band suggested the problem was not due to the method of gDNA extraction (Figure 5.21).

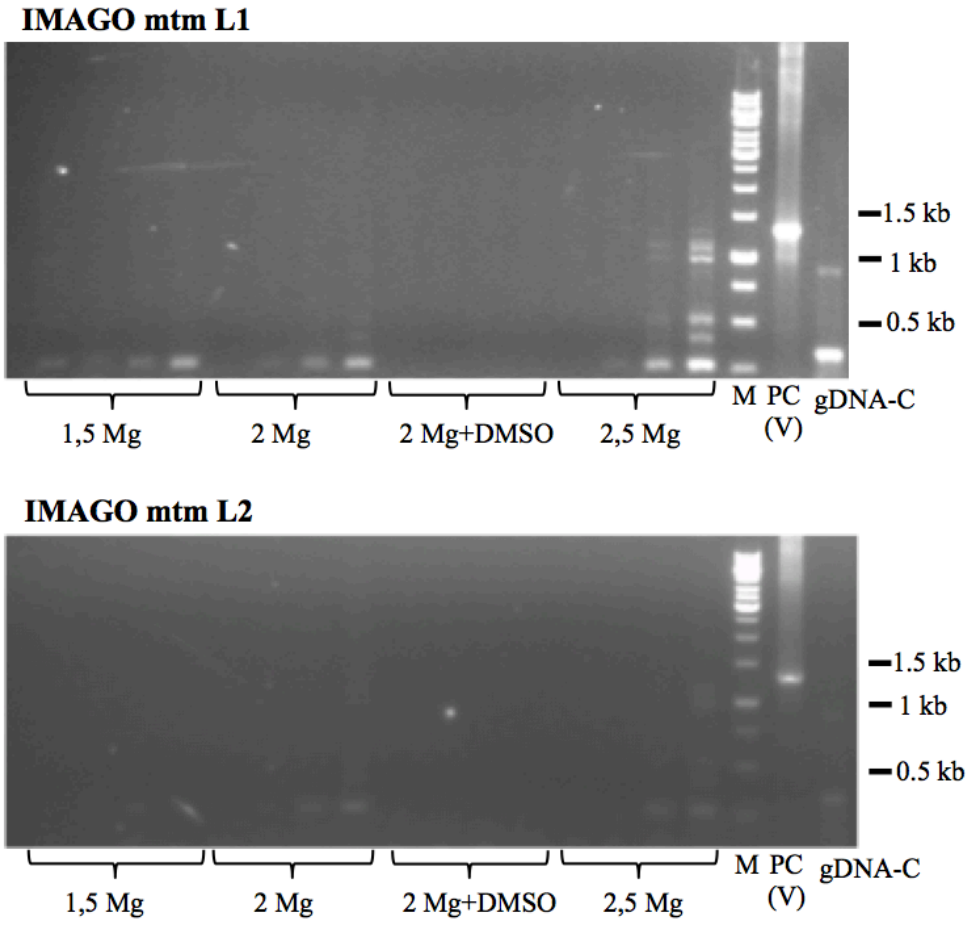

Figure 5.21. Gradient PCR with gDNA of *IMAGO mtm L1* and *L2* flies at increasing $MgCl_2$ concentrations and with/without DMSO. Annealing temperatures: 59.5°C, 56.4°C, 52.1°C, 50°C; $MgCl_2$: 1,5 mM, 2 mM, 2.5 mM (Left to right). M: 1 kb DNA ladder, PC(V): positive control (vector), gDNA-C: gDNA control. CG4623_5HS3 and CG4623_5HRS2 primers were used to amplify a 368 bp region as gDNA control.

A new gradient PCR with same primer pair and addition of glycerol and Tween in different $MgCl_2$ conditions was performed with *IMAGO mtm L1* genomic DNA only since it did give a slight, though probably non-specific band in the vicinity of the expected size. Glycerol increased the specificity and resulted in no bands while Tween increased the non-specific binding. At 2,5 mM $MgCl_2$ concentration and addition of Tween, a band near the expected size of 1314 bp was slightly visible together with other bands again suggesting that it is most probably due to a non-specific amplification (Figure 5.22).

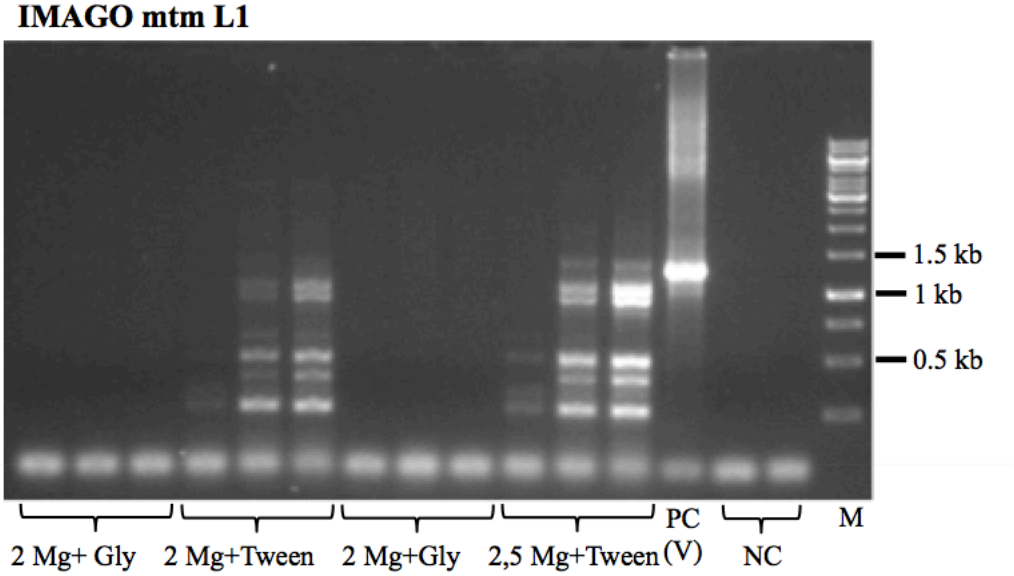

Figure 5.22. Gradient PCR with gDNA of *IMAGO mtm L1* flies at two $MgCl_2$ concentrations and presence of Glycerol (Gly) or Tween. From left to right: Annealing temperatures are 56.4°C, 52.1°C and 50°C, $MgCl_2$ concentrations are 2 mM and 2.5 mM. PC(V): positive control (vector), NC: negative control, M :1 kb DNA ladder.

As a final attempt, to perform nested PCR, a new primer pair (mtm_IMG_SCRF_CK and WplusIMG_SCRR_CK) was designed from 5' homology arm of *mtm* and w^+ gene to check the integration of mtm_ pP{white-STAR} vector to the fly genome (Figure 5.20)., Nested PCR was performed with two primer pairs. The first PCR was performed with gDNA of *IMAGO mtm L1* and *L2* flies and CG9115_5HS5 and IMAGO_CG4623_SCR_R primers. Then, the second PCR was performed with the product of the first PCR and mtm_IMG_SCRF_CK and WplusIMG_SCRR_CK primer pair, which amplifies a region inside the product of the first PCR. Both PCR products were loaded on agarose gel after

the nested PCR however, the expected 1204 bp band was not observed as a result of the second PCR (Figure 5.23).

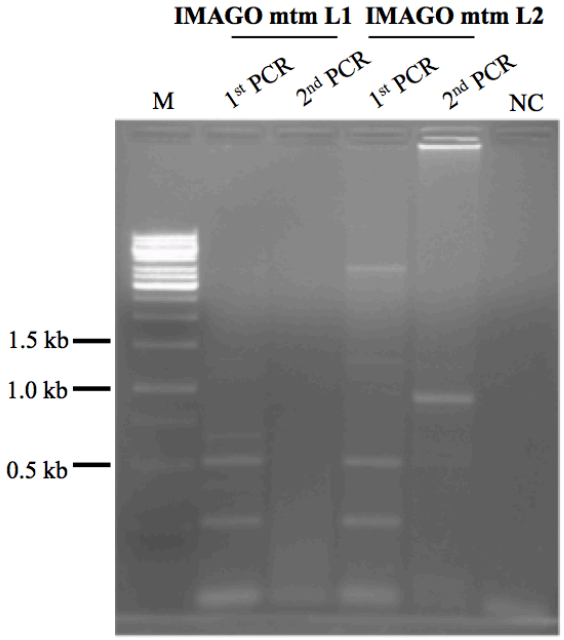

Figure 5.23. Nested PCR with gDNA of *IMAGO mtm L1* and *L2* flies. CG9115_5HS5 and IMAGO_CG4623_SCR_R primer pair is used in the first PCR and mtm_IMG_SCRF_CK and WplusIMG_SCRR_CK primer pair is used in the second PCR. M: 1 kb DNA ladder, NC: negative control.

Although *IMAGO mtm L1* and *L2* lines were both red-eyed (carrying the w^+ gene somehow), verification of the integration of the targeting vector by PCR failed. Thus, integration of the vector was tested by flippase activity, which is explained in Section 5.1.4 in detail. *IMAGO mtm L1* and *L2* lines were crossed with *w;;eyFLP*, *TM3,Sb/TM6B* line separately. F1 progeny was expected to include white-eyed flies in the presence of both *IMAGO* and *eyFLP* alleles since flippase enzyme that is expressed in the eye would cut out the *w+* (red eye) gene from the integrated vector. F1 progeny was selected against *Sb* (short bristle) and screened for white-eyed flies. Even though more than 150 flies were screened for both lines, no white-eyed flies were observed (Table 5.10). These are consistent with the results of PCR experiments. Thus, it was concluded that the targeting vector for IMAGO was integrated to the genome in an incorrect manner.

Table. 5.10. Screening results for F1 progeny to test IMAGO targeting vector integration.

	Number of red-eyed flies	**Number of white-eyed flies**
$\frac{\text{IMAGO mtm,w+ L1}}{+/\rightarrow}$;; $\frac{\text{TM3,Sb eyFLP}}{+}$	233	0
$\frac{\text{IMAGO mtm,w+ L2}}{+/\rightarrow}$;; $\frac{\text{TM3,Sb eyFLP}}{+}$	159	0

6. DISCUSSION

In this study, we aimed to generate *Drosophila* models for CMT, and further investigate them from different aspects. I have focused on two causative genes, *GDAP1* and *MTMR2,* of the autosomal recessive form of the disease (CMT4) since this subtype is more frequent in regions with high percentage of consanguineous marriages like Turkey, and results in more severe symptoms with early onset. We have chosen *GDAP1* because it is one of the few CMT-causative genes in which recessive or dominant mutations lead to demyelinating, axonal or intermediate forms of the disease with ranging onset and/or severity. Furthermore, GDAP1 is thought to have a function in mitochondrial dynamics since abnormalities in mitochondrial morphology and dynamics were described upon changing *GDAP1* expression levels or introducing mutations in *in vitro* and *in vivo* studies (Niemann *et al.*, 2005; Pedrola *et al.*, 2005; Niemann *et al.*, 2014; Lopez Del Amo *et al.*, 2014). Mitochondria are the power supply of the cells; thus disruptions in its morphology and dynamics can distress high energy demanding peripheral neurons and lead to neuropathies with impaired motor performances. Mutations in *MTMR2* also cause autosomal recessive demyelinating CMT, classified as CMT4B1. MTMR2 is known to have a role in regulation of endocytosis and membrane trafficking, which are crucial mechanisms for proper functioning of the neurons. Therefore, both *GDAP1* and *MTMR2* are good candidates to study CMT from functional and behavioral aspects.

Drosophila was chosen as a model organism for our studies since both *GDAP1* and *MTMR2* have functional homologs in the flies. We have decided to model CMT on flies by altering the expression levels of the *CG4623* and *mtm*, homologues of *GDAP1* and *MTMR2,* respectively. Thus, we first verified the downregulation of *CG4623* and overexpression of *CG4623* and *mtm* in the fly lines used at the mRNA level. Furthermore, we investigated the effect of these changes in *CG4623* expression on the locomotor behavior of the flies. Also a polyclonal antibody was produced for *mtm* that can be used in further localization and functional studies. Lastly, we have examined the effects of *CG4623* and *mtm* expression level alterations on the lifespan of the flies.

In order to model CMT through alteration of *CG4623* expression, we have used the commercially available *UAS-CG4623 RNAi* line for downregulation and *UAS-CG4623 OE1, UAS-CG4623 OE2,* and *UAS-CG4623 OE3* lines that were previously generated in our laboratory by Kaya Akyüz, for overexpression. Quantitative RT-PCR revealed that *CG4623* mRNA level was reduced by 96% and 93% in ubiquitous downregulation flies when compared to driver and *UAS- RNAi* line controls, respectively. For the ubiquitous overexpression flies *CG4623* expression showed over 20-fold increase in all three different lines when compared to both driver control and UAS-line controls of each. In these studies, to make sure that the expression level differences were caused only by downregulation and overexpression, we compared the expression levels with a driver control that carries the driver allele, *act5C-Gal4,* on wild type background, and a UAS-line control that carries the relevant UAS responder allele on wild type background. In this way, we eliminated the sole effect of driver and responder alleles on the observed expression levels. All qRT-PCR results were statistically significant confirming that *CG4623* expression levels were successfully altered and these lines are suitable for further experiments.

Since there was no commercially available antibody for *CG4623*, we could not check the expression at the protein level in the time course of this study. However, recently Elif Begüm Gökerküçük from our laboratory has generated a polyclonal antibody against *CG4623* which is promising to be used to profile expression at the protein level.

Once the lines were verified, negative geotaxis assay was performed to shed light onto the effects of alterations in *CG4623* expression levels on the climbing behavior of the adult flies. Our aim was to observe a decline of motor performance with age to recapitulate the CMT phenotype in flies. This assay was a first at our laboratory and department; therefore, optimizations and modifications of a well-established version of the assay were essential in the beginning. A modified version of the Rapid Iterative Negative Geotaxis assay (RING) was developed in our laboratory by changing some of the materials and the recording method (Gargano *et al.*, 2005). We have used longer tubes than suggested to record the climbing behavior at five seconds after the start of the movement. Besides, rather than taking photographs at five seconds we recorded a video of the whole process to perform the analysis easily. Five seconds after the start of the movement was chosen as the

time point to compare the climbing distances of the experiment and control flies because it was long enough for older flies to climb and short enough for youngers not to gather on the top of the tubes. As we wanted to determine whether any observed changes in the behavior were due to a degenerative process, we carried out our experiments at three different time points from young to old: nine, 20 and 30 days old and nine, 12, and 15 days old for flies raised at 25°C and 29°C, respectively. Usually climbing assays are performed on one gender only because it takes less time and the choice of gender is up to the researcher. We have decided to perform the tests on both males and females since we also aimed to optimize the gender selection for the future. According to our results, test performance was not affected by the gender selection; however, the egg rhythm of females could be a confounding factor. Therefore, future tests may be performed on males only.

Negative geotaxis assay was performed using ubiquitous and neuron-specific drivers in order to understand the effect of *CG4623* expression level alterations on motor performance from both a broader and neuronal perspective. Ubiquitous downregulation of *CG4623* did not cause any statistically significant difference in climbing behavior of the younger males and females; however we observed that old males and females of 30 days of age climbed a significantly shorter distance than the controls. Furthermore, ubiquitous overexpression of *CG4623* resulted in longer distance climbing of young (nine days old) males and females whereas old flies (30 days old) again climbed a shorter distance than the controls. All of these statistically significant results indicate that alteration of *CG4623* expression level affects the climbing behavior of the flies. Shorter distance climbing was observed in later times in life in both ubiquitous downregulation and overexpression of *CG4623* suggesting an age-dependent phenotype. Moreover, observing this age-dependent phenotype in high levels of *CG4623* expression contributes to the idea that overexpression of *CG4623* might serve as a model for gain-of function mutations of *GDAP1*.

A neuronal driver with Dicer enzyme was chosen in this study to increase the efficiency of RNA degradation in downregulation of *CG4623*. Dicer works best at higher temperatures; thus, flies were raised at 29°C for neuron-specific downregulation. Since at 29°C the lifespan of *Drosophila* is about a month, the climbing behavior of nine, 12 and 15 days old flies were analyzed. Males with *CG4623* downregulation in neurons climbed a shorter distance than controls, in all age groups whereas only old females (15 days old)

were significantly slower than controls. The age-dependent phenotype observed in both males and females in ubiquitous downregulation of *CG4623* was only observed in females with neuron-specific downregulation. This might be due to our choice of age groups because males live shorter than females and even nine days might be too old to catch the beginning of the phenotype at 29°C. However, the results of neuron-specific downregulation in females are consistent with the ubiquitous downregulation results. This finding suggests a cell autonomous mechanism, supporting the idea that neuronal loss of *CG4623* expression might be sufficient for the progressive decline of motor performance. The results in neuron-specific overexpression flies that were raised at 25°C showed significant shorter distance climbing in aged males (30 days old) only. These findings are also consistent with the age-dependent decline of motor performance phenotype observed in ubiquitous *CG4623* overexpression. They suggest a cell autonomous mechanism indicating that excess CG4623 levels in neurons also lead to impairments in motor abilities. Females with neuron-specific *CG4623* overexpression climbed a longer distance than controls when they were young (nine days old); however as they aged it was impossible to compare since both controls and experimental samples were nearly motionless. This immobility might be caused by the driver. To overcome this unwanted effect in the future, another control carrying only the *UAS-Dicer* allele on wild type background can be analyzed in terms of climbing.

Age-dependent motor performance decline in flies with altered levels of CG4623 recapitulates the CMT phenotype. It is also supported by the findings of Galindo's group in Spain. They have shown that changes in *CG4623* expression level in a tissue-specific approach resulted in abnormal mitochondrial morphology and degeneration in adult retina and muscles with increasing severity in an age-dependent manner (Lopez del amo *et al.*, 2014). Therefore, progressive impairments in mitochondria might be the reason underlying the decline in motor performance. Negative geotaxis assay can be repeated in the future by using muscle-, motor neuron- and glia- specific drivers in order to understand the effects of altered CG4623 levels more thoroughly.

We have optimized and established the negative geotaxis assay in our laboratory even though there is still room for improvement. For instance, experimental sample size can be increased to obtain more solid results especially for *CG4623* expression level

alterations in neurons. In the future, our method can be used to assess motor behavior of any fly model.

In literature, there are very few reports for the analyses of life expectancy in CMT patients and it is expected to be normal. However, lower motor performance and other unknown cellular effects of the mutations may alter the survival rate. In patients with mutations causing the early onset forms of the disease survival may decrease due to the severely affected motor performance. Thus, we wanted to shed light to these hypotheses in our CMT fly models and investigated the effect of *CG4623* expression level alterations on the lifespan of the flies by longevity assay. *CG4623* ubiquitous downregulation in males yielded slightly lowered lifespan with statistical significance while very slight but significant difference in terms of lifespan was observed in females only at the last period of life. Both male and female flies in which *CG4623* is ubiquitously overexpressed yielded mildly lowered lifespan with statistical significance compared to control. These results suggest that expression level alterations in *CG4623* mildly affect the lifespan of the flies. Kaya Akyüz previously showed that loss of *Drosophila* homolog of *Mfn1* and *Mfn2 (Marf)*, which are mitochondrial fusion factors and CMT causative genes, drastically lowered the lifespan of the flies suggesting a vital conserved function (Akyüz, 2013). In the case of *CG4623*, we did not see a drastic effect. Redundancy and compensation of the function of *CG4623* by other factors might be the reasons behind. Furthermore, the expression level alteration might not be sufficient to observe a distinctive change in term of life span; thus analyzing the lifespan of *CG4623* knock-outs and/or mutant *GDAP1* knock-ins might be more illuminative. Moreover, *Mfn2* dominant mutations result in a more severe phenotype with prominent motor deficits in patients when compared to mutations in *GDAP1*. Therefore, loss of *Marf* might be causing a more severe decline of motor performance than *CG4623* expression level alterations resulting in lower survival rates in flies. This phenomenon can be further investigated by performing negative geotaxis assay to the flies lacking Marf.

The results of the negative geotaxis assay and lifespan analysis is promising to suggest that the age-dependent decline of climbing in flies might have an indirect effect on the lifespan. However, in order to test this assumption, further investigation of the cellular functions of CG4623 is necessary.

To model CMT by altering *mtm* expression levels, we have used the commercially available *UAS-mtm RNAi* line and three *UAS-mtm* overexpression lines that were previously generated in our laboratory by Kaya Akyüz. Since ubiquitous downregulation of *mtm* resulted in pupal lethality, expression level differences at mRNA level were quantified for the overexpression lines only. For the first overexpression line, *mtm* mRNA levels were increased by more than 20-fold in flies overexpressing *mtm* ubiquitously compared to both driver and UAS-line controls. This first line was selected to be used in further experiments since in the other two lines increase in expression was significant but lower compared to the first line.

Since an anti-mtm antibody was not commercially available, in order to analyze mtm expression at the protein level, we aimed to generate a polyclonal antibody against it. As an initial step we overexpressed the His-tagged mtm protein in bacteria via IPTG induction. We tried to purify the protein by Nickel column, which has an affinity for His-tag; however we could not elute the protein from the column probably because recombinant mtm protein did not bind to the column due to its large size (74.6 kDa) or it might be forming inclusion bodies *i.e.* insoluble aggregates, which is a common problem encountered in recombinant protein purification from bacteria. Then, the purified protein was obtained by extraction from polyacrylamide gel, and used as an antigen source. The antibody generated in rabbits was tested on western blots of lysates of mtm overexpressing and wild type flies. Overexpression at protein level was confirmed and pre-adsorption of the antibody reduced non-specific results. However, the antibody generated should be further purified to be used in future studies or the overexpression construct may be designed again for a smaller, more distinctive part of *mtm* to avoid the problems in protein purification and non-specificity in western blots. Overall, our antibody is promising and can be used in immunohistochemistry with further optimizations to reveal the expression pattern of mtm. Moreover, determination of subcellular localization of mtm with the optimized antibody would be crucial to elucidate the function and interaction partners of mtm in the vesicle trafficking.

The effect of altered mtm levels on motor performance could not be investigated in the time course of this study since *mtm* downregulation flies are pupal lethal and requires adoption of assays other than negative geotaxis. In the future, an assay that assesses the

movements of the larvae, like larval crawling, may be used. Besides, in order to understand how altered mtm levels affect the motor performance as a whole both up- and down-regulation should be taken into account.

We also investigated the effect of *mtm* expression level alterations on the lifespan of the flies by longevity assay. Pupal lethality in flies was shown to be rescued by overexpression of *hMTMR2* (Velichkova et al., 2010); however, the group did not analyze its effect on lifespan. We found that rescue flies had a normal lifespan and once again verified that *mtm* is the *Drosophila* homolog of *hMTMR2*. Moreover, ubiquitous overexpression of *mtm* or *hMTMR2* did not have any effect on the lifespan of males; only *hMTMR2* overexpression resulted in lower percent survival in females, which was statistically significant compared to wild type. When we compared these results with the effects of *CG4623* expression level alterations on lifespan, we see that downregulation of *mtm* has a more deleterious effect than downregulation of *CG4623* on the survival of the flies implying that mtm has a conserved vital function and it cannot be compensated by other factors in the cell. In the literature, there is only one report showing that CMT patients with *MTMR2* mutations had a shorter lifespan than normal population (Quattrone *et al.*, 1996). Meanwhile, considering early-onset, rapid progression and severity of symptoms in patients with *MTMR2* mutations, it could be assumed that life expectancy could be affected. However, this might not be the case for *GDAP1* since its mutations and phenotype are heterogeneous.

It is important to emphasize that males are more suitable for an 80-90 day long longevity assay. If the females were chosen to be followed in the future, a longer time period for the assay is necessary to obtain more significant results.

In the scope of this study, we also examined the genotype of the flies that were developed at the initial step of *CG4623* and *mtm* knock-out generation. Previously, Kerem Yıldırım and Merve Kılınç aimed to develop CMT fly models by generating *CG4623* and *mtm* mutant lines *via* IMAGO approach. The reason for choosing this approach was the feasibility of creating not only knock-outs of *CG4623* and *mtm*, but also knock-ins of any target sequence. Therefore, it would have been possible to knock-in mutant forms of human homologs of the genes. As a first step of knock-out generation, Yıldırım and Kılınç

designed the IMAGO targeting vectors that carried the marker gene (w^+, red eye) flanked by attP sites (docking sites for the integration of knock-in constructs), 5' and 3' homology arms of *CG4623* or *mtm*, FRT and *ISce*-I sites which were necessary for vector mobilization and linearization and *P*-element arms for initial integration (Figure 5.7 and 5.20, respectively). The vectors were injected into embryos with white-eye background (*w*); however, they did not get any positive results in their further attempts of vector mobilization and linearization crosses, which were necessary for homologous recombination to generate knock-outs. Therefore, in this study the aim was to check the integration of the targeting vectors to the fly genome, in the first place. Even though, fly lines of both genes were red-eyed meaning that they carry the w^+ marker, various genomic PCRs gave negative results for integration. Moreover, no positive results were obtained from the nested PCR, which is a common technique to check vector integration. We have decided to adopt a different approach, and checked the integration by crossing the fly lines with an *eyFLP* line in which flippase enzyme is active in the eye with the expectation to see white-eyed flies in the progeny if the vector was integrated correctly. However, we could not observed white-eyed progeny in any of the fly lines. After long conversations with other colleagues who have used IMAGO for mutant generation, we have concluded that the targeting vectors were integrated to the genome improperly for both *CG4623* and *mtm*. The reason for this could be that the targeting vectors might have been injected to the wrong type of flies. Targeting vectors are designed to integrate to the genome from *P*-element arms via 2-3 delta transposase (Figure 6.1); thus the injection should have been performed to the flies carrying this enzyme. If this was the case, we should have observed white-eyed flies in the progeny of the crosses between the IMAGO lines and the *eyFLP* line since flippase would cut out the w^+ (red eye) gene. However, if the injection was done to flies carrying another enzyme, ΦC31, vectors could have been integrated to the genome randomly from the attP site between the 5' homology arm and w^+ gene. In this case, the 5' homology arm that should have been on the upstream of the w^+ gene would be on the downstream which explains the negative results of the PCRs since the primers do not meet. Moreover, vector backbone would be residing between the FRT sites; therefore, flippase would remove the vector backbone, not the w^+ marker (Figure 6.2). This explains why we could not obtain any white-eyed flies form the eyFLP crosses.

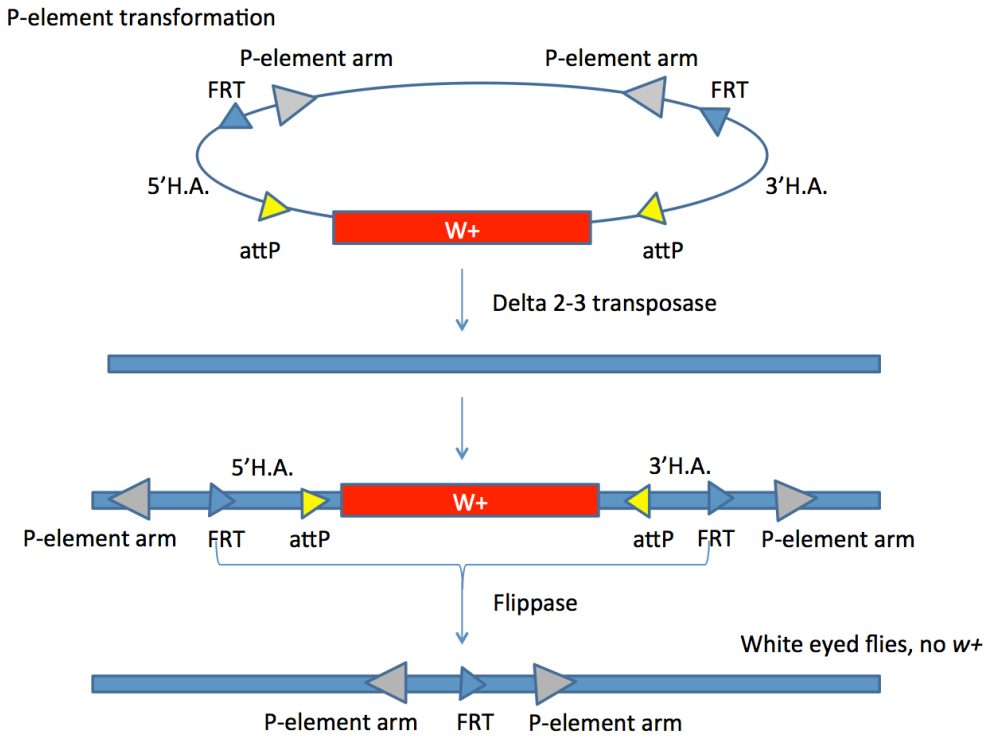

Figure 6.1. Integration of the IMAGO targeting vector (pP{white-STAR}) into the genome via *P*-element transformation.

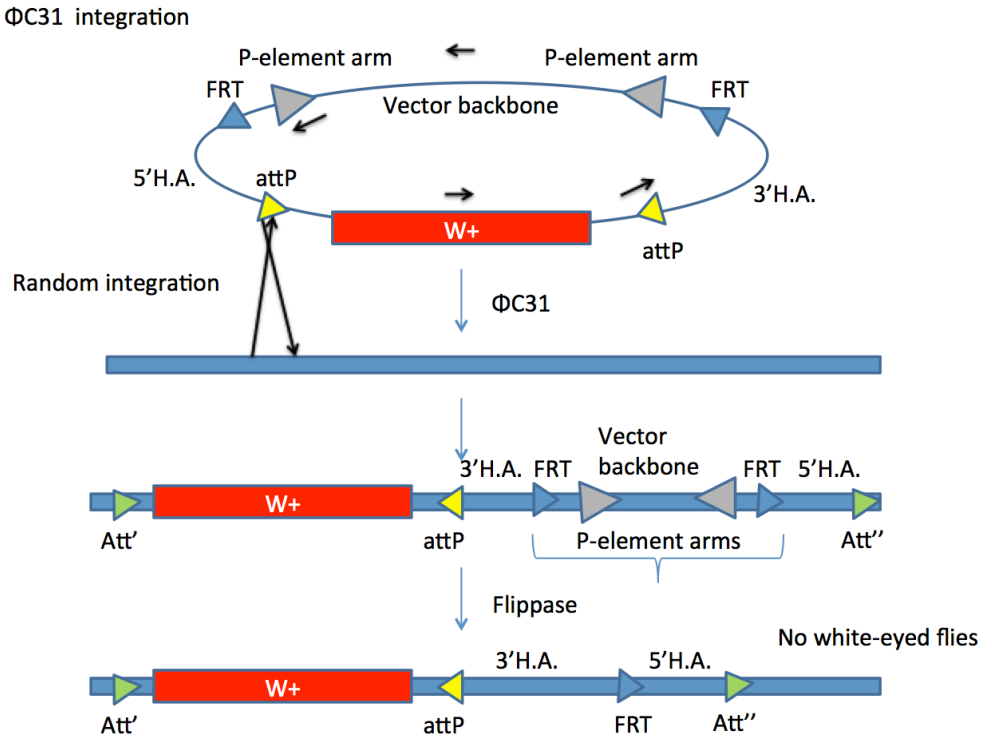

Figure 6.2. Improper integration of the IMAGO targeting vector (pP{white-STAR}) into the genome via ΦC31 integration.

Injections could be repeated to the correct flies in the future in order to generate knock-outs of *CG4623* and *mtm* and further mutant *GDAP1* and *MTMR2* knock-ins, respectively. However, IMAGO has become more time-consuming and exhaustive upon the emergence of the novel approaches in the genome-editing field. For instance, CRISPR system is much more faster and efficient than IMAGO and other homologous recombination techniques. Therefore, adopting novel approaches like CRISPR could be a better choice to generate knock-outs and knock-ins in the future.

We suggest that altering expression levels of *Drosophila* homologs of CMT causative genes is promising to model the disease. In this study, we have recapitulated the CMT phenotype of progressive motor performance decline in flies by altering expression levels of *CG4623*. Also we have produced an antibody against mtm that could be further used to analyze the expression pattern and subcellular localization of the protein. Our longevity analyses suggest expression level alterations of fly homologs of CMT-causing genes might affect survival at different levels depending on the function of the protein. Our results should be verified by repeating these assays on knock-outs and knock-ins of human mutant versions of the genes. Future studies may focus on understanding the functions of these proteins using biochemical methods and *in vivo* live imaging since elucidation of cellular functions of these proteins is essential to understand their contribution to disease mechanisms.

7. CONCLUSION

In this study, we have focused on generating *Drosophila* models of CMT and further investigated them from different aspects. *CG4623* RNAi line and overexpression lines of both *CG4623* and *mtm* were confirmed to alter the expression at mRNA level by qRT-PCR. Negative geotaxis assay revealed that altering *CG4623* expression levels affected the climbing behavior of the flies in an age-dependent manner. Thus, we have recapitulated the CMT phenotype of progressive motor performance decline in flies by altering expression levels of *CG4623.* The anti-mtm antibody that we have developed allowed us to quantify expression level of *mtm* at the protein level by western blot analysis. This antibody could be used in future studies to elucidate the subcellular localization and interaction partners of the protein. Longevity analyses showed that expression level alterations of fly homologs of CMT-causing genes affect survival at different levels depending on the function of the protein. The *Drosophila* models generated for *CG4623* and *mtm* are good candidates to study CMT pathophysiology further, to find biomarkers and, ultimately, to investigate novel therapeutic agents for treatment of peripheral neuropathies.

REFERENCES

Akyüz, H. K., 2013, "*Development of a Drosophila CMT via Overexpression and Knocking-in of GDAP1 gene"*, M.S. Thesis, Boğaziçi University.

Altschul, S. F., J. C. Wootton, E. M. Gertz, R. Agarwala, A. Morgulis, A. A. Schaffer, and Y. K, Yu, 2005, "Protein Database Searches Using Compositionally Adjusted Substitution Matrices", *Federation of European Biochemical Societies Journal*, Vol. 272, No. 20, pp. 5101-5109.

Altschul, S. F., T. L. Madden, A. A. Schaffer, J. Zhang, Z. Zhang, W. Miller, and D. J. Lipman, 1997, "Gapped BLAST and PSI-BLAST: A New Generation of Protein Database Search Programs", *Nucleic Acids Research*, Vol. 25, No. 17, pp. 3389-3402.

Berger, P., A. Niemann, and U. Suter, 2006, "Schwann Cells and The Pathogenesis of Inherited Motor and Sensory Neuropathies (Charcot-Marie-Tooth Disease)", *Glia*, Vol. 54, No. 4, pp. 243-257.

Bier, E., 2005, "Drosophila, The Golden Bug, Emerges as a Tool for Human Genetics", *Nature Reviews Genetics*, Vol. 6, No. 1, pp. 9-23.

Boerkoel, C. F., H. Takashima, M. Nakagawa, S. Izumo, D. Armstrong, I. Butler, P. Mancias, S. C. Papasozomenos, L. Z. Stern, and J. R. Lupski, 2003, "CMT4A: Identification of a Hispanic GDAP1 Founder Mutation", *Annals of Neurology*, Vol. 53, No. 3, pp. 400-405.

Bolino, A., A. Bolis, S. C. Previtali, G. Dina, S. Bussini, G. Dati, S. Amadio, U. Del Carro, D. D. Mruk, M. L. Feltri, C. Y. Cheng, A. Quattrini, and L. Wrabetz, 2004, "Disruption of Mtmr2 Produces CMT4B1-like Neuropathy with Myelin Outfolding and Impaired Spermatogenesis", *The Journal of Cell Biology*, Vol. 167, No. 4, pp. 711-721.

Bolino, A., M. Muglia, F. L. Conforti, E. LeGuern, M. A. Salih, D. M. Georgiou, K. Christodoulou, I. Hausmanowa-Petrusewicz, P. Mandich, A. Schenone, A. Gambardella, F. Bono, A. Quattrone, M. Devoto, and A. P. Monaco, 2000, “Charcot-Marie-Tooth Type 4B is Caused by Mutations in the Gene Encoding Myotubularin-related Protein-2”, *Nature Genetics*, Vol. 25, No. 1, pp. 17-19.

Bonneick, S., M. Boentert, P. Berger, S. Atanasoski, N. Mantei, C. Wessig, K. V. Toyka, P. Young, and U. Suter, 2005, "An Animal Model for Charcot-Marie-Tooth Disease Type 4B1", *Human Molecular Genetics*, Vol. 14, No. 23, pp. 3685-3695.

Brand, A. H., and N. Perrimon, 1993, "Targeted Gene Expression as a Means of Altering Cell Fates and Generating Dominant Phenotypes", *Development*, Vol. 118, No. 2, pp. 401-415.

Cassereau, J., A. Chevrollier, N. Gueguen, V. Desquiret, C. Verny, G. Nicolas, F. Dubas, P. Amati-Bonneau, P. Reynier, D. Bonneau, and V. Procaccio, 2011, “Mitochondrial Dysfunction and Pathophysiology of Charcot-Marie-Tooth Disease Involving GDAP1 Mutations”, *Experimental Neurology*, Vol. 227, No. 1, pp. 31-41.

Chen, H., and D. C. Chan, 2009, “Mitochondrial Dynamics Fusion, Fission, Movement, and Mitophagy in Neurodegenerative Diseases”, *Human Molecular Genetics*, Vol. 18, No. 2, pp. 169-176.

Cherry, S., E. J. Jin, M. N. Ozel, Z. Lu, E. Agi, D. Wang, W. H. Jung, D. Epstein, I. A. Meinertzhagen, C. C. Chan, and P. R. Hiesinger, 2013, "Charcot-Marie-Tooth 2B Mutations in rab7 Cause Dosage-dependent Neurodegeneration due to Partial Loss of Function", *Elife*, Vol. 2, p. e01064.

Chihara, T., D. Luginbuhl, and L. Luo, 2007, "Cytoplasmic and Mitochondrial Protein Translation in Axonal and Dendritic Terminal Arborization", *Nature Neuroscience*, Vol. 10, No. 7, pp. 828-837.

Choi, C. M., S. Vilain, M. Langen, S. Van Kelst, N. De Geest, J. Yan, P. Verstreken, and B. A. Hassan, 2009, "Conditional Mutagenesis in Drosophila", *Science*, Vol. 324, No. 5923, p. 54.

Claramunt, R., L. Pedrola, T. Sevilla, A. Lopez de Munain, J. Berciano, A. Cuesta, B. Sanchez-Navarro, J. M. Millan, G. M. Saifi, J. R. Lupski, J. J. Vilchez, C. Espinos and F. Palau, 2005, "Genetics of Charcot-Marie-Tooth Disease Type 4A: Mutations, Inheritance, Phenotypic Variability, and Founder Effect", *Journal of Medical Genetics*, Vol. 42, No. 4, pp. 358-365.

Davis, C. J., W. G. Bradley, and R. Madrid, 1978, "The Peroneal Muscular Atrophy Syndrome: Clinical, Genetic, Electrophysiological and Nerve Biopsy Studies. I. Clinical, Genetic and Electrophysiological Findings and Classification", *Journal de Genetique Humaine*, Vol. 26, No. 4, pp. 311-349.

Detmer, S. A., and D. C. Chan, 2007, “Functions and Dysfunctions of Mitochondrial Dynamics”, *Nature Reviews Molecular Cell Biology*, Vol. 8, No. 11, pp. 870-879.

Dove, S. K., K. Dong, T. Kobayashi, F. K. Williams, and R. H. Michell, 2009, "Phosphatidylinositol 3,5-bisphosphate and Fab1p/PIKfyve underPPIn Endo-lysosome Function", *Biochemical Journal*, Vol. 419, No.1, pp. 1-13.

Duffy, J. B., 2002, “GAL4 System in Drosophila: A Fly Geneticist's Swiss Army Knife”, *Genesis*, Vol. 34, No. 1-2, pp. 1-15.

Eaton, D. L., and T. K. Bammler, 1999, “Concise Review of the Glutathione S-transferases and Their Significance to Toxicology”, *Toxicological Sciences*, Vol. 49, No. 2, pp. 156-164.

Ermanoska, B., W. W. Motley, R. Leitao-Goncalves, B. Asselbergh, L. H. Lee, P. De Rijk, K. Sleegers, T. Ooms, T. A. Godenschwege, V. Timmerman, K. H. Fischbeck, and A. Jordanova, 2014, "CMT-associated Mutations in Glycyl- and Tyrosyl-tRNA

Synthetases Exhibit Similar Pattern of Toxicity and Share Common Genetic Modifiers in Drosophila", *Neurobiology of Disease*, Vol. 68, pp. 180-189.

Gargano, J. W., I. Martin, P. Bhandari, and M. S. Grotewiel, 2005, "Rapid Iterative Negative Geotaxis (RING): A New Method for Assessing Age-Related Locomotor Decline in Drosophila", *Experimental Gerontology*, Vol. 40, No. 5, pp. 386-395.

Harding, A. E., and P. K. Thomas, 1980, "Genetic Aspects of Hereditary Motor and Sensory Neuropathy (Types I and II)", *Journal of Medical Genetics*, Vol. 17, No. 5, pp. 329-336.

Hirth, F., 2010, "Drosophila melanogaster in the Study of Human Neurodegeneration", *CNS Neurol Disorders Drug Targets*, Vol. 9, No. 4, pp. 504-523.

Houlden, H., R. H. King, N. W. Wood, P. K. Thomas, and M. M. Reilly, 2001, "Mutations in the 5' Region of the Myotubularin-related Protein 2 (MTMR2) Gene in Autosomal Recessive Hereditary Neuropathy with Focally Folded Myelin", *Brain*, Vol. 124, No. Pt 5, pp. 907-915.

Hsu, F., and Y. Mao, 2014, "The Structure of Phosphoinositide Phosphatases: Insights into Substrate Specificity and Catalysis", *Biochimica et Biophysica Acta*, Vol. 1981, No. 14, p. 1388.

Huber, N., S. Guimaraes, M. Schrader, U. Suter, and A. Niemann, 2013, "Charcot-Marie-Tooth Disease-Associated Mutants of GDAP1 Dissociate Its Roles in Peroxisomal and Mitochondrial Fission", *EMBO Reports*, Vol. 14, No. 6, pp. 545-552.

Hummel, T., and C. Klämbt, 2008, "P-element Mutagenesis", *Methods in Molecular Biology*, Vol. 420, pp. 97-117.

Jackson, G. R., 2008, "Guide to Understanding Drosophila Models of Neurodegenerative Diseases", *PloS Biology*, Vol. 6, No.2, p. e53.

Jose, L. E., P. Verstreken, and S. Vilain, 2013, *Genetic Screens in Drosophila and their Application in Motor Neuron Disease Models*, Nova Science Publishers Inc, Leuven.

Juarez, P., and F. Palau, 2012, "Neural and Molecular Features on Charcot-Marie-Tooth Disease Plasticity and Therapy", *Neural Plasticity*, Vol. 2012, p. 171636.

Kılınç, M., 2013, "*Development and Molecular Analysis of CMT4B1 Drosophila Model*", M.S. Thesis, Boğaziçi University.

Kim, Y. J., N. Jahan, and Y. Y. Bahk, 2013, "Biochemistry and Structure of Phosphoinositide Phosphatases", *BMB Reports*, Vol. 46, No. 1, pp. 1-8.

Kuzmicic, J., A. Del Campo, C. Lopez-Crisosto, P. E. Morales, C. Pennanen, R. Bravo-Sagua, J. Hechenleitner, R. Zepeda, P. F. Castro, H. E. Verdejo, V. Parra, M. Chiong, and S. Lavendero, 2011, "Mitochondrial Dynamics: A Potential New Therapeutic Target for Heart Failure", *Revista Espanola de Cardiologia*, Vol. 64, No. 10, pp. 916-923.

Lee H.W., Y. Kim, K. Han, H. Kim, and E. Kim, 2010, "The Phosphoinositide 3-Phosphate MTMR2 Interacts with PSD-95 and Maintains Excitatory Synapsis by Modulating Endosomal Traffic", *The Journal of Neuroscience*, Vol. 30, No. 26, pp. 5508-5518.

Lewis, E. B., 1978, "A Gene Complex Controlling Segmentation in Drosophila", *Nature*, Vol. 276, No. 5688, pp. 565-570.

Li, X., X. Wang, X. Zhang, M. Zhao, W. L. Tsang, Y. Zhang, R. G. W. Yau, L. S. Weisman, and H. Xu, 2013, "Genetically Encoded Fluorescent Probe to Visualize Intracellular Phosphatidylinositol 3,5-Bisphosphate Localization and Dynamics.", *Proceedings of the National Academy of Sciences of the United States of America*, Vol. 110, pp. 21165–21170.

Lloyd, T. E., and J. P. Taylor, 2010, “Flightless Flies: Drosophila Models of Neuromuscular Disease”, *Annals of New York Academy of Sciences*, No. 1184, pp. e1-20.

Lopez Del Amo, V., M. Seco-Cervera, J. L. Garcia-Gimenez, A. J. Whitworth, F. V. Pallardo, and M. I. Galindo, 2015, "Mitochondrial Defects and Neuromuscular Degeneration Caused by Altered Expression of Drosophila Gdap1: Implications for The Charcot-Marie-Tooth Neuropathy", *Human Molecular Genetics*, Vol. 24, No. 1, pp. 21-36.

Lorenzo, O., S. Urbe, and M. J. Clague, 2006, "Systematic Analysis of Myotubularins: Heteromeric Interactions, Subcellular Localisation and Endosome Related Functions", *Journal of Cell Science*, Vol. 119, No. Pt 14, pp. 2953-2959.

Lu, B., 2009, "Recent Advances in Using Drosophila to Model Neurodegenerative Diseases", *Apoptosis*, Vol. 14, No. 8, pp. 1008-1020.

Lu, B., and H. Vogel, 2009, "Drosophila Models of Neurodegenerative Diseases", *Annual Review of Pathology*, Vol. 4, pp. 315-342.

Marco, A., A. Cuesta, L. Pedrola, F. Palau, and I. Marin, 2004, “Evolutionary and Structural Analyses of GDAP1, Involved in Charcot-Marie-Tooth Disease, Characterize a Novel Class of Glutathione Transferase-related Genes”, *Molecular Biology and Evolution*, Vol. 21, No. 1, pp. 176-187.

Morgan, T. H., A. H. Sturtevant, H. J. Muller, and C. B. Bridges, 1915, *The Mechanism of Mendelian Heredity*, Henry Holt, New York.

Muqit, M. M., and M. B. Feany, 2002, "Modelling Neurodegenerative Diseases in Drosophila: A Fruitful Approach?", *Nature Reviews Neuroscience*, Vol. 3, No. 3, pp. 237-243.

Ni, H. M., J. A. Williams, and W. X. Ding, 2014, "Mitochondrial Dynamics and Mitochondrial Quality Control", *Redox Biology*, Vol. 4C, pp. 6-13.

Nichols, C. D., J. Becnel, and U. B. Pandey, 2012, "Methods to Assay Drosophila Behavior", *Journal of Visualized Experiments*. No. 61.

Niemann, A., K. M. Wagner, M. Ruegg, and U. Suter, 2009, "GDAP1 Mutations Differ in Their Effects on Mitochondrial Dynamics and Apoptosis Depending on the Mode of Inheritance", *Neurobiology of Disease*, Vol. 36, No. 3, pp. 509-520.

Niemann, A., M. Ruegg, V. La Padula, A. Schenone, and U. Suter, 2005, "Ganglioside-induced Differentiation Associated Protein 1 is a Regulator of the Mitochondrial Network: New Implications for Charcot-Marie-Tooth Disease", *Journal of Cell Biology*, Vol. 170, No. 7, pp. 1067-1078.

Niemann, A., N. Huber, K. M. Wagner, C. Somandin, M. Horn, F. Lebrun-Julien, B. Angst, J. A. Pereira, H. Halfter, H. Welzl, M. L. Feltri, L. Wrabetz, P. Young, C. Wessig, K. V. Toyka, and U. Suter, 2014, "The Gdap1 Knockout Mouse Mechanistically Links Redox Control to Charcot-Marie-Tooth Disease", *Brain*, Vol. 137, No. Pt 3, pp. 668-682.

Noack, R., S. Frede, P. Albrecht, N. Henke, A. Pfeiffer, K. Knoll, T. Dehmel, Z. U. Meyer, G. Hörste, and M. Stettner, 2012, "Charcot-Marie-Tooth Disease CMT4A: GDAP1 Increases Cellular Glutathione and the Mitochondrial Membrane Potential", *Human Molecular Genetics*, Vol. 21, No. 1, pp. 150-162.

Nusslein-Volhard, C., and E. Wieschaus, 1980, "Mutations Affecting Segment Number and Polarity in Drosophila", *Nature*, Vol. 287, No. 5785, pp. 795-801.

Pandey, U. B., and C. D. Nichols, 2011, "Human Disease Models in Drosophila melanogaster and the Role of the Fly in Therapeutic Drug Discovery", *Pharmacological Reviews*, Vol. 63, No. 2, pp. 411-436.

Parman, Y., E. Battaloglu, I. Baris, B. Bilir, M. Poyraz, N. Bissar-Tadmouri, A. Williams, N. Ammar, E. Nelis, V. Timmerman, P. De Jonge, A. Najafov, F. Deymeer, P. Serdaroglu, P. J. Brophy, and G. Said, 2004, "Clinicopathological and Genetic Study of Early-Onset Demyelinating Neuropathy", *Brain*, Vol. 125, No. 11, pp. 2540-2550.

Patzko, A., and M. E. Shy, 2011, "Update on Charcot-Marie-Tooth Disease", *Current Neurology and Neuroscience Reports*, Vol. 11, No. 1, pp. 78-88.

Pedrola, L., A. Espert, T. Valdes-Sanchez, M. Sanchez-Piris, E. E. Sirkowski, S. S. Scherer, F. Farinas, and F. Palau, 2008, "Cell Expression of GDAP1 in the Nervous System and Pathogenesis of Charcot-Marie-Tooth Type 4A Disease", *Journal of Cellular and Molecular Medicine*, Vol. 12, No. 2, pp. 679-689.

Pedrola, L., A. Espert, X. Wu, R. Claramunt, M. E. Shy, and F. Palau, 2005, "GDAP1, the Protein Causing Charcot-Marie-Tooth Disease Type 4A, is Expressed in Neurons and is Associated with Mitochondria", *Human Molecular Genetics*, Vol. 14, No. 8, pp. 1087-1094.

Pla-Martin, D., C. B. Rueda, A. Estela, M. Sanchez-Piris, P. Gonzalez-Sanchez, J. Traba, S. de la Fuente, L. Scorrano, J. Renau-Piqueras, J. Alvarez, J. Satrustegui and F. Palau, 2013, "Silencing of the Charcot-Marie-Tooth Disease-associated Gene GDAP1 Induces Abnormal Mitochondrial Distribution and Affects Ca2+ Homeostasis by Reducing Store-operated Ca2+ Entry", *Neurobiology of Disease*, Vol. 55, pp. 140-151.

Previtali S.C., B. Zerega, D.L. Sherman, P.J. Brophy PJ, G. Dina, R.H. King, M.M. Salih, L. Feltri, A. Quattrini, R. Ravazzolo, L. Wrabetz, A. P. Monaco, and A. Bolino, 2003, "Myotubularin-Related 2 Protein Phosphatase and Neurofilament Light Chain Protein, both Mutated in CMT Neuropathies, Interact in Peripheral Nerve", *Human Molecular Genetics*, Vol. 12, No. 14, pp. 1713-1723.

Quattrone, A., A. Gambardella, F. Bono, U. Aguglia, A. Bolino, A.C. Bruni, M.P. Montesi, R.L. Oliveri, M. Sabatelli, O. Tamburrini, P. Valentino, C. Van

Broeckhoven, and M. Zappia, 1996, “Autosomal Hereditary Motor and Sensory Neuropathy with Focally Folded Myelin Sheaths: Clinical, Electrophysiologic and Genetic Aspects of a Large Family”, *Neurology*, Vol. 46, No. 5, pp. 1318-1324.

Reilly, M. M., S. M. Murphy, and M. Laura, 2011, "Charcot-Marie-Tooth Disease", *Journal of the Peripheral Nervous System*, Vol. 16, No. 1, pp. 1-14.

Robinson, F. L., and J. E. Dixon, 2005, "The phosphoinositide-3-phosphatase MTMR2 Associates with MTMR13, a Membrane-associated Pseudophosphatase also Mutated in Type 4B Charcot-Marie-Tooth Disease", *Journal of Biological Chemistry*, Vol. 280, No. 36, pp. 31699-31707.

Saporta, M. A., and M. E. Shy, 2013, "Inherited Peripheral Neuropathies", *Neurologic Clinics*, Vol. 31, No. 2, pp. 597-619.

Senderek, J., C. Bergmann, V. T. Ramaekers, E. Nelis, G. Bernert, A. Makowski, S., P. De Jonghe, S. Rudnik-Schöneborn, K. Zerres, and J. M. Schröder, 2003, “Mutations in the Ganglioside-induced Differentiation-associated Protein-1 (GDAP1) Gene in Intermediate Type Autosomal Recessive Charcot-Marie-Tooth Neuropathy”, *Brain*, Vol. 126, No. 3, pp. 642-649.

Shield, A. J., T. P. Murray, and P. G. Board, 2006, “Functional Characterisation of Ganglioside-induced Differentiation-associated Protein 1 as a Glutathione Transferase”, *Biochemical and Biophysical Research Communications*, Vol. 347, No. 4, pp. 859-866.

Skre, H., 1974, "Genetic and Clinical Aspects of Charcot-Marie-Tooth's Disease", *Clinical Genetics*, Vol. 6, No. 2, pp. 98-118.

Storkebaum, E., R. Leitao-Goncalves, T. Godenschwege, L. Nangle, M. Mejia, I. Bosmans, T. Ooms, A. Jacobs, P. Van Dijck, X. L. Yang, P. Schimmel, K. Norga, V. Timmerman, P. Callaerts, and A. Jordanova, 2009, “Dominant Mutations in the Tyrosyl-tRNA Synthetase Gene Recapitulate in Drosophila Features of Human

Charcot-Marie-Tooth Neuropathy", *Proceedings of the National Academy of Sciences*, Vol. 106, No. 28, pp. 11782-11787.

Tazir, M., M. Bellatache, S. Nouioua, and J. M. Vallat, 2013, "Autosomal Recessive Charcot-Marie-Tooth Disease: from Genes to Phenotypes", *Journal of the Peripheral Nervous System*, Vol. 18, No. 2, pp. 113-129.

Timmerman, V., A. V. Strickland, and S. Zuchner, 2014, "Genetics of Charcot-Marie-Tooth (CMT) Disease within the Frame of the Human Genome Project Success", *Genes (Basel)*, Vol. 5, No.1, pp. 13-32.

Vaccari, I., G. Dina, H. Tronchere, E. Kaufman, G. Chicanne, F. Cerri, L. Wrabetz, B. Payrastre, A. Quattrini, L. S. Weisman, M. H. Meisler, and A. Bolino, 2011, "Genetic Interaction Between MTMR2 and FIG4 Phospholipid Phosphatases Involved in Charcot-Marie-Tooth Neuropathies", *PLoS Genetics*, Vol. 7, No. 10, p. e1002319.

Velichkova, M., J. Juan, P. Kadandale, S. Jean, I. Ribeiro, V. Raman, C. Stefan, and A. A. Kiger, 2010, "Drosophila Mtm and Class II PI3K Coregulate a PI(3)P Pool with Cortical and Endolysosomal Functions", *Journal of Cell Biology*, Vol. 190, No. 3, pp. 407-425.

Vienna Drosophila RNAi Center, 2013, http://stockcenter.vdrc.at/control/howtornaidmel [Accessed January 2015].

Wishart, M. J., and J. E. Dixon, 2002, "PTEN and Myotubularin Phosphatases: from 3-phosphoinositide Dephosphorylation to Disease", *Trends in Cell Biology*, Vol. 12, No. 12, pp. 579-585.

Yamamoto, S., M. Jaiswal, W. L. Charng, T. Gambin, E. Karaca, G. Mirzaa, W. Wiszniewski, H. Sandoval, N. A. Haelterman, B. Xiong, K. Zhang, V. Bayat, G. David, T. Li, K. Chen, U. Gala, T. Harel, D. Pehlivan, S. Penney, L. E. Vissers, J. de De Ligt, S. N. Jhangiani, Y. Xie, S. H. Tsang, Y. Parman, M. Sivaci, E. Battaloglu,

D. Muzny, Y. W. Wan, Z. Liu, A. T. Lin-Moore, R. D. Clark, C. J. Curry, N. Link, K. L. Schulze, E. Boerwinkle, W. B. Dobyns, R. Allikmets, R. A. Gibbs, R. Chen, J. R. Lupski, M. F. Wangler and H. J. Bellen, 2014, "A Drosophila Genetic Resource of Mutants to Study Mechanisms Underlying Human Genetic Diseases", *Cell*, Vol. 159, No. 1, pp. 200-214.

Yang, J. S., H. J. Nam, M. Seo, S. K. Han, Y. Choi, H. G. Nam, S. J. Lee, and S. Kim, 2011, "OASIS: Online Application for the Survival Analysis of Lifespan Assays Performed in Aging Research", *PLoS One*, Vol. 6, No. 8, p. e23525.

Yıldırım, K., 2013, "*Development of Drosophila CMT4A Model Using IMAGO Approach*", M.S. Thesis, Boğaziçi University.

Zuchner, S., and J. M. Vance, 1993, *Charcot-Marie-Tooth Neuropathy Type 4A*, GeneReviews, Seattle (WA).

Zuchner, S., and J. M. Vance, 2006, "Molecular Genetics of Autosomal-dominant Axonal Charcot-Marie-Tooth Disease", *Neuromolecular Medicine*, Vol. 8, No. 1-2, pp. 63-74.